

Bulgarian Geophysical Journal

2012, Vol. 38

C O N T E N T S

T. Harinarayana, B. Srebrov, K. Veeraswamy, K. Bojadgieva, V. Hristov – Magnetoelluric survey in Burgas hydrothermal basin (se Bulgaria)	3
B. Markova, R. Mitzeva – Instability indices as an indicator of thunderstorms in Eastern Bulgaria - preliminary results	12
A. Deleva – Lidar monitoring of clouds and aerosol layers	21
E. Botev, V. Protopopova, I. Popova, B. Babachkova, S. Velichkova, I. Tzoncheva, S. Dimitrova, V. Boychev, D. Lazarov, P. Raykova – Data and analysis of the events recorded by NOTSSI in 2011	34
P. Trifonova, D. Solakov, S. Simeonova, M. Metodiev – Black Sea earthquake safety Net(work) – ESNET	44
P. Trifonova, M. Metodiev – Annual report of the observed geomagnetic activity in Panagyurishte observatory	51
A. Deleva – Lidar investigations of the troposphere performed during summer 2011 measurement campaign	79
E. Botev, V. Protopopova, I. Popova, B. Babachkova, S. Velichkova, I. Tzoncheva, S. Dimitrova, V. Boychev, D. Lazarov, P. Raykova – Data and analysis of the events recorded by NOTSSI in 2012	93

MAGNETOELLURIC SURVEY IN BURGAS HYDROTHERMAL BASIN (SE BULGARIA)

T. Harinarayana¹, B. Srebrov², K. Veeraswamy¹, K. Bojadgieva³, V. Hristov³

¹National Geophysical Research Institute, Hyderabad, India

²National Institute for Geophysics, Geodesy and Geography, Bulgarian Academy of Sciences

³Geological Institute, Bulgarian Academy of Sciences

Abstract. The results from the first magnetotelluric (MT) survey in Bulgaria on hydrothermal reservoirs are presented. The project was initiated under Indo-Bulgarian collaborative program supported by Department of Science and Technology, New Delhi, India and Bulgarian Academy of Sciences, Sofia, Bulgaria. The main objective of this study was to search for deep seated reservoirs for the need of geothermal energy use. Field visits were made to 15 sites in Bulgaria to identify the existence of suitable conditions for magnetotelluric investigations. Three reservoirs in Burgas basin (SE Bulgaria) have been selected after complex analysis of available geological, hydrogeological and geophysical data. MT data acquisition and processing are discussed. The results are presented as distribution of apparent resistivity and phase versus frequency. A deep seated conductivity medium is clearly outlined near Polyanovo.

Key words: magnetotelluric method (MT), hydrothermal reservoirs, thermal waters

Introduction

Thermal water use has an ancient tradition in Bulgaria. The temperature of discovered water does not exceed 100°C and is used only for direct application – balneology, heating of buildings and greenhouses, bottling, etc. (Bojadgieva et al. 2011). The need of electricity generation requires exploration of thermal waters with temperatures above 100°C. This article presents the results obtained during the first magnetotelluric survey on geothermal structures in the country. MT allows detection of electro-conductive zones associated with productive structures, including faults and presence of a cap rock. The investigation depth ranges from 300 m below ground down to 10,000 m or deeper with long-period soundings. The earth's natural electromagnetic field contains a very wide spectrum of frequencies as low ones are useful in probing to depths of several hundreds of kilometers. The method works best where seismic has problems in areas of high-velocity

cover such as volcanic provinces, carbonate cover, salt, etc.

This study was conducted by a team of Indian and Bulgarian scientists under Inter-governmental program of cooperation in science & technology.

The paper aims at presenting the application of MT-methodology for probing deep seated hydrothermal deposits in Bulgaria and to discuss the obtained results for the selected region.

Selection criteria for geothermal sites

The selection of geothermal reservoirs suitable for MT survey was made after analysis of available geological information, basic hydrogeological parameters, conducted geophysical surveys and field conditions. The site should be significantly away from power transmission lines, highways, human settlements, large water bodies, undulating topography, etc.

Three geothermal sites located in Burgas region (NE Bulgaria) – Polyanovo, Aitos and Sadievo have been selected after visiting 15 hydrothermal deposits located in nine geothermal basins in the country. The study started with the analysis of the existing geological and geothermal data. Temperature field distribution in depth is analyzed based on the well-log data, water temperature, measured at the wellhead and calculated temperature by chalcedony geothermometer (Bojadgieva et al. 2007).

Temperature field in Polyanovo has been studied in more details due to the largest number of wells and temperature logs in them and for the highest hydrothermal potential (Bojadgieva et al. 2006).. The measured water temperature is 49°C in Polyanovo and 50°C in Aitos. Higher temperatures are expected in deeper seated reservoirs.

The available geological and hydro geological information for the region (Vlaskovski, 1997) was used to layout the measuring stations along profile lines.

Methodology of MT sounding

MT is a geophysical method that measures naturally occurring, time varying magnetic and electric fields. The solar wind (plasma) disturbs the earth's magnetic field and cause ultra low-frequency signal (generally less than 1 Hertz) to penetrate the earth's surface. The higher frequency signal (greater than 1 Hertz) is created by thunderstorms, usually near the equator. Both of these sources create time varying electromagnetic waves. The signals vary in strength over hours, days, weeks and even over the sunspot cycle. The MT field measurements last for hours at each station to get a good statistical average of data signal, especially when measuring them at the lowest frequencies (about 0.001 Hertz). The main parameter that is derived from MT is electrical resistivity. The factors affecting resistivity are lithology, hydro geological processes, pressure and temperature.

Electromagnetic (EM) theory is originated from four fundamental equations proposed by J.Maxwell (Zhdanov, 1994). The orthogonal components of the electric (E_x and E_y) and magnetic (H_x, H_y and H_z) fields are simultaneously recorded. The relationship

between them can be expressed as a complex impedance tensor $Z(\omega)$ at each frequency (1),(2):

$$[Z] = \begin{bmatrix} Z_{xx} & Z_{xy} \\ Z_{yx} & Z_{yy} \end{bmatrix} \quad (1)$$

where

$$Z_{xy}(\omega) = \frac{E_x(\omega)}{H_y(\omega)} \quad (2)$$

As an electromagnetic wave penetrates the Earth, its amplitude will decay at a rate dependent on the conductivity of the rocks and the rate of time variation of the frequency. The apparent resistivities (ρ) could be derived from the amplitudes (3):

$$\rho_{a,xy}(\omega) = \frac{1}{\omega\mu} \left| \frac{E_x(\omega)}{H_y(\omega)} \right|^2 \quad (3)$$

where μ is a constant.

A typical MT station layout is given in Fig.1

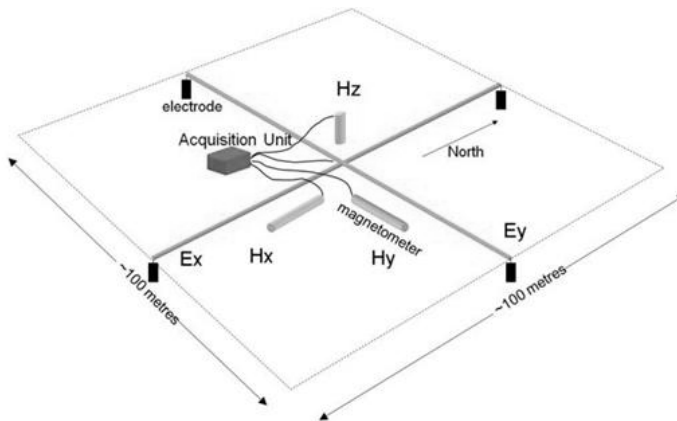


Fig. 1. MT setup (<http://www.moombarriga.com>)

Five components (Hx, Hy, Hz, Ex and Ey) are measured at the surface as a set of time series. The vertical electric field is not measured because it is assumed to be zero. Several processing steps are run after acquiring these data and as a result noise is removed from them. The data are transformed from a time-domain to a frequency domain. This is achieved by using Fourier transforms. The data would be further inverted to produce a cross section of resistivity vs. depth (Zhdanov, 1994).

Field survey

The location of the study region is presented in Fig.2. It is built of Quaternary and Neogene sediments and Upper Cretaceous sediment and volcano-sediment rocks, intersected by tectonic faults. The Upper Cretaceous sediments consist of alternation of marls, siltstones, argillites, clayey limestone and sandstones, while the volcanic complex comprises andesites, basaltic andesites and tuffs. Quaternary and Neogene sediments are thin (from 0-59 m) and built mainly of clays and gravels. The thickness of Upper Cretaceous is very high and its bottom hasn't been reached. Polyanovo geothermal area has been identified for conducting MT field investigations as this area is well studied compared to other nearby geothermal sites such as Sadievo and Aitos and also suitable due to less cultural noise (e.g. power lines, vehicular traffic etc.), Fig.2. the reservoir represents an unstratified fractured type water collector, which is characterized with a high filtration and thermal inhomogeneity (Vlaskovski, 1997).

MT measurements are done in totally 14 stations. Seven of them are placed along a regional profile (1), which is 35 km long and oriented in north-south direction (stations between 13 and 14), Fig. 2a. Four shorter profiles about 1 to 3 km long are placed around Polyanovo for more detailed survey, Fig.2b.

MT data processing and interpretation

The MT field survey in Bulgaria has been carried out by equipment provided by National Geophysical Research Institute in Hyderabad, India (Harinarayana et al. 2008). The ADU (Analogue Digital Unit)-06 is the main unit of the Metronix multi-channel geophysical measurement system GMS-06. The electric and magnetic field sensors are connected directly to the ADU-06 unit. Between ten to thirty channels are recorded at one time. The ADU can be operated either by using the control software GMS (offline recording mode) or by MAPROS (online recording mode and data processing) which runs under Windows 95/98 or Windows NT/2000/XP operating system. The measured time series at 14 sounding locations are processed using Mapros MT time series analysis and processing software to estimate the best MT impedance values in the frequency range 1000 Hz – 0.001 Hz. The processed MT apparent resistivity and phase curves in the measured directions (XY – geomagnetic north-south and YX- geomagnetic east-west) are drawn for along the five profile lines.

The apparent resistivity and phase data for the station 3 (Polyanovo), located near the central part of the study region, is presented in Figure 3. The data are plotted on a log-log

curve. One curve shows the apparent resistivity (ρ_{XY}) determined from the electric field, in the north direction (E_x) and the magnetic field, in the east direction (H_y). The other curve (ρ_{YX}) plots the data for the other two orthogonal horizontal fields, E_y and H_x .

The sediments of Quaternary, Neogene and the upper weathered part of Upper Cretaceous have exhibited conductive as compared to the below Upper Cretaceous volcano-sediment rocks. This can be seen clearly showing the apparent resistivity values of 10 Ohm.m in (100 – 1000 Hz) frequency range. For lower frequencies (10 - 1 Hz) the apparent resistivity steeply raises indicating the presence of high resistive basement below the sedimentary cover. For further lower frequency range (1 - 0.01 Hz) the apparent resistivity values show a decreasing trend indicating for the presence of deeper anomalous structure in the central part of the study area. The same trend is confirmed by the data measured in station 4 (Fig.2b), located also in Polyanovo area.

An example of MT data is presented for the station 13 located away from Polyanovo area towards southern part near Vinarsco village (Figure 4). It has exhibited relatively high resistive layer at the high frequency range indicating that the site is located over a high resistivity formations as compared to the stations 3 and 4 (near Polyanovo).

Further for the lower frequency range the apparent resistivity has shown small gradient for the station 13. The same trend is exhibited for a station 14 located towards northern end of the study area (near Shivarovo). From these stations 13 and 14 it is clear that the deeper anomalous conductor indicated near the central part of the profile 1 of the study area has not extended to far away locations.

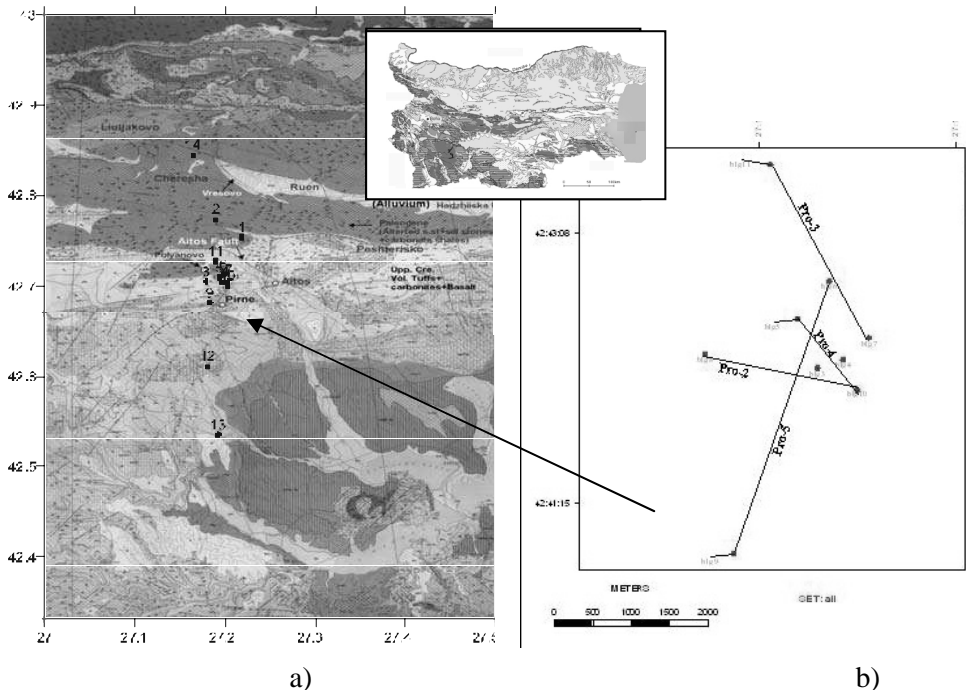


Fig. 2. Location of MT stations and regional profile -1 (a) and short profiles - 2,3, 4 and 5 layout in Polyanovo area (b)

The pseudo-section prepared using apparent resistivity data along both xy and yx are presented along the stations of regional profile-1 (Figure 5). The stations located towards north covering the stations 14, 2, 1 and also another station 12 towards south have exhibited relatively high resistivity as compared to the stations 11, 5, 9 located near centre of the profile. Near the center shallow section corresponds to high frequency up to about 100 Hz conducting sediments of Quaternary, Neogene and weathered volcano-sediments rocks of Upper Cretaceous. This is followed by high apparent resistivity for the frequencies (10-1) Hz and further lower frequencies has tendency to show conductive formations at 0.1 Hz.

Similarly, phase pseudo-section for profile 1 is presented in Fig.5. The high frequency band near the middle part of the profile has phase values ranging between 35 and 55 and as the frequency decreases the phase value also decreases to 10 to 30 and for further lower frequencies the phase again exhibited higher values of 35 to 50. This is compatible with the apparent resistivity pseudo section in the form of conductor-resistor-conductor layers near the central part of the profile 1.

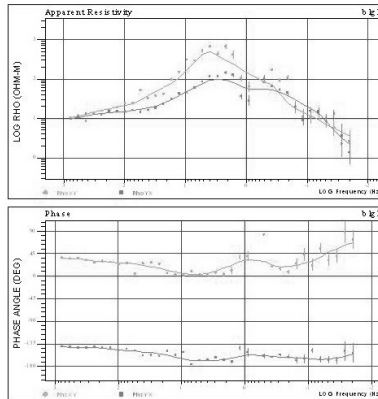


Fig. 3.. MT data for station 3 after processing

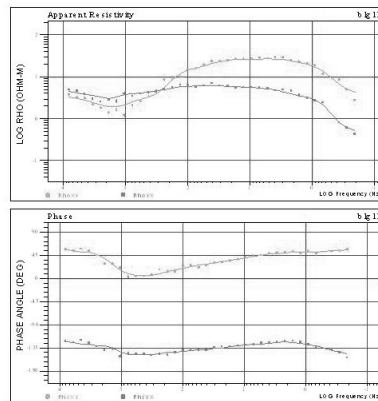


Fig. 4. MT data for station 13 after processing

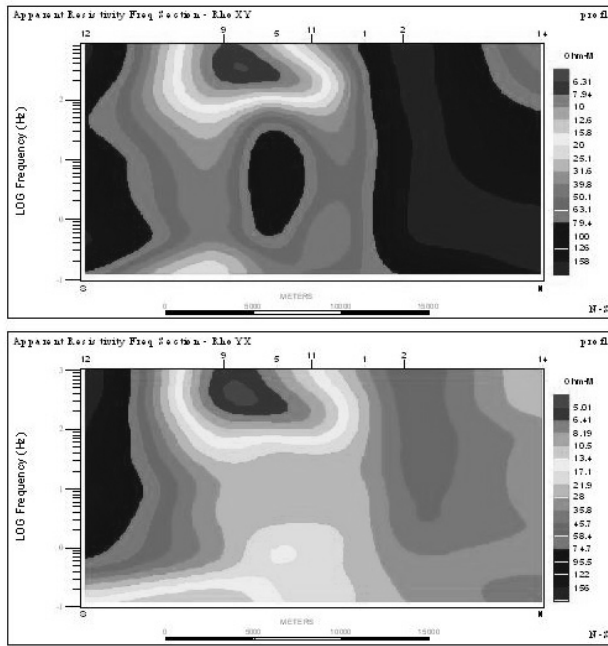


Fig.5. Regional distribution of apparent resistivity as a function of frequency (profile-1)

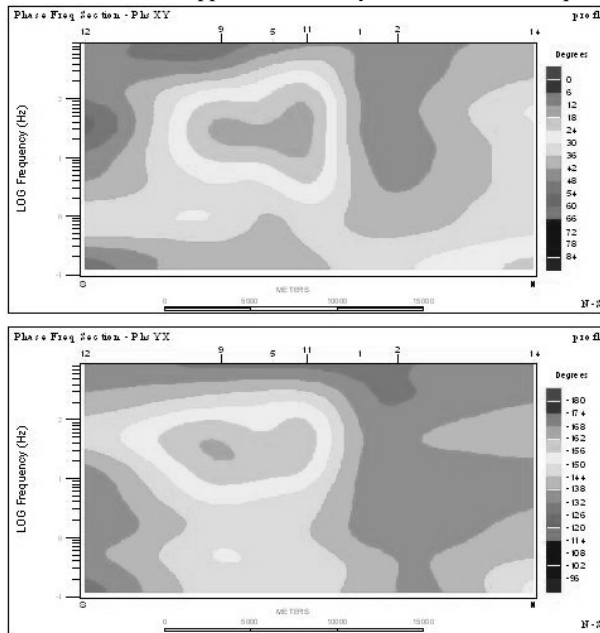


Fig. 6. Regional distribution of phase values as a function of frequency (profile 1).

The existing conductive zone in the middle of profile-1 is marked also on the apparent resistivity and phase pseudo-sections along profiles 2 and 4, located in the Polyanovo hydrothermal zone.

Indications of deep seated hydrothermal zones are registered in other hydrothermal basins in the country, where suitable conditions for MT sounding are also available.

Conclusions

About 15 geothermal sites in Bulgaria were visited to select the best conditions for conducting magneto telluric sounding - Polyanovo geothermal reservoir (SE Bulgaria). A detailed study of temperature field distribution, geological and hydrogeological conditions in Polyanovo had been done before the execution of the magnetotelluric survey.

The distribution of apparent resistivity and phase values along one regional and four local profiles clearly define two conductive zones. The next step is the assessment of resistivity variations versus depth.

Acknowledgements

We are thankful to the Municipality of Aitos town (Burgas region) for the great help rendered for all the places of the field work. We are also grateful to the financial support extended by DST, India, Ministry of Education and Sciences, Bulgaria.

References

1. Bojadgieva, K., A. Benderev, 2011, Geothermal resources and utilization in Bulgaria. 711-718 In: *Compt. rend. Acad. bulg. Sci.* 64.No.5.
2. Bojadgieva, K., V. Hristov, and B. Srebrov, Feb. 2007, Temperature field study of fractured hydrothermal reservoirs in SE Bulgaria (Bourgas basin). pp.8-15. 2007, *Journal of the Balkan Geophysical Society*, v.10, No.1.
3. Bojadgieva, K., V. Hristov, B. Srebrov, T. Harinarayana, and K. Veeraswamy, 2006, Temperature investigations in Polyanovo hydrothermal reservoir (SE Bulgaria), *Bulg. Geophys. Journal*, vol.32.
4. Vlaskovski, I. (ed), 1997, Reassessment of geothermal resources in Bulgaria (Report), pp. 247, *Geonika, Jambol, National Geofund*,
5. Zhdanov, M.S. and G.V. Keller, 1994, *The geoelectrical methods in geophysical exploration*. Elsevier.
6. Harinarayana, T., B. Srebrov, K. Veeraswamy, K. Bojadgieva, 2008, Mapping of subsurface geoelectric structure to assess geothermal potential of Bulgaria using magneto-telluric studies, Technical Report NGRI, Hyderabad, India,.

Магнитотелурични проучвания в Бургаския хидротермален басейн (СИ България)

Харинараяна Т., Сребров Б., Веерасуами К., Бояджиева К., Христов В.

Резюме. Представени са резултати от първите магнитотелурични (МТ) проучвания на хидротермален резервоар в България. Този проект беше инициран в рамките на Българско-Индийската програма за сътрудничество между Департамента за наука и технологии, Ню Дели, Индия и Българската академия на науките. Главния цел на това изследване е да се търсят дълбоки геотермални резервоари за добиване на геотермална енергия. Бяха посетени 15 обекта в България за да се определят такива, с подходящи условия за провеждане на магнитотелурични изследвания. Бяха избрани три резервоара в Бургаския басейн (СИ-България) за комплексен анализ на наличните геологични, хидрогеологични и геофизични данни. В статията е представено получаването на МТ данни и тяхната обработка. Резултатите са представени като разпределение на привидното съпротивление и фазата в зависимост от честотата. В резултат от проведеното МТ проучване е намерена зона с висока електропроводимост в близост до с. Поляново.

INSTABILITY INDICES AS AN INDICATOR OF THUNDERSTORMS IN EASTERN BULGARIA - PRELIMINARY RESULTS

B. Markova^{1,2}, R. Mitzeva²

¹National Institute of Meteorology and Hydrology –Varna, Department Weather Forecast, 10 Sv. Nikola mst., 9010 Varna, Bulgaria, e-mail: b_markova@abv.bg

² Sofia University, Faculty of Physics, Department of Meteorology and Geophysics, 5 James Boucher Blvd., 1164 Sofia, Bulgaria, e-mail: rumypm@phys.uni-sofia.bg

Abstract. The work is directed to test the ability of some instability indices to be used as an indicator of lightning from convective clouds. Three instability indices (CAPE, Lifted Index and K Index) are calculated using environmental conditions of 98 days with precipitation, detected in eleven synoptic stations located in eastern Bulgaria in the period April – September 2006. For the statistical analyses the cases have been divided in two samples – ordinary precipitating clouds and thunderstorms. The results reveal that the distributions of the studied indices are significantly different in the both samples. The critical values (thresholds) of the three instability indices that may separate the studied cases into two groups (ordinary clouds and thunderstorms) are established. The best discrimination between thunderstorms and ordinary precipitating clouds is obtained using the threshold values of Lifted index. The performed multiple discriminant analysis shows that the classification function obtained by combination of instability indices does not improve the skill to predict the occurrence of thunderstorms in comparison to the single use of Lifted index.

Key words: Instability indices, thunderstorms, discriminant analyses

Introduction

It is well known that standard weather prediction methods have a limited ability to forecast severe weather events (tornado, hail, strong wind, thunderstorms, etc.) especially to predict the location of their development. That is why several studies (Doswell et al. (1996), Rasmussen et al. (1998), Craven et al. (2002), Markowski et al. (2002), Brooks et al. (2003), Brooks et al. (2007), and Doswell et al. (2003)) focus on the determination of critical values of various parameters “describing” the environmental conditions for severe events. Furthermore, it is known that the established thresholds depend on geographical regions, season, and climatic conditions.

The aim of the present work is to explore if any of the three instability indices Li, K and CAPE or combination of them can be used as an indicator of thunderstorms development over eastern Bulgaria. The choice of the above parameters is based on the previous studies which reported that Lifted Index (Galway, 1956) and K Index (George, 1960) predict the likelihood of thunderstorms. Vertically integrated measures of instability such as the convective available potential energy, CAPE (Moncrieff and Miller, 1976), provide a more detailed physical representation of the state of the atmosphere (Blanchard, 1998). Based on the analyses of thermodynamic and kinematic environmental characteristics in Europe during the summer months it is concluded (Kaltenbock et al., 2009) that CAPE has considerable skill to predict the occurrence of thunderstorms.

Data and Methodology

The environmental conditions of 98 days with precipitating clouds developed in the afternoon hours over eastern Bulgaria from April to September 2006 are analyzed. The proximity aerological sounding at 1200 UTC are used to calculate three instability indices (CAPE, Lifted Index and K Index; Table 1) for the days when precipitation is detected in eleven synoptic stations of the National Institute of Meteorology and Hydrology (NIMH), located in eastern Bulgaria. Six of the stations are situated along the coast and the others five are inland stations. The proximity soundings are obtained by downloading the data of the numerical model GFS <http://www.arl.noaa.gov/ready/cmnet.html>. Surface level meteorological data (pressure, humidity, temperature and a maximum temperature for the day), taken from <http://www.ogimet.com/synops.phtml.en> are utilized for processing the data from the soundings.

Table 1. Summary of thermodynamic, kinematic parameters and skill scores used: T is temperature ($^{\circ}\text{C}$), T_d is dewpoint temperature ($^{\circ}\text{C}$), θ is potential temperature (K), θ_e is equivalent potential temperature (K), g is the acceleration of gravity (m s^{-2}), z is height (m), LFC - the level of free convection, EL - the equilibrium level of the parcel, TP_{500} - temperature of a parcel after it has been lifted pseudo-adiabatically to 500 hPa from its original level, x - the number of correctly classified thunderstorms cases, y - the number of incorrectly classified thunderstorms cases, w - the number of incorrectly classified ordinary clouds cases. Subscripted numbers indicate constant pressure levels.

Parameter	Code and units	Equation
Convective Available Potential Energy	CAPE, J kg^{-1}	$CAPE = g \int_{LFC}^{EL} \frac{\theta - \theta_e}{\theta_e} dz$
Lifted index	Li, deg	$Li = T_{500} - TP_{500}$
K index	K, deg	$K = (T_{850} - T_{500}) + T_{d850} - (T_{700} - T_{d700})$
Probability of detection	POD	$POD = \frac{x}{x + y}$
False alarm ratio	FAR	$FAR = \frac{w}{x + w}$

All precipitating cases (373) were divided into two samples – ordinary (without lightning) precipitating clouds (216) and thunderstorms (precipitation concurrent with lightning) (157), according to synoptic reports in eastern Bulgaria. The ordinary precipitating clouds (without lightning) and thunderstorms hereafter are denoted as *or* and *th* respectively.

The descriptive statistics (mean, mode, median, etc.) for the three instability indices (CAPE, Li, and K) are estimated. The statistical analyses (F- and t-test with significance level $\alpha=0.05$) is performed to establish if there is a statistical significant difference between any of the instability indexes (CAPE, Li and K) in the both considered samples - ordinary precipitating clouds, *or* and thunderstorms, *th*.

The distributions of the CAPE, Li and K values in the *or* and *th* samples are investigated.

The discriminant analyses (StatSoft, Inc., 2001) is carried out to establish if any of the three instability indices Li, K and CAPE or combination of them is able to classify the clouds as ordinary precipitating cloud or thunderstorm. The probability of detection (POD) and false alarm ratio (FAR) are calculated (Donaldson et al., 1975) for the derived classification functions (see Table 1). The critical values (thresholds) of the three instability indices (CAPE, Li and K) that may separate the studied cases in two groups (ordinary clouds and thunderstorms) are established.

Results

The results presented in Fig. 1 reveal that the frequency distribution of the CAPE *th* values (black columns) is shifted towards larger values in comparison to the frequency distribution of CAPE *or* (grey columns). The maximum percentage (mode) of CAPE *or* is less than 250 J kg^{-1} , while the mode of CAPE *th* is approximately 1050 J kg^{-1} . The results also reveal that thunderstorms may developed at very low CAPE values ($\text{CAPE} < 200 \text{ J kg}^{-1}$) however, their percentage is less than 3 %, while ~ 27 % of ordinary clouds develop at $\text{CAPE} < 200 \text{ J kg}^{-1}$.

The more detailed analysis of the frequency distribution shows that ~57 % of the considered thunderstorms and ~18 % of ordinary precipitating clouds developed at CAPE values in the interval for “moderate instability” ($1000\text{--}2500 \text{ J kg}^{-1}$), while most of the ordinary clouds (80 %) developed at CAPE values in the interval for “marginal instability” ($0\text{--}1000 \text{ J kg}^{-1}$). The above mentioned classification of the degree of instability is in accordance with the study <http://www.crh.noaa.gov/lmk/soo/docu/indices.php>, performed for the USA regions.

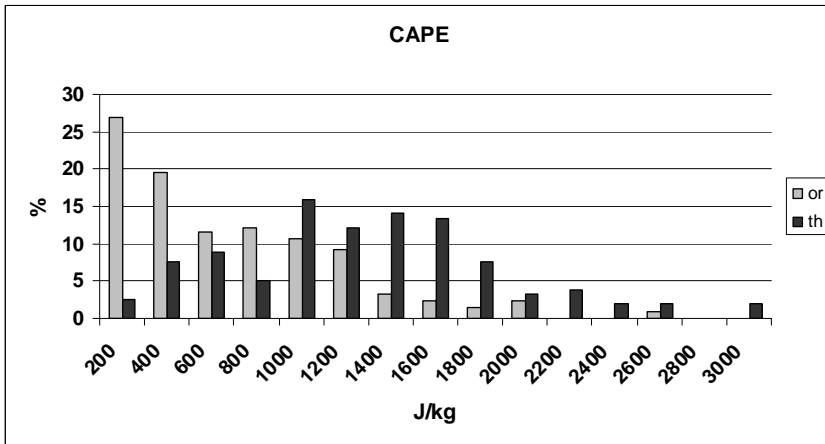


Fig.1. Frequency distribution of CAPE values (in percentages) at the development of ordinary precipitating clouds (grey columns) and at the development of thunderstorms (black columns)

Fig. 2 and Fig. 3 show the frequency distributions of Li and K values for the both samples - ordinary clouds, *or* and thunderstorms, *th*. It is seen (Fig. 2) that the frequency distribution of the Li *th* values (black columns) is shifted towards lower (negative) values in comparison to the frequency distribution of Li *or* (grey columns), while the percentages of higher K values are larger at the development of thunderstorms in comparison to the development of ordinary precipitating clouds. The detailed analysis of the frequency distribution of Li indicates that according to the classification <http://www.crh.noaa.gov/lmk/soo/docu/indices.php> most of the thunderstorms (~53 %) developed at “moderate instability” (-3 to -6 deg), 11 % at “strong instability” (Li < -9 deg) and 33 % at “marginal instability” (-3 < Li < 0 deg). Most of the ordinary clouds (46 %) developed at “marginal instability”, 19 % at “moderate instability” and only 2 % at strong instability. It has to be mentioned that 33 % of the considered ordinary precipitating clouds developed according to <http://www.crh.noaa.gov/lmk/soo/docu/indices.php> at stable atmosphere (0 < Li < 3 deg) when “there is a weak probability for convection if a strong lifting is present”. The highest percentage (66 %) of K values at the development of ordinary precipitating clouds are K < 30 deg, while ~64 % of thunderstorms developed at K > 30 deg.

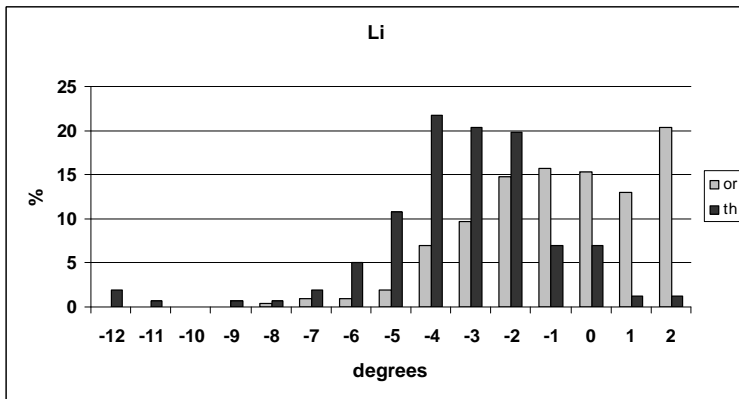


Fig.2. Frequency distribution of Li values (in percentages) at the development of ordinary precipitating clouds (grey columns) and at the development of thunderstorms (black columns)

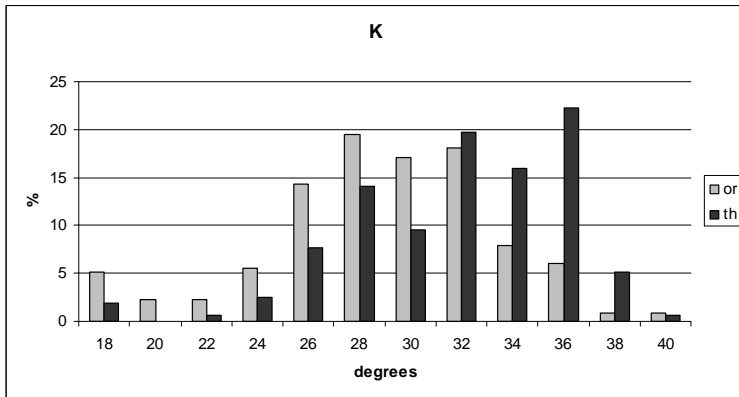


Fig.3. Frequency distribution of K values (in percentages) at the development of ordinary precipitating clouds (grey columns) and at the development of thunderstorms (black columns)

The statistical analyses (t- and F-tests with a significance level $\alpha=0.05$) indicates that the differences in the mean values of the three indices for thunderstorms and ordinary precipitating clouds are statistically significant. The Box and Whiskers plots for CAPE (Fig.4a), Li (Fig.4b) and K (Fig.4c) illustrate that there is a well pronounced difference between their corresponding mean values at the development of thunderstorms, *th* and at the development of ordinary precipitating clouds, *or*. The results reveal that thunderstorms over eastern Bulgaria developed at significantly higher mean values of CAPE and K and significantly lower mean values of Li, compared to the corresponding mean values at the development of ordinary thunderstorms.

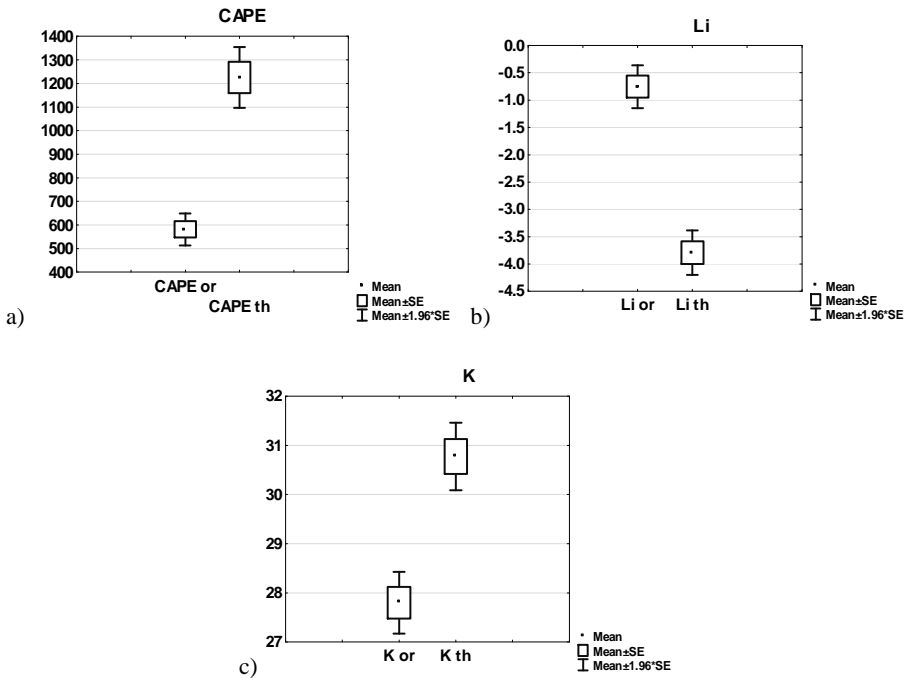


Fig.4. Box and Whiskers plot of a) CAPE , b) Lifted index, Li and c) K values for ordinary precipitating clouds *or* and thunderstorms *th*. ♦Mean±SE±1.96*SE

Table 2. Threshold values of instability indices for the type of clouds, percentage of correctly determined cases - thunderstorm *th* or ordinary *or*, and skill scores POD and FAR

Index	Threshold	Correct classification %			POD	FAR
		all	th	or		
CAPE, J kg ⁻¹	903	72.9	67.5	76.9	0.68	0.32
Li, deg	-2.3	73.9	80.3	69.4	0.80	0.34
K, deg	29	63	67.5	59.7	0.68	0.45

The threshold values of CAPE, Li and K at the development of thunderstorms over eastern Bulgaria derived by general discriminant analysis (StatSoft, Inc., 2001), the percentage of correctly classified cases (*th* or *or*) and calculated skill scores are presented in Table 2. The results show that when thunderstorms developed over eastern Bulgaria 67.5% of CAPE and K values are higher than the established threshold (903 J kg⁻¹ and 29 deg respectively) and at the development of ordinary clouds 76.9 % of CAPE values and 59.7 % of K values are lower than the established thresholds. The best results are obtained using the threshold values of Lifted index. At Li < -2.3 deg - 73.9 % of the cases are correctly discriminate in accordance to the type of clouds (ordinary precipitating or thunderstorms). This threshold is very close to the reported (Kunz, 2007) Li threshold for thunderstorm development over Southwest Germany. The calculated skill scores (POD, FAR) given in

Table 2 reveal that only Lifted index, Li has approximately a good forecasting ability (POD = 0.8 and FAR = 0.34) for occurrence of thunderstorms in eastern Bulgaria.

In an attempt to obtain better discrimination between the ordinary precipitating clouds and thunderstorms the multiple discriminant analyses (StatSoft, Inc., 2001) with various combination of the instability indices are carried out (Table 3). At $F(\text{th,or}) > 0$ the case is classified as thunderstorm; at $F(\text{th,or}) \leq 0$ the case is classified as ordinary cloud. The percentage of correctly classified cases in accordance to the type of the clouds (*or* or *th*), the POD and FAR values indicate that the combination of instability indices does not improve the classification ability of the derived function in comparison to the single use of Lifted index.

Table 3. Classification functions $F(\text{th,or})$ for the type of clouds, and the percentage of correctly classified cases - thunderstorm th or ordinary or, using combination of instability indices and skill scores POD and FAR

Index	Function	Correct classification %			POD	FAR
		all	th	or		
CAPE, Li, K	$F(\text{th,or}) = 0.0004 \text{ CAPE} - 0.2988 \text{ Li} + 0.0167 \text{ K} - 1.4965$	74.3	77.1	72.2	0.77	0.33
CAPE, Li	$F(\text{th,or}) = -0.3184 \text{ Li} + 0.0003 \text{ CAPE} - 1.0314$	74.3	77.7	71.6	0.78	0.33
CAPE, K	$F(\text{th,or}) = 0.0013 \text{ CAPE} + 0.0631 \text{ K} - 3.0172$	73.2	70.7	75.0	0.71	0.33
Li, K	$F(\text{th,or}) = -0.3742 \text{ Li} + 0.0127 \text{ K} - 1.2220$	73.7	78.3	70.4	0.78	0.34

Conclusion

Three instability indices - CAPE, Lifted Index and K Index, were calculated using environmental conditions of 98 days with precipitation over eastern Bulgaria from April to September 2006. For the analyses the cases were divided into two samples – ordinary precipitating clouds and thunderstorms. The statistical analyses (F- and t-test) were performed to check if there is a significant difference between CAPE, Li and K values at the development of ordinary precipitating clouds and thunderstorms over eastern Bulgaria. Discriminant analyses were carried out to obtained classification functions and threshold values of the considered indices that are able to discriminate thunderstorms from ordinary precipitating clouds. The main results are:

- The frequency distributions of the considered indices (CAPE, K and absolute values of Li) at the development of thunderstorms are shifted towards larger values in comparison to the frequency distributions at the development of ordinary precipitating clouds in eastern Bulgaria;

- The higher probability of detection of thunderstorms (POD = 0.8) has Lifted index. The established critical Li values (Li = -2.3 deg) are able to discriminate correctly ~74 % of cases in accordance to the type of the considered clouds;
- The combination of instability indices does not improve the classification ability of the derived function in comparison to the single use of Lifted index.

In an attempt to search classification functions (threshold values) with higher probability of detection of thunderstorms it is worth to consider separately the inland and coastal cloud cases developed over eastern Bulgaria, using larger number of precipitating cases.

References

- Blanchard, D. O., 1998. Assessing the vertical distribution of convective available potential energy. *Wea. Forecasting*, 13, 870–877.
- Brooks, H.E., J.W. Lee, J.P. Craven, 2003. The spatial distribution of severe thunderstorm and tornado environments from global reanalysis data. *Atmos. Res.*, 67–68, 73–94.
- Brooks, H.E., A.R. Anderson, K. Riemann, I. Ebberts, H. Flachs, 2007. Climatological aspects of convective parameters from the NCAR/NCEP reanalysis. *Atmos. Res.*, 83, 294–305.
- Craven, J.P., H.E. Brooks, J.A. Hart, 2002. Baseline climatology of sounding derived parameters associated with deep, moist convection. Preprints 21st Conf. on Severe Local Storms, San Antonio, Texas, 12–16 August 2002. Amer. Meteor. Soc., Boston, pp. 643–646.
- Donaldson, R., R. Dyer, M. Krauss, 1975. An objective evaluator of techniques for predicting severe weather events. Preprints: 9th Conf. Severe Local Storms, Norman, Oklahoma. Amer. Meteor. Soc. 321–326.
- Doswell III, C.A., H.E. Brooks, R.A. Maddox, 1996. Flash flood forecasting: an ingredients-based methodology. *Weather Forecast.*, 11, 560–580.
- Doswell III, C.A., J.S. Evans, 2003. Proximity sounding analysis for derechos and supercells: an assessment of similarities and differences. *Atmos. Res.*, 67–68, 117–133.
- Galway, J.G., 1956. The lifted index as a predictor of latent instability. *Bull. Am. Meteorol. Soc.*, 37, 528–529.
- George, J., 1960. *Weather Forecasting for Aeronautics*. Academic Press. 673 pp.
<http://www.arl.noaa.gov/ready/cmet.html> NOAA Air Resources Laboratory.
- <http://www.ogimet.com/synops.phtml.en> Professional information about meteorological conditions in the world
- <http://www.crh.noaa.gov/lmk/soo/docu/indices.php> NOAA's National Weather Service Weather Forecast Office, Science and Technology, NWS Louisville, KY Convective Season Environmental Parameters and Indices.
- Kaltenbock, R., G. Diendorfer, N. Dotzek, 2009. Evaluation of thunderstorm indices from ECMWF analyses, lightning data and severe storm reports. *Atmos. Res.*, 93, 381–396.
- Kunz, M., 2007. The skill of convective parameters and indices to predict isolated and severe thunderstorms. *Nat. Hazards Earth Syst. Sci.*, 7, 327–342.
- Markowski, P.M., J.M. Straka, E.N. Rasmussen, 2002. Direct surface thermodynamic observations within rearflank downdrafts of nontornadic and tornadic supercells. *Mon. Weather Rev.*, 130, 1692–1721.
- Moncrieff, M., M. Miller, 1976. The dynamics and simulation of tropical cumulonimbus and squall lines. *Quart. J. Roy. Meteor. Soc.*, 102, 37–394.

Rasmussen, E.N., D.O.Blanchard, 1998.A baseline climatology of soundingderived supercell and tornado forecast parameters.Weather Forecast., 13, 1148–1164.
StatSoft, Inc. (2001). STATISTICA (data analysis software system), version 6.1, www.statsoft.com

Индекси на неустойчивост като индикатори на гръмотевични облаци в Източна България – предварителни резултати

Б. Маркова, Р. Мицева

Резюме. Работата е насочена към установяване, дали някои индекси на неустойчивост могат да се използват като индикатори за гръмотевични облаци. Пресметнати са три индекса на неустойчивост (CAPE, Lifted Index and K Index), като се използват приземни данни и от апроксимирани сондажи за 98 дни с валежи, регистрирани в 11 синоптични станции в Източна България за периода април – септември 2006 г. За статистически анализ случаите са разделени на две извадки – обикновени дъждовни облаци и гръмотевични облаци. Резултатите показват, че разпределението на стойностите на пресметнатите индекси са съществено различни за двете извадки. Установени са критични стойности (прагове) на трите индекса на неустойчивост, които могат да разделят използваните случаи на две групи (обикновени дъждовни облаци и гръмотевични облаци). Най-добро класифициране като гръмотевични или обикновените дъждовни облаци се получава при използване на критичната стойност за Lifted index. С помощта на дискриминантен анализ е получена класификационна функция, комбинация от трите индекса на неустойчивост (CAPE, Lifted Index and K Index), която може да се използва като индикатор на гръмотевични облаци. Резултати показват, че функцията получена от комбинацията на трите индекса на неустойчивост не разделя двете извадки по-добре от функцията, получена при използване само на стойностите на Lifted index.

LIDAR MONITORING OF CLOUDS AND AEROSOL LAYERS

A. Deleva

Institute of Electronics, 72 Tsarigradsko Chaussee Blvd., 1784 Sofia, Bulgaria, e-mail:
adeleva@ie.bas.bg

Abstract. Aerosols and clouds are of central importance for global climate, atmospheric chemistry and physics, ecosystems and public health. In order to better understand effects on the environment, knowledge of their vertical structure, including parameters such as the thickness, location, top and bottom height, is necessary. In this work we present several examples of lidar monitoring of clouds and aerosols layers which are chosen from the measurements performed in the period 2006-2012. The investigations are carried out with an aerosol lidar, equipped with Nd:YAG laser at wavelengths 532 nm and 1064 nm. Lidar is located in the Institute of Electronics of Bulgarian Academy of Sciences. Experimental data are presented in terms of vertical backscatter coefficient profiles and color maps of the atmospheric field stratification evolution. The results of our atmospheric studies have demonstrated that clouds could be formed with widely differing thicknesses (in the interval 0.5–5 km) and could exist at various heights (2-16 km) in the troposphere up to the tropopause. Some experiments illustrate simultaneously detection of clouds and Saharan dust layers. Also, here we include results of lidar detection of anthropogenic aerosol load over Sofia city. We employed HYSPLIT (HYbrid Single-Particle Lagrangian Integrated Trajectory) backward trajectories and DREAM (Dust REGIONal Atmospheric Model) forecasts to make conclusions about atmospheric aerosol's origin. Depicted measurements are extracted from regular lidar investigations of the atmosphere within the framework of the European Aerosol Research Lidar Network (EARLINET).

Key words: lidar, aerosols, clouds, Saharan dust, troposphere.

Introduction

The atmosphere is a complex system with many components interacting through a large number of processes on a wide range of scales. Aerosols and clouds participate in determining the Earth's radiative budget, climate and weather (J.E. Penner et al., 2001; Guibert, S. et al., 2005; Solomon, S. et al., 2007). The changes in the energy fluxes of solar radiation (maximum intensity in the visible spectral region) and terrestrial radiation

(maximum intensity in the infrared spectral region) in the atmosphere induced by changes of atmospheric compositions and/or surface properties are referred to as “radiative/climate forcing”.

Aerosols are liquid or solid particles suspended in the air. They come from a variety of natural and human processes. On a global basis, the bulk of aerosols originate from natural sources, mainly sea salt, dust, volcanoes and wildfires. Desert dust particles represent a large fraction (of the order of 30-50%) (Gian Paolo Gobbi et al., 2000) of the naturally occurring tropospheric aerosols and the scientific community has made great efforts to document and understand the interactions of mineral aerosols (dust) with environment. The Saharan desert is the largest source of dust and produces more aeolian mineral particles than any other world desert (Prospero M. Joseph, 1999; Vukmirović Z.M. et al., 2004; Perez L. et al., 2008). At present the quantity of anthropogenic emissions in the atmosphere increases because of rapid growth of the industry, transport, processes of urbanization, etc. Human-produced particles can be dominant form of aerosol in highly populated and industrialized regions, and in areas of intense agricultural burning. Urban aerosols have been identified as important species of concern due to their potential health and environmental impacts (U. Pöschl, 2005; Tasić M. et al., 2006; Atanaska Deleva et al., 2010). Key parameters for determining the impacts of aerosols to climate forcing and ecological state of the environment are their optical parameters (extinction and backscatter coefficients), as well as their spatial distribution. Aerosol effects on climate are generally classified as direct or indirect with respect to radiative forcing of the climate system. The direct aerosol impact is caused by scattering or absorbing sunlight, and absorbing and emitting some terrestrial infrared radiation. The indirect effect is provoked by the aerosol capability to act as cloud condensation nuclei. Also, aerosols alter warm, ice and mixed-phase cloud formation processes by increasing droplet number concentrations and ice particle concentrations. In this manner, aerosols influence cloud cover, cloud optical properties and lifetime (Natalie M. Mahowald, 2003). The effect of aerosols on the radiative properties of Earth's cloud cover is defined as indirect effect of aerosols, or indirect climate forcing.

Clouds are groups of tiny water droplets or ice crystals in the air and are formed by different processes. They can come in all sizes and shapes, and can form near the ground or high in the troposphere. Clouds contribute differently to short-wave and long-wave radiation depending on their type, altitude, thickness, structure, particle size, etc. On the one hand, they act like greenhouse gases, absorbing infra-red thermal radiation from the Earth and trapping the heat in the lower atmosphere. On the other hand, they reflect incoming solar radiation back into space (albedo effect), effectively cooling the planet. The information with respect to cloud vertical distribution is required because light scattering and absorption are altitude dependent, as are cloud properties (Ulrike Lohmann et al., 1995; S. Veerabuthiran, 2004; L. L. Pan et al., 2011). For example, the greenhouse effect is weak for low altitude clouds, so their albedo effect dominates. In contrast, cold high altitude clouds (Cirrus clouds) may either cool or warm the climate depending of their geometrical characteristics and location. These two opposing effects are an important difference between Cirrus clouds and other hydrometeor layers in the atmosphere. Most frequently Cirrus clouds are thin and wispy. They are presented at all latitudes and are formed in the upper levels of the troposphere at heights greater than 6 km. Cirrus clouds are composed

predominately or wholly of ice non-spherical crystals, reflecting the extreme cold, and they can take a variety of shapes and thickness. As a general rule, Cirrus clouds are thin enough to be transparent or very close to it because humidity is low at such high altitudes.

Low-altitude clouds play an important role in global climate forcing, weather, and precipitation. In particular, low clouds often have large liquid water part and are involved in interactions with anthropogenic aerosols in the planetary boundary layer. Therefore, it is a significant challenge to accurately measure their optical and geometrical properties in order to assimilate them into global climate model. Unfortunately, for satellite sensors with visible and near-infrared channels, measurement of low and optically thin clouds from space is very difficult due to their partial transparency, land surface emission, and fact that they are relatively warm. On the other hand, lidars (LIDAR-Light Detection And Ranging) are an excellent way to obtain high-resolution aerosol or cloud data to complement satellite data. They are increasingly used because the investigated atmospheric parameters could be retrieved with high spatial and temporal resolution. Lidar measurements can elucidate the aerosol concentration, optical depth, cloud position and thickness which are important for a better understanding of the Earth-radiation budget and climate. The largest active aerosol research project in Europe EARLINET (European Aerosol Research Lidar Network) can provide an important contribution in the aerosol study. It is founded as a coordinated network of lidar stations that uses advanced methods for vertical profiling of the atmosphere. EARLINET was the first very important step in our continent to unite the lidar groups with the main goal of establishing a quantitative comprehensive statistical data base of both horizontal and vertical aerosol distribution on a continental scale. Additional more specific measurements (on Saharan dust, volcanic ash, forest fire) are also included in the project work program (Papayannis A. et al., 2008). Bulgarian lidar station at Sofia was involved in systematic investigations on a regular base of three measurements per week according to the schedule of the EARLINET project (EARLINET:<http://www.earlinet.org>).

In this work, we present results of laser remote detection of aerosol layers and clouds in the troposphere over Sofia. Some experimental examples illustrate observations of clouds during Saharan dust transport. We should emphasize that the results reported here not only illustrate the exceptional opportunities offered by lidars concerning sounding of the atmosphere, but also the good technical capabilities of our lidar system, which permits us to observe the whole troposphere with high spatial and temporal resolution.

Technical equipment and data processing

The results presented here are based on measurements with an elastic backscatter Nd:YAG lidar. It is described in details elsewhere (Atanaska D. Deleva et al., 2008; A. Deleva et al., 2010), and for that reason only brief description of its set-up is given below. Lidar system is configured in a mono-static biaxial alignment pointing at angle 32° with respect to the horizon, as determined by its disposition in the lab. Therefore despite signals from as far as 30 km distance are recorded the maximum sounding height is limited to 16.4 km above ground level. A solid-state Q-switched frequency-doubled Nd:YAG laser (pulse energy: up to 600 mJ at 1064 nm, 80 mJ at 532 nm; pulse duration 15 ns FWHM, laser-beam divergence 3 mrad, fixed repetition rate 2 Hz) is utilized as a light source. Laser

radiation backscattered by the atmosphere is received by a Cassegrain telescope (aperture: 35 cm; focal distance: 200 cm). The output beam from the telescope is passed to the spectrum analyzer for separation of the incoming optical signals. Data acquisition system includes hardware and software components. The hardware have been designed as an integrated photo-receiver modules consisting of photo-receiving sensor, controlled photo-receiver power supply, amplifier, 14-bit analog-to-digital converter (ADC), and USB-interface for computer connection. The data acquisition software contains two main programs. The first one is designed for real-time control of the lidar system during measurements. Received signals are digitized every 100 ns with an ADC, resulting in a 15 m range resolution (about 7.5 m altitude resolution). Thus, the lidar measures the temporal evolution of atmospheric aerosol backscatter with high time and range resolution. The second main program is a package providing the calculation of the atmospheric backscatter coefficient and determination of the error in the estimates. The well known Klett-Fernald-Sasano inversion algorithm is used in these retrievals (J. D. Klet, 1981; F. G. Fernald, 1984; Ya Sasano et al., 1985). The Nd:YAG lidar entered on operation in the beginning of 2006, equipped with only one spectral channel at wavelength 532 nm. At that time the lidar was included in the EARLINET network and we started to perform regular lidar measurements with accord to the project schedule. In 2008 was put into operation the second spectral channel for registration of lidar signals with wavelength 1064 nm and thus we were able to perform atmospheric monitoring with the first and second harmonic of the laser radiation. The decision to use one or two laser wavelengths depends on the working condition of the system and the weather. The daily investigations in sunny weather are performed with the first harmonic (1064 nm) most often because the background of the received signal is lower and there is no risk of saturation of the photo-receiver. Thus, presented here backscatter coefficient profiles from 2006 till now are obtained by single- or double wavelength monitoring of the atmosphere.

Lidar observations and comments

Lidar measurements described below are obtained within the frame of the EARLINET. A large database is created accumulating the aerosol backscatter profiles until now. The calculated data are uploaded on the common EARLINET-server in Germany. During EARLINET project, DREAM (Dust Regional Atmospheric Model) is used to make conclusions about the type and the origin of the aerosol layers, observed by the lidar (DREAM:<http://www.bsc.es/projects/earthscience/DREAM>). DREAM-weather forecast maps elaborated by Barcelona Supercomputing Center (BSC) give an image of the wind direction and speed, position of clouds and magnitude of dust load in the atmosphere above North Africa and Europe. In this paper, the location of Bulgaria on the DREAM-maps is indicated by a black circle. HYSPLIT (HYbrid Single-Particle Lagrangian Integrated Trajectory) model provides additional information about the origin of the detected aerosol layers (Draxler R. et al., 2003; Rolph G., 2011). It represents a complete system for computing simple air parcel trajectories to complex dispersion and deposition simulations. The calculations of backward air mass trajectories give a plot of the road that the air mass

traversed for a chosen time period before to arrive to the location of lidar observations. Both DREAM and HYSPLIT models are freely available on the Web.

We analyze the results of the lidar atmospheric sounding calculating vertical backscatter coefficient profiles and compiling time evolution maps of these profiles or maps of the range-corrected measurement signals (RCS). Since the magnitude of the atmospheric backscatter coefficient value is proportional to the aerosol density, the changes of the calculated profiles in time and space illustrate the temporal evolution and the stratification of the aerosol fields or clouds over the lidar station. RCS is produced by subtracting the estimated background noise from the raw lidar signal and multiplying by the square of the distance to the backscattering atmospheric sample. We present here the results mainly in terms of vertical atmospheric backscatter profiles (x-axis represents the value of the calculated atmospheric backscatter coefficient; y-axis – the altitude above sea level, ASL). The measurement date and laser sounding wavelength are written over the lidar profile plot. Also, in this work we conventionally call the clouds observed “low” and „high” depending on their location in the troposphere. The first group comprises clouds situated roughly up to 6 km, the second one - clouds above 6 km.

Figure 1 shows the results of simultaneous lidar observations of the Saharan dust load and low clouds. This is expected because aerosol particles can act as cloud condensation nuclei that form clouds (Sassen, K. et al., 2003). The measurements are performed on 31 March 2009 and 3 October 2012. Experimental examples described below illustrate Saharan dust transport over Sofia in early spring and in the beginning of the autumn. Saharan dust outbreaks over the eastern Mediterranean, including the Balkans, occur predominantly during spring and early summer, but autumn can also be considered a period with Saharan incursions. As a partner of EARLINET we participate in the Saharan-dust-transport network activities (A. Deleva, 2010).

The measurement on 31 March 2009 was performed in the morning (7:51-9:47 UTC, universal time coordinate). For this day DREAM-model (Fig.1 c) forecasted strong Saharan dust load over Mediterranean Sea and Central Europe, including Bulgaria. The lidar profile (Fig.1 a) outlines the registered cloud with center of mass at 5.8 km (cloud’s base and top 5.5 km and 6.5 km, respectively) and the aerosol layer just below it in the range 3.5-5.5 km with center of mass at about 4.5 km. Besides that it is visible that the atmosphere was aerosol loaded also below 3.5 km as below that altitude the concentration of particles gradually increases. For the period of the measurement we found HYSPLIT backward trajectories (for 100 hrs duration) in the altitude range 1.5-6 km, which pass over Northern Africa/Sahara desert and across the highly-dusted space over Mediterranean Sea before the end point above Sofia. This is a reason to suppose that the air masses in the range 1.5-6 km were transported desert aerosols from Africa. As before mentioned, HYSPLIT backward trajectories show how the air masses had moved for chosen period of time (here 100 hours) before they arrive over the lidar station on particular altitude (here the range 1.5-6 km). In Fig.1b we include three of the calculated air mass trajectories, two of which (4.5 km and 5.8 km) coincide with the abovementioned mass centers of the detected layer and cloud. The third trajectory (2 km) is in the range 2-3.5 km, where we most often register Saharan dust layers above PBL (planetary boundary layer). The high-altitude trajectory originated from above the Atlantic Ocean, passed over Sahara and, as seen in Fig.1b, has kept the direction of their motion semi-constant until reaching Sofia. Probably, these

quickly moving air streams brought humidity from above the Atlantic, which we observed as a cloud. The lower trajectories display that the air masses at altitudes 4.5 km and 2 km have been moving, accordingly very close above Sahara's surface and Libyan desert some days before. It is certain that they have been transporting a large amount of African desert dust. Based of the two models' forecast, we draw the conclusion that the aerosols registered by us in the range 3.5-5.5 km were of Saharan origin. Additionally the image of the trajectory on 2 km altitude supports our opinion that the air under that layer contained not only anthropogenic aerosols typical for PBL over city, but also long-distance transported particles from Africa.

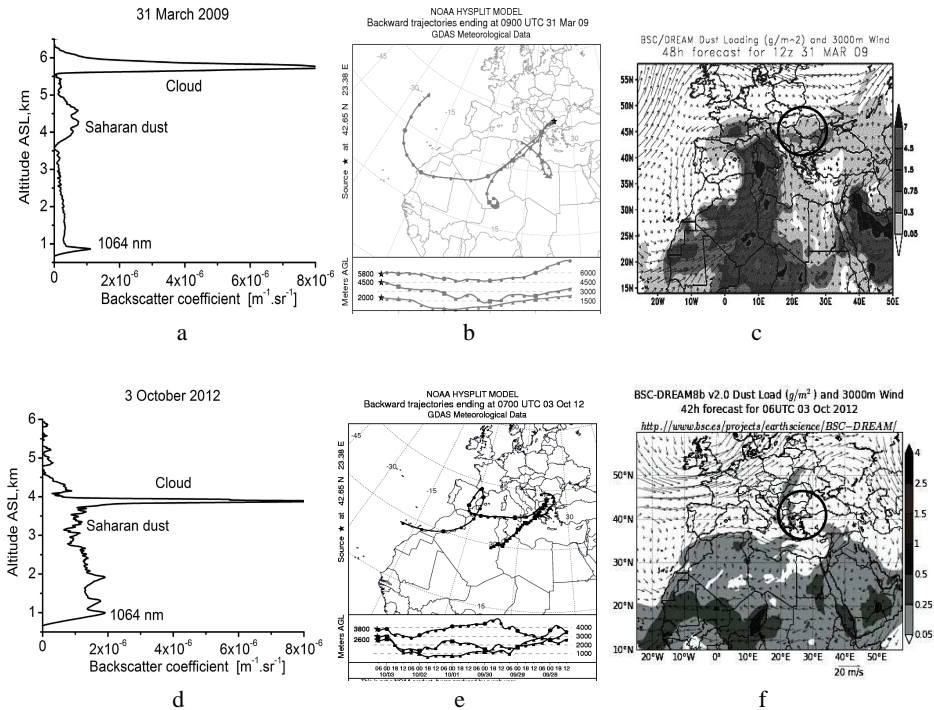
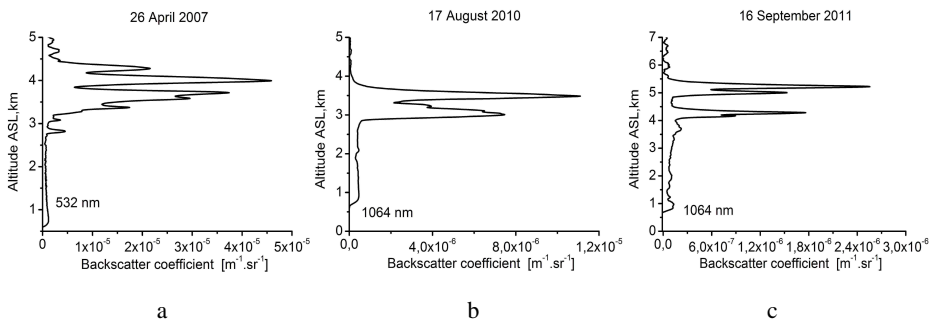


Fig.1. Lidar observations of Saharan dust and clouds: a), d) – retrieved atmospheric backscatter coefficient profiles; b), e) – HYSPLIT model backward trajectories and c), f) – DREAM forecast maps showing Saharan dust transport over Bulgaria (Sofia) on 31 March 2009 and 3 October 2012.

On 3 October 2012 we also registered low cloud during Saharan dust incursion (Fig.1 d, e, and f). The investigation started at 7:37 UTC and ended at 8:52 UTC. We registered a thin cloud with a mass center at about 3.8 km and an aerosol load over Sofia reaching 4.5 km (Fig.1. d). It is interesting to comment on the DREAM-model forecast for the time of the measurement (Fig.1 f). According to this forecast, a narrow plume of Saharan dust would be raised, be directed towards Europe and reach the northern parts of the continent. The dust should spread over Bulgaria's western parts, where Sofia is located. For the period of the measurement we calculate HYSPLIT air mass backward trajectories (for 140 hrs duration) in the altitude range 1.5-5 km. We should note in advance here that the analysis of the corresponding HYSPLIT maps revealed that the movement of the air

flows in the range 3-5 km and of those in the lower atmosphere up to 2.7 km differ substantially. The difference is in the fact that the air masses in the shown higher range have moved over Sahara, as the ones in the lower parts of the atmosphere the air flows were kept and moved in closer to Bulgaria regions. Besides that in accordance with the DREAM forecast the atmosphere over the most part of these regions was not loaded with Saharan dust. The described till now is illustrated with the HYSPLIT map in Fig.1e where we include three backward trajectories, which are located at altitude 2.6 km, 3 km and 3.8 km. The black-and-white image makes hard distinguishing the trajectories in altitude, so we will clarify it in more detail. The trajectory which starts over the Atlantic ocean and moves over Sahara shows the movement of the air masses which during the investigation were over the lidar station on height 3.8 km. They transported humidity and desert dust which most probably have participated in the creation of the registered cloud over the lidar station. The movement of the which during the investigation are on 3 km over Sofia is shown with the trajectory which starts from Sahara. On the lower part of HYSPLIT-map is visible that these air flows were moving close over the Sahara and Mediterranean surface. That led us to the conclusion that the upper part (3-4.5 km) of the observed aerosol layer contains substantial amount of Saharan dust. Totally opposite is our conclusion for the origin of the aerosols in the atmosphere up to 2.7 km altitude. As before mentioned the analysis of the HYSPLIT trajectories showed that the lower air flows were moving close to or directly above Earth surface in regions close to Bulgaria (HYSPLIT map shows the trajectory at 2.6 km). That's why above all the low air streams were carrying anthropogenic aerosols and ones emitted by the Earth surface. The described up to now we can summarize as follows. On 3 October 2006 we have registered an aerosol load of the atmosphere above Sofia which extended up to 4.5 km height. In the region 3-4.5 km the aerosols had Saharan origin while at lower levels prevailed anthropogenic and ground-emitted aerosols. The measurement described here is interesting because we have registered Saharan dust event in the autumn, which is possible, but rare. However that incursion could be expected because the weather in the beginning of October 2012 was unusually warm for the season (at places with temperatures above 30°C). The reason for those summer temperatures was the penetration of hot air masses from Africa in Europe. On the basis of the lidar results we could conclude that the air currents from South have transported considerable amount of aerosols from the Sahara desert.

On Fig.2.(a-c) we show some more examples of lidar observation of low clouds, situated on different height and with different stratification.



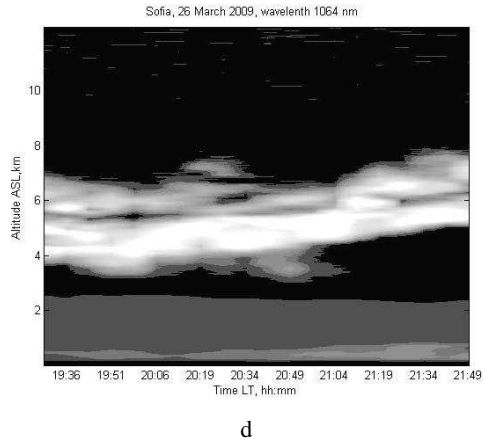


Fig.2. Lidar observations of low clouds: a), b), c) - retrieved atmospheric backscatter coefficient profiles; d) - RCS-color map of the spatial distribution of cloud field over Sofia on 26 March 2009.

Figure 3 presents the results of several measurements of Cirrus clouds, located above 6 km.

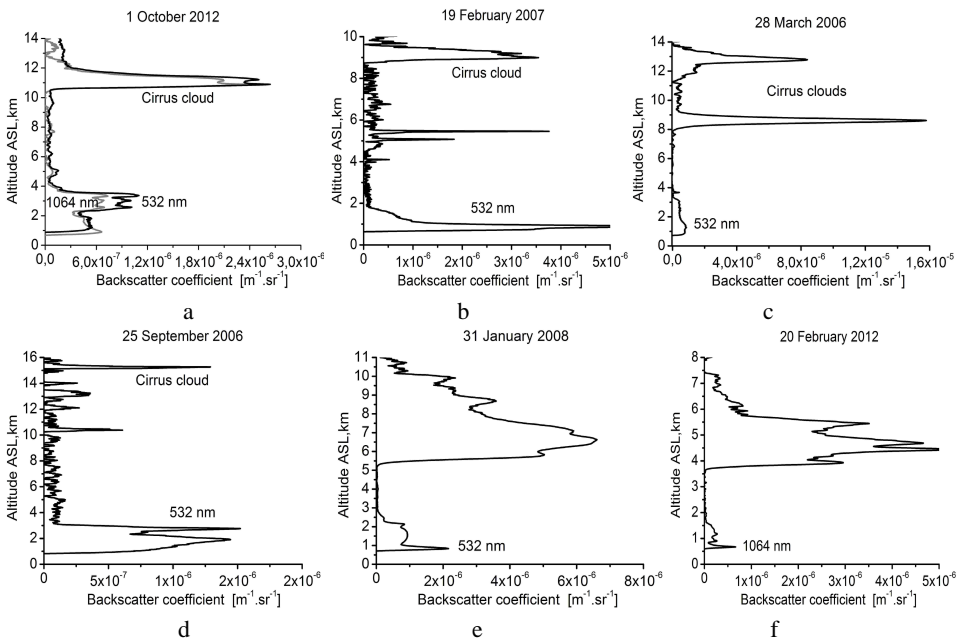


Fig.3. Lidar observations of high altitude Cirrus clouds.

We conventionally call the Cirrus clouds lidar detected “thin, typical and thick” depending on their geometric thickness (the difference between the cloud’s top and base). The first group comprises high clouds with thickness up to 0.5 km, the second, with thickness 1-2 km, and the third, more than 3 km. Following our proper data set of Cirrus

cloud observations from 2006 till now, we could make a rough estimate concerning registration frequency of different types of high altitude clouds, as follows. In most of the lidar observations we have observed typical Cirrus clouds with thickness 1-2 km situated within the range of heights 9-13 km (Fig.3 a, b). We registered thin clouds at various heights (Fig.3 b, c, d) very rarely. Thick clouds (Fig.3 e, f) exist in the atmosphere predominantly in the cold winter months. The base and top of the Cirrus clouds observed cover a large altitude range (5-16 km) in the upper troposphere.

Figure.4 illustrates simultaneous lidar observations of clouds situated in the large altitude range (4-13 km). The measurement was performed over the lidar station on 6 April 2009.

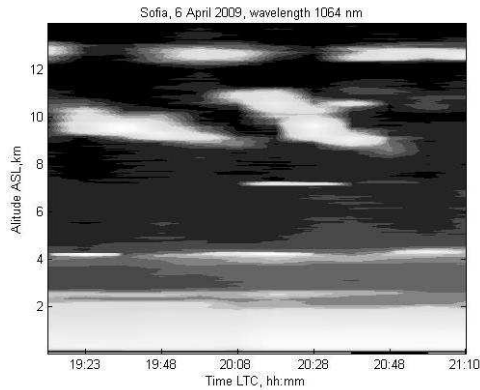


Fig.4. RCS-map of the cloud field stratification measured on 6 April 2009.

In Fig.5 we present the results of several lidar measurements performed on no-Saharan-dust-affected days. The retrieved lidar profiles from the observations carried out on 6 July 2006, 23 June 2011, and 16 September 2011 display we detected aerosol layers extended to 3.5 km and 5.5 km heights.

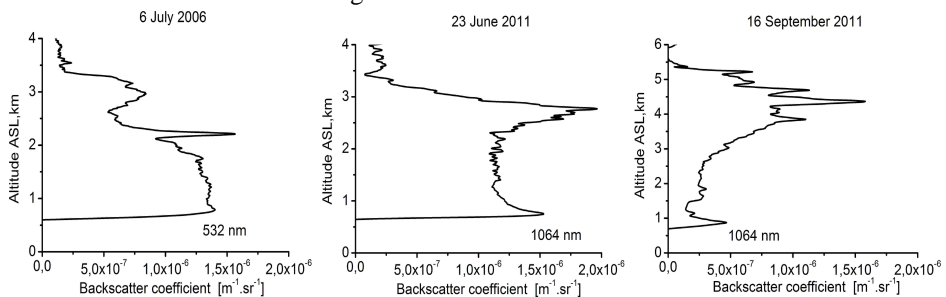


Fig.5. Retrieved atmospheric backscatter coefficient profiles showing considerable aerosol loading over Sofia on no-Saharan dust affected days.

DREAM forecasts (Fig.6) for the days of lidar monitoring show an atmosphere free of desert dust over Balkans.

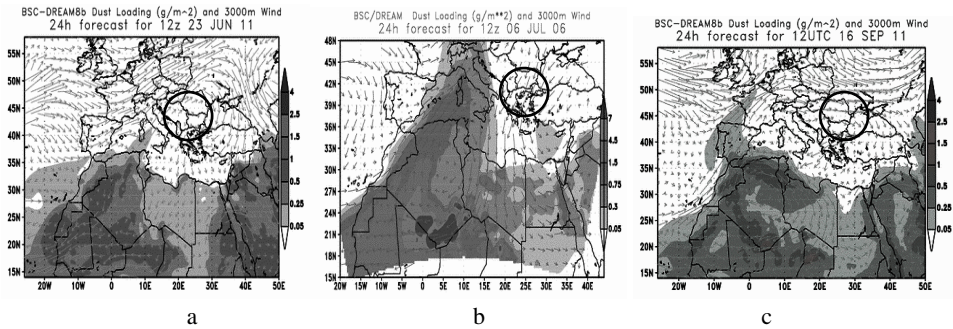


Fig.6. Forecast maps of Saharan dust load in the atmosphere, provided by Barcelona Supercomputer Center (BSC) for the days of lidar measurements: a). 6 July 6 2006; b). 23 June 2011; c). 16 September 2011.

The HYSPLIT trajectories (Fig.7) for the particulate measurements are calculated for 40 hrs duration. Their heights are chosen according to the lidar profile delineations.

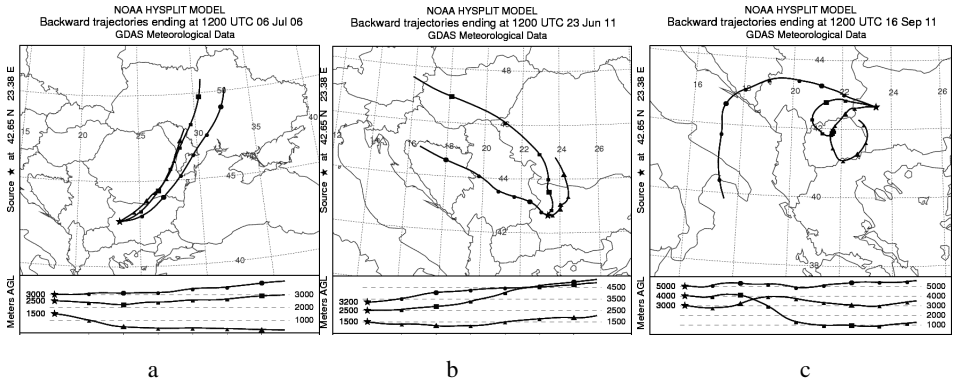


Fig.7. Backward air mass trajectories, calculated using HYSPLIT model: a). 6 July 6 2006; b). 23 June 2011; c). 16 September 2011. They show the origin and the way of air mass three days before arrival over the lidar site.

HYSPLIT trajectories reveal that shortly before its arrival above Sofia, the air masses on altitude 1.5 km (Fig.7 a, b) and 4 km (Fig.7 c) were moving just above the ground of the continental regions close to Bulgaria. Thus they were transporting considerable amounts of continental and anthropogenic aerosols, which are characteristic for the low troposphere above more densely populated regions. It's worth notice the trajectory on 5 km, calculated on 16 September 2011 (Fig.7 c). Its beginning is somewhere above the Mediterranean and moves almost horizontally to its end above Sofia. That gives a reason to conclude that the air in the higher part of the registered layer (3-5 km) where we registered strong backscattered signals was with higher humidity and contained small watered aerosol particles. All other trajectories calculated for the three measurement days have beginning over the continent and HYSPLIT backward trajectories show that the air masses at their heights pass over continental regions where atmosphere was not loaded with Saharan dust. Therefore we conclude that in the days of the described measurements the air

above Sofia up to height of 3.5 km and 5 km contained substantial amount of anthropogenic aerosol.

Conclusions

The results presented in this paper are derived from a long term remote sensing monitoring of the atmosphere above Sofia performed with Nd:YAG lidar. The experimental examples described here emphasize on the detection of clouds and aerosol layers because aerosols, clouds and aerosol-cloud interactions are recognized as the key factors influencing the Earth's radiative budget and the ecological state of the environment. The analysis of our results from 2006 till now shows that clouds could be formed with widely differing thicknesses (in the interval 0.5–5 km) and could exist at various heights (2–16 km) in the troposphere up to the tropopause. Some experiments illustrate detection of clouds during Saharan dust transport over the lidar station. Also, here we include results of lidar observation of aerosol loading over our city up to 4–5 km heights on no-Saharan dust affected days. As neither other source of aerosols, nor dust transport from Sahara over the Balkans was forecasted for the days of lidar investigations, our conclusion was that the anthropogenic aerosols of human activities and traffic in town caused the observed aerosol stratification.

Acknowledgments. The research leading to these results has received funding from the European Union Seventh Framework Programme (FP7/2007-2013) under grant agreement n° 262254". The financial support for EARLINET by the European Commission under grant RICA-025991 is also gratefully acknowledged.

The authors gratefully acknowledge the NOAA Air Resources Laboratory (ARL) for the provision of the HYSPLIT model for air mass transport and dispersion and/or READY website used in this publication.

The authors would like also to express their gratitude to the Earth Sciences Division, Barcelona Supercomputing Center, Spain, for the provision of the DREAM model aerosol dust data used in this publication.

References

- A. Deleva, A. Slesar, and S. Denisov, 2010. Investigations of the aerosol fields and clouds in the troposphere with Raman-aerosol lidar, *Bulgarian Geophysical Journal*, 36, 26-39
- A. Deleva, 2010. Lidar monitoring of Saharan dust transport over the city of Sofia in the period 2006-2008, *Bulgarian Geophysical Journal*, 36, 18-25
- Atanaska D. Deleva, Ivan V. Grigorov, Lachesar A. Avramov, Vladimir A. Mitev, Alexander S. Slesar, and Sergey Denisov, 2008. Raman-elastic-backscatter lidar for observations of tropospheric aerosol, Proc. SPIE 7027, 70270Y-1+70270Y-8
- Atanaska Deleva, and Ivan Grigorov, 2011. Lower Troposphere Observation over Urban Area with Lidar at 1064 nm, *International Journal of Navigation and Observation*, ID 769264, 8 pages, doi:10.1155/2011/769264
- DREAM: <http://www.bsc.es/projects/earthscience/DREAM/>

- Draxler, R., and Rolph G., 2003. HYSPLIT (HYbrid Single-Particle Lagrangian Integrated Trajectory), Model access via NOAA ARL (READY) Website (<http://www.arl.noaa.gov/ready/hysplit4.html>), NOAA Air Resources Laboratory, Silver Spring, MD, (2003).
- EARLINET; <http://www.earlinet.org>
- F. G. Fernald, 1984. Analysis of atmospheric lidar observations: some comments, *Appl. Opt.*, 23, 652-653
- Gian Paolo Gobbi, Francesca Barnaba, Riccardo Giorgi, Alessandra Santacasa, 2000. Altitude-resolved properties of a Saharan dust event over the Mediterranean, *Atmospheric Environment*, 34, 5119-5127
- Guibert, S., Matthias V., and Schulz M., 2005. The vertical distribution of aerosol over Europe - synthesis of one year of EARLINET aerosol lidar measurements and aerosol transport modeling with LMDZT-INCA, *Atmospheric Environment*, 39, 2933-2943
- J. E. Penner, M. Andreae, H. Annegarn, L. Barrie, J. Feichter, D. Hegg, A. Jayaraman, R. Keaitch, D. Murphy, J. Nganga, and G. Pitari, 2001: in *Climate Change 2001: The Physical Scientific Basis, Contribution of Working Group I to the Third Assessment Report of the Intergovernmental Panel on Climate Change*, B. Nyenzi and J. Prospero, Eds., http://unfccc.int/resource/cd_roms/na1/mitigation/Resource_materials/IPCC_TAR_Climate_Change_2001_Scientific_Basis/TAR-05.pdf
- J. D. Klett, 1981. Stable analytical inversion solution for processing lidar returns, *Appl. Opt.*, 20, 211-220
- L. L. Pan, and L. A. Munchak, 2011. Relationship of cloud top to the tropopause and jet structure from CALIPSO data, *Journal of Geophysical Research*, 16, D12201, doi:10.1029/2010JD015462
- Natalie M. Mahowald, and Lisa M. Kiehl, 2003. Mineral aerosols and cloud interactions, *Geophysical Research Letters*, 30, 1475, doi:10.1029/2002GL016762
- Papayannis, A., Amiridis V., Mona L., Tsaknakis G., Balis D., Bösenberg J., Chaikovski A., De Tomasi F., Grigorov I., Mattis I., Mitev V., Müller D., Nickovic S., Pérez C., Pietruczuk A., Pisani G., Ravetta F., Rizi V., Sicard M., Trickl T., Wiegner M., Gerding M., Mamouri R.E., D'Amico G., and Pappalardo G., 2008. Systematic lidar observations of Saharan dust over Europe in the frame of EARLINET (2000-2002), *Journal of Geophysical Research D: Atmospheres*, 113 (10), art. no. D10204.
- Perez L., Tobias A., Querol X., Pey J., Künzli N., Pey J., Alastuey A., Viana M., Valero N., González-Cabré M., and Sunyer J., 2008. Coalescence particles from Saharan dust and daily mortality, *Epidemiology*, 96, 800-807
- Prospero M. Joseph, 1999. Long-range transport of mineral dust in the global atmosphere: Impact of African dust on the environment of the southeastern United States. <http://www.pnas.org/content/96/7/3396.full?ck=nck>
- Sassen, K., DeMott, P., Joseph J. Prospero, J., J., et al., 2003. Saharan dust storms and indirect aerosol effects on clouds: CRYSTAL-FACE results, *Geophysical Research Letters*, 30 (12), 1633, doi:10.1029/2003GL017371
- Solomon, S., D. Qin, M. Manning, Z. Chen, M. Marquis, K.B. Averyt, M. Tignor, and H.L. Miller (eds.), 2007: in *Climate Change 2007: The Physical Science Basis, Contribution of Working Group I to the Fourth Assessment Report of the Intergovernmental Panel on Climate Change*, Cambridge Univ. Press (http://www.ipcc.ch/publications_and_data/ar4/wg1/en/contents.html), New York
- Quicklooks of Sofia lidar station: <http://www.ie-bas.dir.bg/Departments/LidarData/Quicklooks.htm>
- Rolph, G. D., 2011. Real-time Environmental Applications and Display sYstem (READY) Website (<http://ready.arl.noaa.gov>). NOAA Air Resources Laboratory, Silver Spring, MD.
- S. Veerabuthiran, 2004. High-altitude cirrus clouds and climate, *Resonance*, 9, no. 3, pp. 23-32, 2004

- Tasić M., Rajšić S., and Mijić Z., 2006. Atmospheric aerosols and their influence on air quality in urban areas, *Facta Universitatis*, **4**, 83-90
- U. Pöschl, 2005. Atmospheric Aerosols: Composition, Transformation, Climate and Health Effects, *Atmospheric chemistry*, **44**, 7522-7540
- Ulrike Lohmann, and Erich Roeckner, 1995. Influence of cirrus cloud radiative forcing on climate and climate sensitivity in a general circulation model, *Journal of Geophysical Research*, **100**, 16305-16323
- Vukmirović Z. M., Unkašević L. Lazić, Tošić I, Rajšić S., and Tašić M., 2004. Analysis of the Saharan dust regional transport. *Meteorol Atmos. Phys.* **85**, 265-273
- Ya Sasano, E. Browell, and S. Ismail, 1985. Error caused by using constant extinction/backscattering ratio in the lidar solution, *Appl. Opt.*, **24**, 3929-3932

Лидарен мониторинг на облаци и аерозолни слоеве

А. Делева

Резюме. Аерозолите и облациите силно влияят върху глобалния климат и екологичното състояние на околната среда. Това зависи преди всичко от локализацията им, от техните геометрични (дебелина) и оптични (разсейване, поглъщане) параметри. В тази работа описваме резултати от лазерен дистанционен мониторинг на облаци и аерозолни слоеве над София, които са част от базата-данни от систематични изследвания на атмосферата, извършени от 2006 до 2012г.. Изследванията са направени с Nd:YAG-аерозолен лидар с дължини на вълната 532 nm и 1064 nm. Лидарът е разположен в лаборатория „Лазерна локация” на Института по електроника, Балгарската Академия на Науките. Тук експерименталните данни са представени като изчислени вертикални профили на коефициента на обратно разсейване и цветни карти на височинно-времевата еволюция на регистрираните аерозолни полета в атмосферата. Резултатите от нашите лидарни наблюдения показват, че облациите могат да имат силно различаващи се дебелини (в интервала 0.5–5 km) и могат да съществуват на различни височини (2–16 km) в тропосферата чак до тропопаузата. Някои от примерите илюстрират едновременна регистрация на облаци и аерозолни слоеве, съдържащи прах от пустинята Сахара. Също така в тази работа сме включили резултати от лидарен мониторинг на антропогенни аерозоли във въздуха над София. При анализа на експерименталните данни ние сме използвали прогнозите на HYSPLIT (HYbrid Single-Particle Lagrangian Integrated Trajectory) и DREAM (Dust REGIONAL Atmospheric Model) моделите за дните на измерванията, за да направим изводи за произхода на регистрираните аерозоли във въздуха. Описаните измервания са част от регулярните изследвания на атмосферата, които се извършват с Nd:YAG-лидара в изпълнение на работната програма на европейския аерозолен изследователски проект EARLINET.

DATA AND ANALYSIS OF THE EVENTS RECORDED BY NOTSSI IN 2011

E.Botev, V.Protopopova, I.Popova, B.Babachkova, S.Velichkova, I.Tzoncheva, S.Dimitrova, V.Boychev, D.Lazarov, P.Raykova

Geophysical Institute, BAS, Akad. G. Bonchev street, bl.3, Sofia, Bulgaria, e-mail: ebotev@geophys.bas.bg

Abstract. A map of epicentres of 1836 earthquakes that occurred during 2011 in the Balkan Peninsula (sector outlined by latitude $\varphi = 37^{\circ} - 47^{\circ}\text{N}$ and longitude $\lambda = 19^{\circ} - 30^{\circ}\text{E}$) is presented. Expert generalized analysis of the seismicity over the territory of Bulgaria and its very adjacent lands (with more than 1200 localized events) is proposed. Catalog of earthquakes with magnitude $M > 2.5$ is applied.

Key words: Balkan Peninsula, Bulgaria, seismicity

The present scientific communication contains generalized information on the results of collection, processing and analysis of the data about the seismic events recorded by the National Operative Telemetric System for Seismological Information (NOTSSI) in 2011. The expanded information about the realized seismicity is suggested as a natural generalization and supplementation of the monthly compilations of the preliminary seismological bulletin of NOTSSI. The analysis and evaluation of the space, time and energy distribution of the seismicity, periodically been made, open up possibilities for searching for time correlations with the parameters of different geophysical fields aiming to find out eventual precursor anomalies.

The recording and space localization of the seismic events in NOTSSI during 2011 is realized by means of the new digital network (Solakov et al., 2005). The routine processing and acquisition of the initial data is organized in a real time duty regime. The operations are fulfilled by the authors of this communication. In such a way the main goal of NOTSSI, namely the seismicity monitoring in order to help the authorities' and social reaction in case of earthquakes felt on the territory of the country, is realized. The computing procedure for determining the parameters of the seismic events is an adaptation of the widespread product HYPO71 (Solakov, 1993). The energy parameters of the events are presented mainly by the magnitude M calculated according to the record's duration by the formula (Christoskov and Samardjieva, 1983)

$$M = 1.92 + 2.72\log\tau - 0.026\Delta$$

The focal mechanism parameters are obtained by means of a program FOCMEC (Snoke,2009). The high sensitivity of the seismographs allows recording and processing of a great number of long distance earthquakes. As a result of the achieved experience in the authors interpretation work, different magnitude's lower threshold for successful determination of local, regional and long distance earthquakes is established: $M=1.5$ for the territory of Bulgaria, $M=3.0$ for the central part of the Balkans, $M=5.0$ for long distance events. The precision of the epicenter's determination is different; except on the distance it depends also on the specific position of the epicenter in relation to the recording network. The parameters of seismic events occurring at a distance more than 100-150 km outside the territory of Bulgaria should be accepted only informatively and cannot be used for responsible seismotectonic investigation.

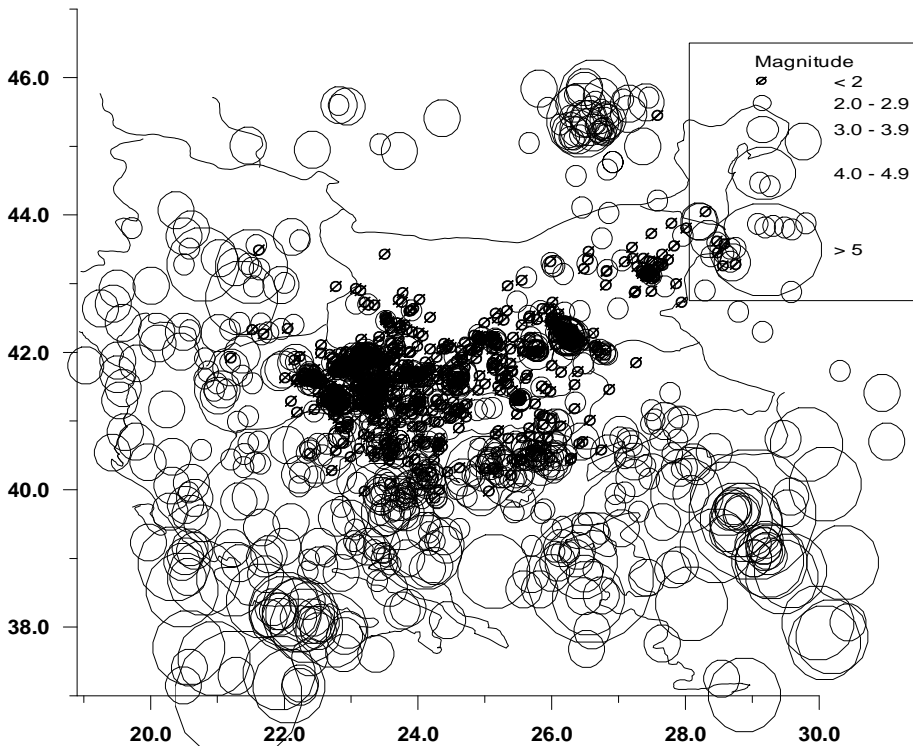


Fig.1. Map of epicenters in Central Balkans during 2011.

For the period of observations presented in this communication, the primary data about 2000 local, regional, distant earthquakes and industrial explosions on the territory of Bulgaria are recorded, classified and processed (as a work bulletin) in NOTSSI. After comprehensive analysis of the records and application of the above mentioned calculation procedures it is established that 1836 of all registered earthquakes are in the Balkan Peninsula region outlined by geographic latitude $37^{\circ} - 47^{\circ}$ N and longitude $19^{\circ} - 30^{\circ}$ E. The

epicenters of the earthquakes differentiated by magnitude levels are plotted on Fig.1. The number of the events in the magnitude interval $M=0.5-1.9$ is 993, in $M=2-2.9$ - 549, in $M=3-3.9$ - 238, in $M=4-4.9$ - 46 earthquakes. During this not so active period there are 3 events with magnitude $M>5$. The maximum magnitude value is $M=5.8$.

As a whole, the seismic situation in the study part of the Balkans during 2011 is characterized by comparatively high activity - 1829 events against 2401 in 2010, 2744 in 2009, 1775 in 2008, and around 1100- 1400 for most of the previous years. The maximum realized earthquake is with magnitude $M=5.8$ while this value for the previous years is lower than five, as a rule. It can be noted that the observed tendency of high increase of the activity compared with the former years is partly due to the high level of earthquake activation in Marmara sea, Central Greece, Serbia, Romania, and also due to increase of number of microearthquakes in the territory of Bulgaria.

The strongest event outside Bulgaria during the study period occurred in the region situated to the south of Marmara sea (Turkey) ($M=5.8$ and intensity $I=III-IV$ of MSC scale in Kurdzhali region). Other shakable effect because of outside attack during the study period occurred around of Lesvos island - eastern edge of central part of Aegean sea (magnitude $M=5.5$ and intensity $I=II-III$ in Kardzhali).

As a whole, events with $M<3.0$ which occur outside Bulgaria are difficult to be localized by the national seismological system; consequently, not all of them have been marked on the scheme in Fig.1.

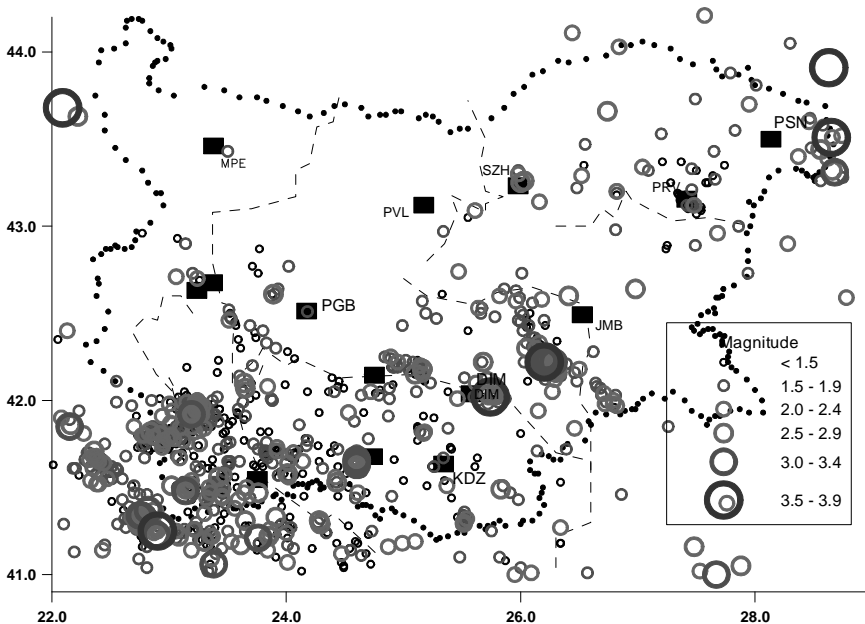


Fig.2. Map of epicenters in Bulgaria and adjacent lands during 2011

Fig.2 illustrates the seismicity just in the territory of Bulgaria and nearby lands ($\varphi = 41^{\circ} - 44.5^{\circ}N$, $\lambda = 22^{\circ} - 29^{\circ}E$). The earthquakes are differentiated by magnitude intervals. The seismic stations are also noted in the same figure by rectangular. The parameters of

relatively stronger earthquakes are presented in Table 1.

Table 1. List of earthquakes with $M \geq 2.5$ in Bulgaria and adjacent lands during 2011

Date			Time	Coordinates		H,km	M
2011	1	3	20:43	41.19	23.3	3	2.6
2011	1	5	17:14	42.07	23.65	8	2.6
2011	1	6	17:16	41.35	22.72	15	2.5
2011	1	8	11:20	42.22	26.28	8	3.1
2011	1	14	03:31	42.25	26.23	6	2.5
2011	1	14	15:49	42.18	25.16	4	2.8
2011	1	20	19:05	41.71	22.36	7	2.5
2011	1	24	12:14	42.15	25.1	2	2.8
2011	1	28	16:30	42.3	26.05	5	2.5
2011	2	2	20:00	41.51	23.02	8	2.5
2011	2	7	22:25	41.56	23.42	10	2.5
2011	2	7	18:00	41.49	23.14	3	2.8
2011	2	7	16:22	41.51	23.17	2	2.9
2011	2	7	10:39	41.48	23.14	2	3.2
2011	2	27	34:32	42.61	23.89	10	2.5
2011	2	28	18:28	42.18	25.16	3	2.9
2011	3	13	18:02	41.36	22.87	1	2.6
2011	3	15	18:00	42.24	26.2	7	3.2
2011	3	18	06:27	41.06	23.38	1	3.1
2011	3	27	10:27	41.22	23.85	12	2.6
2011	3	28	17:21	42.21	26.3	5	2.6
2011	3	28	18:04	42.24	26.2	7	3.2
2011	3	29	09:46	42.03	25.78	2	2.5
2011	3	29	17:03	42.17	26.29	7	2.5
2011	3	29	02:55	41.86	22.16	4	2.8
2011	3	29	02:56	41.85	22.15	2	3.1
2011	3	29	07:29	42.02	25.74	10	3.7
2011	3	30	11:22	42.18	26.28	6	2.8
2011	3	31	05:25	41.22	23.08	2	2.7
2011	4	1	19:44	42.21	26.23	6	2.8
2011	4	2	00:07	43.26	26.03	3	2.5
2011	4	14	03:40	41.58	24.01	15	2.5
2011	4	18	14:18	41.25	22.9	2	3.5
2011	4	22	21:33	43.32	28.66	26	2.9
2011	4	22	21:27	43.31	28.68	25	3.1
2011	5	1	08:36	41.16	27.48	15	2.8
2011	5	4	18:40	43.63	22.22	8	2.7
2011	5	5	01:07	41.21	23.76	2	3.4
2011	5	7	19:14	43.25	26	2	2.6
2011	5	22	22:39	41.05	27.88	5	2.5
2011	6	6	12:01	42.22	26.24	8	2.6
2011	6	6	22:52	42.22	26.24	5	3.2
2011	6	24	17:32	42.24	26.23	3	2.6

2011	6	24	17:47	42.19	26.27	5	2.7
2011	6	24	17:44	42.22	26.2	4	3.6
2011	7	6	13:32	42.64	26.98	10	2.5
2011	7	22	12:57	41.33	23.91	10	2.6
2011	7	22	19:16	41.91	23.2	5	2.6
2011	7	23	07:32	41.92	23.19	1	3
2011	7	26	03:71	43.66	26.74	5	2.5
2011	7	31	17:37	41.49	25.83	5	2.8
2011	8	5	02:16	42.22	26.2	9	3.4
2011	8	5	02:17	42.25	26.22	2	3.4
2011	8	7	20:26	42.1	23.64	4	2.7
2011	8	11	02:57	41.31	22.78	5	2.6
2011	8	20	20:50	41.37	22.82	2	3.3
2011	8	23	08:30	41.3	22.83	2	2.5
2011	8	24	19:59	43.91	28.63	5	3.8
2011	9	2	11:17	41.17	23.61	2	2.7
2011	9	5	13:23	43.68	22.09	10	3.6
2011	9	11	18:52	42.03	25.73	11	2.7
2011	9	15	10:25	41.91	23.17	2	2.7
2011	9	20	11:28	42.22	25.68	15	2.6
2011	10	3	11:53	41.53	24.43	11	2.5
2011	10	5	07:23	42.19	26.23	3	2.5
2011	10	6	15:08	41.34	22.76	2	3.1
2011	10	6	15:55	41.34	22.75	1	3.4
2011	10	7	12:33	41.32	22.77	0	2.8
2011	10	8	16:06	42.25	26.16	2	2.5
2011	10	11	19:49	43.51	28.53	18	3.8
2011	10	15	41:08	42.16	26.3	6	2.5
2011	10	20	10:28	43.44	28.56	14	2.5
2011	10	21	13:18	41.61	24.6	7	2.5
2011	10	21	05:12	41	27.67	2	3.1
2011	10	21	12:26	41.66	24.6	7	3.2
2011	10	23	18:13	41.82	22.84	11	2.5
2011	10	23	13:09	41.66	24.6	11	2.6
2011	10	30	04:48	41.64	24.63	9	2.7
2011	10	30	05:54	41.65	24.61	7	3
2011	10	30	04:47	41.63	24.6	5	3.2
2011	11	10	22:20	41.31	23.65	4	2.8
2011	11	11	18:48	41.29	22.73	7	2.5
2011	11	17	15:10	41.29	24.29	5	2.5
2011	11	19	18:58	41.31	24.28	4	2.6
2011	11	29	12:20	41.47	23.76	13	2.8
2011	12	17	06:13	42.6	26.41	11	2.5
2011	12	18	21:56	41.35	22.75	2	2.7
2011	12	26	08:10	42.26	26.21	2	2.8

On the territory of Bulgaria a very much high degree of activity of weak earthquakes is observed during 2011 - 1205 events against 1607 in 2010, 2017 in 2009,

1079 in 2008, and 600-800 for most of the previous years. The earthquakes of a magnitude higher than 3.0 are in normal amount - 25 events compared with an averaged number of about 20-30 for most of the all previous years (exception is 2009 with 147 events because of the aftershocks of Valandovo $M=5.2$ earthquake.). The maximum realized magnitude $M=3.8$ in the region of Shabla is almost normal too, in comparison with the maximum magnitude in the course of previous years. As usually, the largest concentration of epicenters is marked in the southwestern part of the territory presented in Fig.2. The Kroupnik seismic source is known with the strongest crustal earthquakes in Europe ($M=7.8, 7.1$) for the last 160 years. In 2011 about 80 events of $M<3.0$ and only 2 of $M\geq 3.0$ occurred in this region. The strongest felt earthquake for the south-western part of Bulgarian territory is with magnitude $M=3.2$, it is felt on 07 February in Petrich region (southern slopes of Belasitza mountain) by intensity of III EMS.

The Bulgarian seismic sources in 2011 are relatively not so active than during the previous years. They produced not more than 25 earthquakes affecting different localities in this country by intensity of up to IV degrees EMS. The maximum number of felt earthquakes is occurred around the Monastery uplift. About ten cases of magnitudes less than 3.0 aroused shocks of intensity three or a bit more and about 6 with $M>3$ are felt in Monastery Highland territories with intensities up to V – VI degree of MSC. The maximum event with $M=3.6$ caused V- VI of MSK on 24 June. A strong event $M=3.7$ in the neighbor region of Simeonovgrad caused effects of V degree of MSC. In the rest part of the 2011 felt events caused excitation of lesser intensity. The strongest event with magnitude $M_s=3.8$ occur in north-eastern Bulgaria on 11 October and caused macroseismic impact with intensity of V degree EMS scale in village of Shabla on the Black sea coast. One relatively big seismic activity is associated with the Smolyan fault structure in the Rhodopean Region region where three shocks during the time of ten days shook the city of Chepelare with intensity of III EMS since 21 October to 30 October.

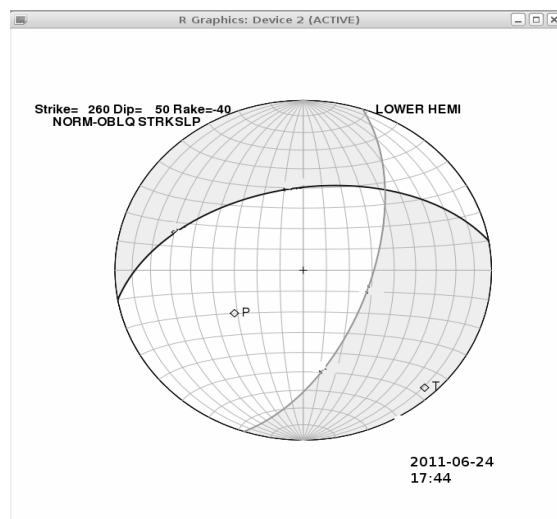


Fig.3. Focal plane solution of the strongest Monastery uplift earthquake (24.06.2011)

For the determination of the earthquake mechanism is used program FOCMEC. Input are polarities of the P wave. In the double - couple focal mechanism are included 12 first motion polarities data from seismological stations in Bulgaria and surrounding area taken from NOTSSI and ISC database (<ftp://www.orfeus-eu.org/pub/data/continuous/2011/>) - Fig.3. The solution is displayed on lower hemisphere. The polarities from ISC are not check as waveform. The polarities from seismological stations KAVA and PGB are poor and the solution is not with very good quality. The fault plane solutions of the some other events are with very bad quality because of a low number of polarities.

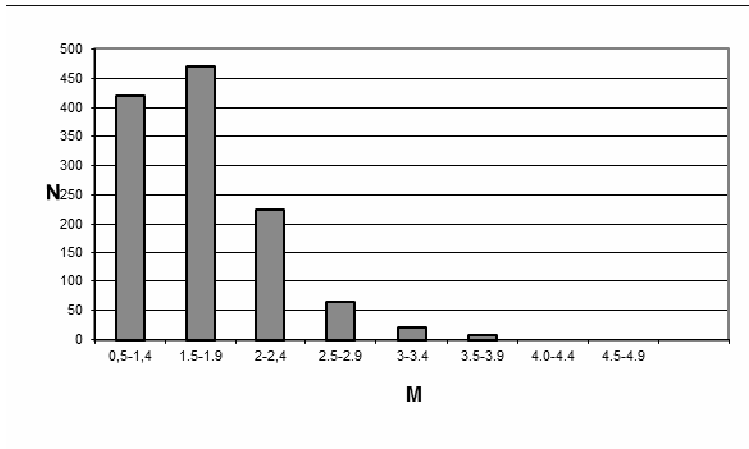


Fig.4. Magnitude - frequency distribution of the earthquakes

A detailed analysis of seismicity in the individual seismic zones is hard to be fulfilled because of the insufficient quantity of events and the narrow magnitude range of the earthquakes. The joint statistics of all the events in Fig.2 characterize predominantly the seismicity parameters of the southwestern part of the territory under investigation.

The magnitude-frequency distribution for the entire data set is presented in Fig.4. The number of localized events increases with the magnitude decreasing: for $M=3.5-3.9$ is 6 events, for $M=3.0-3.4$ is 19 events, for $M=2.5-2.9$ - 64, for $M=2.0-2.4$ - 225 and so on. The abrupt diminishing of the number of earthquakes in the first two intervals ($M < 1.5$) in Fig.4 determines also the registration power of the seismic stations network.

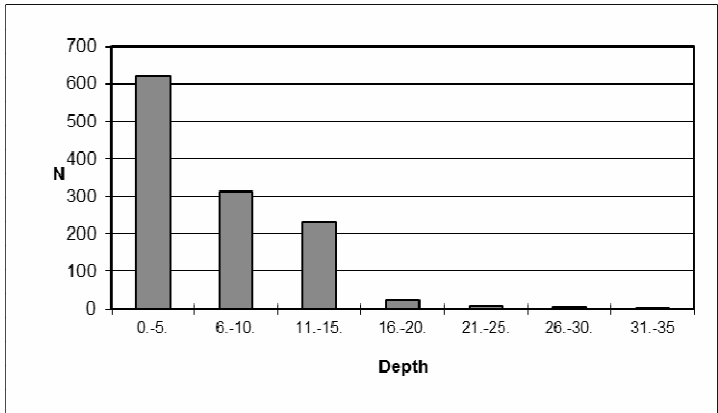


Fig.5. Depth - frequency distribution of the earthquakes

Taking the latter into account, it can be supposed that the magnitude sample for levels with $M > 1.5$ is comparatively closer to the reality for the bigger part of the Bulgarian territory.

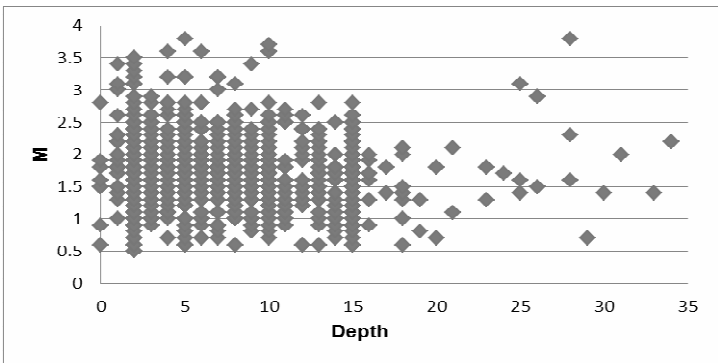


Fig.6. Magnitude - depth dependence

The picture of the depth distribution in Fig.5 shows that the majority of events occur down to 20 km depth. The number of events decreases smoothly with increase of the depth. It is possible the established predominating depth (from 0 to 5 km) to be also due to the presence of unidentified industrial explosions. In the same time the number of events in the interval 15-20 km is bigger. The magnitude distribution of the events in depth (Fig.6) do not permits to note some differentiation of depth "floors" with the increase of magnitude - the maximums can be traced out for all of the depth interval from 2 to 20 km. It is remarkable that the strongest events are not deep situated.

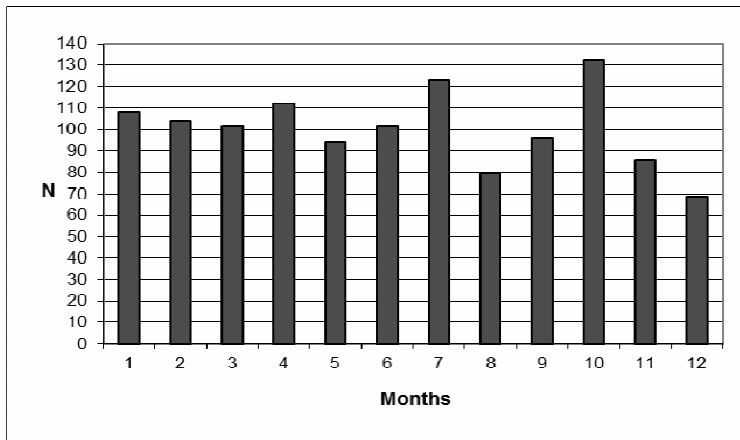


Fig.7. Time distribution of the earthquakes.

Fig.7 illustrates the distribution of seismicity in time according to the number of events per months. The biggest earthquake's amount is displayed in October, when more than 130 earthquakes occurred, approximately the similar situation in July is observed – 123 events. The lowest earthquake quantity is in August, 80 events. The energy release suggests that in October, when 132 events occurred, is the month with maximum of energy release.

Additionally, about 1100 distant earthquakes have been recorded in the period under study, as well as more than 700 industrial explosions, processed and classified in the preliminary monthly bulletins. In order to identify the artificial seismic sources the methodical approach described by Deneva et al. (1988) and some information about the quarry sites in Bulgaria have been used.

Acknowledgements: The authors owe their gratitude to the engineering staff for the perfect software and hardware ensuring of NOTSSI.

References

- Christoskov L. and E. Grigorova, 1968. Energetic and space characteristics of the destructive earthquakes in Bulgaria since 1900. *Izv.BAS, vol XII*.
- Christoskov L. and E. Samardjieva, 1983. Investigation on the duration of the seismic signals like a energetic characteristic of the earthquakes. *BGJ, vol.IX, N1*.
- Christoskov L. et al., 1987. Real time and background data processing in the Bulgarian seismological network. *Proc. Xx gen. Assembly 1986, Kiel, , Zurich*.
- Deneva D. et al., 1988. On the discrimination between industrial explosions and weak earthquakes using records of local seismics networks. *Proc. of conference in Liblice, 1988, Praha*.
- Snoke J.A, 2009. FOCMEC: FOCal MECanism Determinations. VirginiaTech, Blacksburg, VA, USA, 2009, Manual.
- Solakov, D., 1993. An algorithm for hypocenter determination of near earthquakes. *Bulg. Geophys. J.* 19 (1), 56-69

Solakov, D. et al., 2005. National Seismological Network – state and development. Proceedings of Scientific-practical conference on management in extraordinary situations and people protection, BAS, Sofia, 2005, 265-272.
[ftp://www.orfeus-eu.org/pub/data/continuous/2006/](http://www.orfeus-eu.org/pub/data/continuous/2006/)

Данни и анализ на сеизмичните събития регистрирани от НОТССИ през 2011

Е.Ботев, В.Протопопова, И.Попова, Бл.Бабачкова, С.Величкова, И.Цончева,
С.Димитрова, Вл.Бойчев, Д.Лазаров, Пл.Райкова

Резюме. Предлаганото научно съобщение съдържа обобщена информация за резултатите от събирането, обработката и анализа на първичните данни за сеизмичните събития, регистрирани от Националната Оперативна Телеметрична Система за Сеизмологична Информация (НОТССИ) през 2011 г. Представена е карта на епицентрите на общо 1836 земетресения в частта от Балканския полуостров, ограничена от географска ширина 37° - 47° N и дължина 19° - 30° E. По-подробно се анализира сеизмичността за територията на България и прилежащите ѝ земи (1205 сеизмични събития в район с координати $\lambda = 22^{\circ}$ - 29° E и $\varphi = 41^{\circ}$ - 44.5° N). Предлага се и каталог на земетресенията с магнитуд $M > 2.5$. Сеизмогенните прояви се обсъждат по зони, сравнени със съседни периоди време.

BLACK SEA EARTHQUAKE SAFETY NET(WORK) – ESNET¹

P. Trifonova, D.Solakov, S. Simeonova, M. Metodiev.

Dept. of Geophysics, National Institute of Geophysics, Geodesy and Geography-BAS, Acad. G. Bonchev Str., Bl.3, 1113 Sofia, Bulgaria, ptrifonova@geophys.bas.bg

Abstract *ESNET* project is working in the frame of the Joint Operational Programme “Black Sea Basin 2007-2013” financed by EU and national co-financing. The project objective is to contribute to the prevention of natural disasters generated by earthquakes in Black Sea basin by developing a joint monitoring and intervention concept between the partner countries (Romania, Bulgaria, Moldova and Turkey, see Fig. 1). Its duration is 24 months starting in March 2012 and has five major groups of activities. In the end of project implementation the disaster potential, with accent on the seismic risk degree and the earthquakes effects in the intervention area will be assessed, an integrated seismic monitoring and intervention concept will be developed and the capacity of local emergency intervention units for joint response activities in case of disasters will be increased. The present paper describes the expected cross-border impact of the action, its methodology and final results and outputs for the project’s beneficiaries.

Key words: cross-border cooperation, JOP “Black Sea Basin 2007-2013”, seismic risk, seismic monitoring, joint intervention concept

Program framework

The Black Sea Basin is one of the main areas of interaction between the European Union (EU) and its eastern neighbor countries. In order to address the challenges emerging in this area and in terms of relations with the other southern and eastern EU neighbours, the EU released a comprehensive new strategy in May 2004, the European Neighbourhood

¹ This publication has been produced with the assistance of the European Union. The content of this publication is the sole responsibility of its authors and can in no way reflect the views of the European Union

Policy (ENP)². To implement this Strategy, financial means are being made available through the European Neighbourhood and Partnership Instrument (ENPI)³. The core policy objectives of cross-border cooperation (CBC) on the external borders of the Union are to support sustainable development along both sides of the EU's external borders, to reduce differences in living standards across these borders, and to address the challenges and opportunities following EU enlargement or otherwise arising from the proximity between regions across European land and sea borders. The Black Sea Basin eligible area occupies a territory of 834,719 sq. km. and includes a population of 74.2 million people. It involves ten countries, some of which include the whole of their national territory (Armenia, Azerbaijan, R. Moldova and Georgia), while for some others those regions closest to the Basin (Bulgaria, Greece, Romania, Russia, Turkey⁴ and Ukraine).



Fig. 1. ESNET partner's institutions.

In order to achieve stronger regional partnerships and cooperation the program is aimed at contributing to its key objective: “a stronger and more sustainable economic and social development of the regions of the Black Sea Basin”. The ESNET project is released under OBJECTIVE 2: WORKING TOGETHER TO ADDRESS COMMON CHALLENGES of the Black Sea Basin ENPI-CBC programme, Priority 2: Sharing resources and competencies for environmental protection and conservation.

² European Neighbourhood Policy STRATEGY PAPER COMMUNICATION FROM THE COMMISSION COM (2004) 373 final Brussels, 12.5.2004

³ Regulation (EC) No 1638/2006 of the European Parliament and of the Council of 24 October 2006 laying down general provisions establishing a European Neighbourhood and Partnership Instrument.

⁴ Turkey as a negotiating candidate country is not covered by the ENPI Regulation (EC) N° 1638/2006 but allowed to participate in the Black Sea Basin Programme in accordance with art. 86(4) of the Commission Regulation (EC) No 718/2007 and the Article 9(5) of ENPI Regulation.

Project objectives

The overall objective of the project is to contribute to the prevention of natural disasters generated by earthquakes in Black Sea basin by developing a joint monitoring and intervention concept. All the countries involved in the project have their own studies, strategies, prevention and intervention systems in case of earthquakes, but until now there has not been an integrated approach so far in the Black Sea basin. Given the cross-border character of seismic activity results, it is necessary to have a cross-border approach on prevention, monitoring and intervention in case of earthquakes. There are also three specific objectives:

1. To assess the disaster potential, with accent on the seismic risk degree and the earthquakes effects in the intervention area. The first step in achieving the project main objective is to have an accurate and up-to-date assessment of the potential of disasters provoked by earthquakes in the project area/regions. This assessment will be carried out at national level and will be used in designing the common concept/approach for dealing with earthquakes at regional level, thus ensuring the cross-border character of the objective.

2. To develop an integrated seismic monitoring and intervention concept. This integrated concept, built on the basis of the previous objective, will have a cross-border relevance and is at the core of the action. The monitoring and intervention in case of earthquakes will be coordinated among the participating countries based on this concept, thus a more effective and efficient approach being ensured.

3. To increase the capacity of local institutions emergency intervention units for joint response activities in case of disasters. By involving the local emergency units and public administration in the project activities, especially in trainings, conferences and consultations, a better cooperation at cross-border level will be achieved. Step by step, the respective bodies will increase the cooperation and will benefit from each other's expertise.

Target groups aimed for achieving these objectives are: bodies in the partners countries and regions acting in the earthquakes research sector; emergency intervention units in the areas covered by the project; local public authorities in the areas covered by the project; NGOs acting in the field of information and intervention in case of natural disasters

Methodology

The project methodology was chosen in line with the specificity of the needs and constraints of the target groups. The activities proposed will gather the added-value of each target group and will lead through its outputs and results to the fulfillment of the overall and specific objectives of the ESNET action.

The activities follow logically and are scheduled so as to deliver the best possible results in a reasonable timeframe. The implementation methods are based on permanent cooperation among partners and on-line meetings will take place every time it is necessary to ensure a good coordination. The project team (Fig. 2) is large enough to allow each partner to make sure that is able to fulfill its activities and also that the legal and financial regulations and requirements are observed.



Fig. 2. ESNET project team at the Bulgarian study visit, organized in Varna.

NIEP is the most authorized entity in the field of earthquakes in Romania. The same can be said about the Bulgarian (NIGGG) and Moldavian (IGS) partners. The Turkish partner (IBC) is an NGO with a long history in the field of protection to disasters and intervention in case of catastrophes.

All partners have the capacity to involve relevant stakeholders from their countries (local public administrations, emergency units, NGOs), based on the long-term cooperation history.

Activities

ESNET project implementation is organized in five groups of activities:

Activity 1: Assessment of the current situation. Aim of this group of activities is to provide a high level of mutual knowledge regarding the current status of the national frameworks, strategies, policies and procedures regarding the prevention, monitoring and intervention in case of earthquake. At this moment, each country has its own systems, methodologies and institutions dealing with earthquakes/disasters, but very little have been achieved in what concerns the cooperation among them at regional level. Sharing expertise and benefiting from each other's experience is the basic tool for a cross-border project and the partners are determined to make the most out of using them.

Activity 2: Increase the sector cooperation by setting up the Black Sea Safety Network. The aim of the action is to create a platform for long-term cooperation among the

stakeholders in the participating countries, in the field of preventing, monitoring and intervention in case of earthquakes. This platform will take the form of a network whose tools will be: a web portal, monitoring and early warning software and communication tool (e-group). In order to make sure that the network will be operational on long term, an agreement shall be signed by all project partners, providing for clear commitment concerning the active participation to the network activity (e.g. supply of information and documents to be posted on the portal, inviting the network members to attend sector events etc). The portal will be a good mean to communicate with the stakeholders but also with the citizens on issues of common interest regarding the earthquakes. The network will also communicate with similar networks in order to ensure synergy of the activities instead of overlapping.



Fig. 3. Visit to the Dobrogea Seismological Observatory (Eforie)

Activity 3 Capacity building. The aim of the action is to increase the administrative capacity of dealing with earthquakes in the Black Sea area covered by the countries participating in the network. Joint curricula will be developed according to the needs assessment data identified during country assessments carried out in Group of Activities 1 and based on the regional strategic requirements. The training will be delivered by trainers from each country to the emergency units staff from the respective country.

Activity 4 Visibility of the Action. The aim of this group of activities is to make the project and the EU contribution widely known to the general public in the participating countries and even further. This will be achieved through conferences and press conferences, distribution of promotion materials, dissemination of press releases, net book and regular project updates.

Activity 5 Management and coordination of the Action. The last group of activities aims to ensure a smooth project implementation, in agreement with the EU and national

(where applicable) laws and regulations. Face to face as well as on-line meetings of the project team members will ensure the strong cooperation between partners. Evaluation of activities and expenditure verification will ensure that the project and the grant contract provisions are observed and no irregularities are made.

Expected results and outputs

Execution of the first group of activities will result in: 1) Broad expert knowledge shared on the earthquake related issues for each participating country; 2) Support of the public authorities for the elaborated reports and proposed plans; and 3) Basis for creating a long-term cooperation network. Four study visits (Fig. 3) and four county assessment reports resulted in estimation of the existing framework in the field of prevention, monitoring and intervention related to earthquake (potential) disasters in the region.

Envisaged long-term cooperation among the stakeholders in the participating countries, in the field of preventing, monitoring and intervention in case of earthquakes will be achieved through one “Seismic Safety Net(work) Web Portal” developed and launched, and One “Black Sea Joint Seismicity Monitoring and Early Warning System” set up as a software tool.

A “Regional Capacity Building Start-up Curricula” elaborated, with approx. 10 training subjects included and 2 days training sessions in each country, with the participation of 20 professionals from the emergency units in each participating country will be the results from *Capacity building* package. These will ensure training support for the professionals in the sector of earthquake monitoring, early warning and intervention as well as increased capacity of emergency units to react to earthquake disasters.

Planned visibility actions will contribute to spreading a broad knowledge of the project and its donors to the public in the participating countries.

Acknowledgements

The project is financed by the European Neighbourhood and Partnership Instrument and national co-financing under the Joint Operational Programme “Black Sea Basin 2007-2013”, grant contract Ref. № 1.2.1.65963.80 MIS-ETC 250.

Черноморска мрежа за сеизмична безопасност - ESNET

П. Трифонова, Д. Солаков, С. Симеонова, М. Методиев

Резюме Проект ESNET се изпълнява в рамките на съвместна оперативна програма на Черноморския басейн 2007-2013, финансиран от ЕС и национално съ-финансиране.

Целта на проекта е да допринесе за превенцията на природни бедствия, генерирани от земетресения в региона на западния бряг на Черно море, чрез разработване на система за съвместен мониторинг и концепция за реакция между партньорските страни (Румъния, България, Молдова и Турция). Неговата продължителност е 24 месеца, с начало март 2012 г. и съдържа пет основни групи дейности. В края на изпълнението на проекта ще бъдат оценени потенциалите за бедствие, с акцент върху степента на сеизмичен риск и възможните ефекти от земетресения в областта, ще бъдат разработени интегрирана система за сеизмичен мониторинг и концепция за намеса и ще бъде увеличен капацитета на местните звена за реакция при кризи и съвместни дейности в случай на бедствие. Статията представя информация за очаквания трансграничен ефект на предвидените дейности, методологията и крайните резултати за бенефициентите по проекта.

ANNUAL REPORT OF THE OBSERVED GEOMAGNETIC ACTIVITY IN PANAGYURISHTE OBSERVATORY

P. Trifonova, M. Metodiev

Dept. of Geophysics, National Institute of Geophysics, Geodesy and Geography-BAS, Acad. G. Bonchev Str., Bl.3, 1113 Sofia, Bulgaria, p.trifonova@abv.bg

Abstract. Presently, in the era of Internet communication the preliminary time series (INTERMAGNET's reported data) acquired in geomagnetic observatories are available in near-real time, while the final absolute time series (definitive data) are disseminated with many months delay, being subject to many checks. This paper reports the quasi-definitive geomagnetic data obtained in Panagyurishte observatory in 2012, prepared in the form of local geomagnetic indices and absolute time-series of hourly mean values plots. Verification of data quality is performed according to "IAGA guide for magnetic measurements and observatory practice".

Key words: PAG observatory, geomagnetic variations, geomagnetic activity, hourly mean values.

Introduction

The Geomagnetic observatory in Panagyurishte (PAG) is established in 1937 – first on the Balkan Peninsula and unique in Bulgaria and during more than 75 years performs the absolute measurements of the geomagnetic field elements and continuous registration of their variations. From 2008 PAG observatory was equipped with digital systems for the recording of geomagnetic field element's variations. Thus, the observatory implement the technical requirements and was joined to the INTERMAGNET (International Real-time Magnetic Observatory Network), which establishes a global network of cooperating digital magnetic observatories, and facilitate data exchanges and geomagnetic products in close to real time. Preliminary recorded time series and local geomagnetic k-indices are published on the NIGGG web page (http://data.geophys.bas.bg/magn_data1/dailymag_bg.php) and automatically reported to INTERMAGNET. The present paper provides quasi-definitive geomagnetic data which are checked and processed to comply with the IAGA standards for observatory practices.

Local geomagnetic indices (K , A_K , ΣK) calculated at PAG observatory.

The K-index is often used as a quantitative measure of local magnetic activity. It is a 3-hour quasi-logarithmic scale developed to measure magnetic activity ranging from 0 to 9, with 0 indicating completely quiet conditions and 9, representing extreme magnetic activity. It is intended to measure geomagnetic disturbances outside the normal diurnal quiet time variations. In order to have a somewhat consistent scale of magnetic activity between observatories at high latitudes, where field variations can be quite large in amplitude, and those at low latitudes, each observatory is assigned its own set of amplitude ranges corresponding to the various K-index levels. Thus, for example, a K-index of 5 at College (212.4°E, 64.87°N) corresponds to a lower limit of magnetic activity range of 350 nT over the 3-hour interval, while at San Juan (293.85°E, 18.117°N) this same K-index level corresponds to a lower limit of magnetic activity of 40 nT. The idea is to have K-index compensation for the influence of latitude on magnetic activity, so that a K-index of 7 at College and San Juan would represent the same magnetic storm intensity despite the actual differences in the range of magnetic fluctuation amplitudes at the two latitudes.

The ranges of the individual K numbers in PAG observatory (24.177°EN, 42.515°N) are defined as follows:

Deviation from the normal S_q variation [nT]	<5	5 -10	10 - 20	20 - 40	40 - 70	70 - 120	120 -200	200-330	330-500	> 500
K	0	1	2	3	4	5	6	7	8	9

The eight three-hourly K numbers are calculated by a computer code (FMI method) from the digital recordings of three component flux-gate variometer FGE.

Description of the geomagnetic storms and their possible effects on people and systems can be found at NOAA Space Weather Scale for Geomagnetic Storms (<http://www.swpc.noaa.gov/NOAAscales/index.html#GeomagneticStorms>).

A_K [nT] is the local equivalent daily amplitude index which is determined by converting K -indices into eight 3-hour equivalent linear amplitudes a_K , and calculating the mean value. The 3-hour equivalent amplitude a_K is assigned for each K value using the following table:

K	0	1	2	3	4	5	6	7	8	9
a_K [nT]	0	3	7	15	27	48	80	140	240	400

ΣK is the daily sum of the eight K numbers.

Table 1. Local geomagnetic indices (K , A_K , ΣK) calculated at PAG observatory in January 2012.

Activity indices			
PAG Observatory		January 2012	
Day	K	A _k [nT]	ΣK
1-Jan-12	2 1 1 1 2 2 2 1	5	12
2-Jan-12	1 1 1 1 1 1 3 2	5	11
3-Jan-12	3 3 1 1 1 2 2 1	7	14
4-Jan-12	2 1 2 2 1 0 1 1	4	10
5-Jan-12	1 1 1 1 3 2 2 2	6	13
6-Jan-12	2 1 2 2 1 2 3 3	8	16
7-Jan-12	3 2 1 1 2 2 1 3	8	15
8-Jan-12	2 1 2 2 1 1 2 2	6	13
9-Jan-12	2 2 2 2 2 3 2 2	8	17
10-Jan-12	1 1 1 2 2 1 2 1	5	11
11-Jan-12	2 2 2 2 1 1 2 2	6	14
12-Jan-12	1 2 1 1 1 2 3 3	7	14
13-Jan-12	2 2 2 0 1 1 0 1	4	9
14-Jan-12	1 0 1 1 1 0 0 1	2	5
15-Jan-12	1 1 1 1 1 1 2 3	5	11
16-Jan-12	2 1 2 3 3 3 3 2	11	19
17-Jan-12	3 2 1 2 1 1 2 1	6	13
18-Jan-12	2 1 1 2 1 1 1 1	4	10
19-Jan-12	1 1 1 0 0 1 1 1	2	6
20-Jan-12	2 2 1 1 0 1 2 1	4	10
21-Jan-12	1 2 2 2 2 2 2 2	7	15
22-Jan-12	1 2 4 4 4 4 5 5	27	29
23-Jan-12	4 3 2 1 1 0 1 2	8	14
24-Jan-12	4 2 2 2 2 4 5 4	20	25
25-Jan-12	3 3 3 4 3 2 2 2	14	22
26-Jan-12	2 1 1 2 1 3 3 2	8	15
27-Jan-12	2 1 3 1 2 2 1 1	6	13
28-Jan-12	2 2 1 1 1 1 3 3	7	14
29-Jan-12	3 2 1 1 0 2 3 3	8	15
30-Jan-12	0 0 0 1 1 4 4 4	11	14
31-Jan-12	2 1 1 0 1 0 1 1	3	7

Table 2. Local geomagnetic indices (K , A_K , ΣK) calculated at PAG observatory in February 2012.

Activity indices			
PAG Observatory		February 2012	
Day	K	A _K [nT]	ΣK
1-Feb-12	2 2 2 2 1 1 1 1	5	12
2-Feb-12	2 1 1 1 1 0 1 1	3	8
3-Feb-12	2 2 1 2 2 2 1 0	5	12
4-Feb-12	2 2 2 2 3 2 2 3	9	18
5-Feb-12	3 2 1 2 3 2 4 2	11	19
6-Feb-12	2 2 1 1 1 3 3 2	8	15
7-Feb-12	1 2 2 3 3 3 5 4	17	23
8-Feb-12	3 2 2 2 3 2 3 2	10	19
9-Feb-12	1 1 1 2 2 3 3 1	7	14
10-Feb-12	1 1 1 1 1 1 3 2	5	11
11-Feb-12	2 1 1 1 1 1 2 2	5	11
12-Feb-12	2 1 1 2 0 1 1 1	4	9
13-Feb-12	2 1 3 2 3 3 3 3	12	20
14-Feb-12	3 2 2 1 2 3 4 5	16	22
15-Feb-12	2 4 2 3 2 3 5 4	19	25
16-Feb-12	2 1 2 2 2 1 0 1	5	11
17-Feb-12	0 0 1 1 1 0 0 0	1	3
18-Feb-12	0 0 1 1 0 1 2 4	5	9
19-Feb-12	5 4 1 2 1 2 2 3	15	20
20-Feb-12	3 4 2 2 3 4 3 4	18	25
21-Feb-12	3 2 1 1 1 1 1 3	7	13
22-Feb-12	3 3 3 3 2 2 2 1	11	19
23-Feb-12	0 0 1 1 1 1 1 3	4	8
24-Feb-12	2 3 1 1 2 2 2 1	7	14
25-Feb-12	0 0 2 2 3 2 3 2	7	14
26-Feb-12	2 1 2 1 1 0 2 3	6	12
27-Feb-12	3 2 1 3 4 5 6 2	25	26
28-Feb-12	2 2 4 2 2 3 1 3	11	19
29-Feb-12	3 2 3 1 0 1 1 2	7	13

Table 3. Local geomagnetic indices (K , A_K , ΣK) calculated at PAG observatory in March 2012.

Activity indices			
PAG Observatory		March 2012	
Day	K	A _k [nT]	ΣK
1-Mar-12	1 3 3 3 2 3 5 4	18	24
2-Mar-12	3 3 2 2 2 2 2 2	9	18
3-Mar-12	2 1 1 2 1 3 1 3	7	14
4-Mar-12	3 3 3 3 2 3 4 2	15	23
5-Mar-12	3 1 2 3 1 2 3 3	10	18
6-Mar-12	3 2 2 2 2 3 3 3	11	20
7-Mar-12	3 3 4 4 5 5 5 4	32	33
8-Mar-12	2 2 3 5 4 4 4 4	23	28
9-Mar-12	4 5 6 5 5 5 3 3	41	36
10-Mar-12	4 4 2 2 2 3 4 2	16	23
11-Mar-12	2 1 1 2 2 3 3 4	11	18
12-Mar-12	3 2 2 5 5 4 4 3	24	28
13-Mar-12	4 2 1 2 2 2 2 2	9	17
14-Mar-12	2 2 1 2 2 3 2 3	9	17
15-Mar-12	3 2 1 2 5 6 5 4	29	28
16-Mar-12	3 2 2 3 3 5 5 4	23	27
17-Mar-12	4 3 3 2 3 4 5 5	25	29
18-Mar-12	4 3 2 3 2 2 3 3	14	22
19-Mar-12	2 3 2 2 3 1 3 4	12	20
20-Mar-12	1 1 2 2 1 1 2 3	6	13
21-Mar-12	1 1 2 2 2 2 3 3	8	16
22-Mar-12	1 1 1 1 1 1 3 4	8	13
23-Mar-12	2 0 1 1 1 1 2 1	4	9
24-Mar-12	1 2 3 2 2 2 3 3	10	18
25-Mar-12	2 1 2 2 2 1 1 0	5	11
26-Mar-12	1 1 2 2 1 1 1 2	5	11
27-Mar-12	2 2 2 3 3 3 4 4	15	23
28-Mar-12	5 3 2 2 3 2 3 2	15	22
29-Mar-12	0 1 0 0 1 1 2 3	4	8
30-Mar-12	3 2 2 1 1 1 0 1	5	11
31-Mar-12	1 1 2 1 2 3 3 1	7	14

Table 4. Local geomagnetic indices (K , A_K , ΣK) calculated at PAG observatory in April 2012.

Activity indices			
PAG Observatory		April 2012	
Day	K	A _k [nT]	ΣK
1-Apr-12	2 2 1 2 1 2 2 3	7	15
2-Apr-12	3 2 2 1 2 2 1 2	7	15
3-Apr-12	2 1 1 1 1 1 2 3	6	12
4-Apr-12	2 2 0 1 1 2 2 3	6	13
5-Apr-12	2 2 2 3 3 3 2 3	11	20
6-Apr-12	1 1 1 1 0 1 0 2	3	7
7-Apr-12	2 2 2 2 3 1 1 2	7	15
8-Apr-12	2 1 1 1 1 2 2 1	5	11
9-Apr-12	1 1 2 1 0 1 2 2	4	10
10-Apr-12	3 2 1 2 2 2 2 3	9	17
11-Apr-12	2 1 3 2 2 1 1 3	8	15
12-Apr-12	1 2 2 2 1 3 5 3	13	19
13-Apr-12	5 4 3 3 2 3 3 3	20	26
14-Apr-12	3 2 2 2 2 2 3 1	9	17
15-Apr-12	0 1 2 2 1 2 3 2	6	13
16-Apr-12	1 1 1 1 2 2 2 2	5	12
17-Apr-12	2 1 2 2 2 2 4 2	9	17
18-Apr-12	3 2 2 2 2 1 2 2	8	16
19-Apr-12	1 1 2 1 0 1 3 3	6	12
20-Apr-12	1 3 3 2 1 1 1 2	7	14
21-Apr-12	1 0 1 2 0 2 3 3	6	12
22-Apr-12	3 2 1 3 2 1 1 1	7	14
23-Apr-12	2 4 3 2 2 4 4 4	18	25
24-Apr-12	5 5 3 2 2 3 4 4	24	28
25-Apr-12	3 3 3 2 2 4 4 4	18	25
26-Apr-12	2 4 2 2 3 2 3 3	13	21
27-Apr-12	2 2 2 1 2 2 2 2	7	15
28-Apr-12	2 1 1 3 1 2 2 3	8	15
29-Apr-12	2 1 1 1 1 1 2 1	4	10
30-Apr-12	1 1 1 0 0 0 1 1	2	5

Table 5. Local geomagnetic indices (K , A_K , ΣK) calculated at PAG observatory in May 2012.

Activity indices			
PAG Observatory		May 2012	
Day	K	A _k [nT]	ΣK
1-May-12	0 1 1 1 1 1 1 3	4	9
2-May-12	3 1 0 1 1 0 1 3	5	10
3-May-12	2 2 2 2 2 1 2 3	8	16
4-May-12	2 2 0 1 1 2 1 1	4	10
5-May-12	0 1 1 1 1 1 1 1	3	7
6-May-12	1 2 2 2 2 1 1 0	5	11
7-May-12	1 2 1 2 2 2 1 1	5	12
8-May-12	1 2 1 1 2 3 3 4	10	17
9-May-12	4 4 3 3 4 4 5 4	27	31
10-May-12	3 3 2 2 2 2 2 4	12	20
11-May-12	3 2 2 2 1 3 2 2	9	17
12-May-12	3 1 2 2 2 2 3 3	10	18
13-May-12	3 2 2 2 2 3 3 2	10	19
14-May-12	3 2 1 1 2 1 1 1	6	12
15-May-12	2 2 2 1 1 0 0 2	4	10
16-May-12	2 1 1 2 3 2 3 4	11	18
17-May-12	2 1 1 1 1 1 2 2	5	11
18-May-12	3 2 1 2 1 2 2 2	7	15
19-May-12	2 2 2 2 2 1 2 1	6	14
20-May-12	3 4 3 2 3 2 1 1	12	19
21-May-12	0 2 1 1 0 1 4 2	6	11
22-May-12	3 4 2 2 4 4 4 4	21	27
23-May-12	3 3 3 3 2 2 2 2	11	20
24-May-12	2 2 2 2 2 2 3 2	8	17
25-May-12	2 2 1 2 2 2 2 2	7	15
26-May-12	2 1 1 1 1 1 0 0	3	7
27-May-12	1 2 1 2 0 1 1 1	4	9
28-May-12	0 2 1 1 2 3 2 2	6	13
29-May-12	1 2 0 1 2 2 2 3	6	13
30-May-12	3 3 1 2 2 2 2 1	8	16
31-May-12	3 2 3 2 2 3 3 1	11	19

Table 6. Local geomagnetic indices (K , A_K , ΣK) calculated at PAG observatory in June 2012.

Activity indices			
PAG Observatory		June 2012	
Day	K	A _k [nT]	ΣK
1-Jun-12	1 2 1 3 2 -1 -1 -1	4	9
2-Jun-12	-1 -1 -1 -1 -1 -1 3 4	5	7
3-Jun-12	3 2 2 3 5 4 4 2	19	25
4-Jun-12	2 3 2 4 3 3 3 4	16	24
5-Jun-12	2 3 4 3 3 3 3 4	17	25
6-Jun-12	4 3 2 3 3 3 4 2	16	24
7-Jun-12	2 2 2 2 2 2 3 2	8	17
8-Jun-12	2 2 2 3 1 1 2 1	7	14
9-Jun-12	2 2 1 2 2 2 3 2	8	16
10-Jun-12	0 1 1 2 2 2 -1 -1	3	8
11-Jun-12	-1 -1 -1 2 2 3 4 5	13	16
12-Jun-12	4 4 2 2 1 1 1 1	10	16
13-Jun-12	2 2 2 2 1 1 1 1	5	12
14-Jun-12	2 2 1 1 1 1 1 1	4	10
15-Jun-12	1 2 1 1 1 1 0 1	3	8
16-Jun-12	2 2 1 3 3 3 4 6	21	24
17-Jun-12	4 3 3 5 4 4 3 3	24	29
18-Jun-12	4 4 3 2 2 2 2 0	12	19
19-Jun-12	1 1 0 1 1 0 0 0	2	4
20-Jun-12	1 2 1 2 1 1 1 0	4	9
21-Jun-12	1 1 1 1 1 1 1 1	3	8
22-Jun-12	0 2 2 2 2 2 1 0	5	11
23-Jun-12	0 1 2 2 2 3 1 1	6	12
24-Jun-12	2 1 1 2 2 2 2 1	6	13
25-Jun-12	1 2 2 2 3 3 2 2	9	17
26-Jun-12	2 2 2 2 1 2 1 2	6	14
27-Jun-12	1 2 1 2 2 2 1 1	5	12
28-Jun-12	2 2 2 2 2 1 1 1	6	13
29-Jun-12	1 2 1 1 1 1 2 3	6	12
30-Jun-12	3 3 3 4 4 3 3 4	20	27

Table 7. Local geomagnetic indices (K , A_K , ΣK) calculated at PAG observatory in July 2012.

Activity indices			
PAG Observatory		July 2012	
Day	K	A _k [nT]	ΣK
1-Jul-12	3 3 3 3 3 3 3 4	17	25
2-Jul-12	3 4 3 3 4 3 3 2	17	25
3-Jul-12	2 2 3 3 2 3 2 2	10	19
4-Jul-12	3 2 1 2 2 2 1 2	7	15
5-Jul-12	3 3 2 4 4 3 3 3	17	25
6-Jul-12	2 3 2 2 3 4 4 4	17	24
7-Jul-12	2 2 2 3 2 2 3 3	10	19
8-Jul-12	2 3 2 3 3 3 2 4	14	22
9-Jul-12	5 3 3 4 4 5 3 4	28	31
10-Jul-12	3 2 3 3 2 3 3 2	12	21
11-Jul-12	2 2 3 4 2 2 2 3	12	20
12-Jul-12	3 3 3 2 2 2 1 2	10	18
13-Jul-12	1 2 1 1 1 1 1 1	4	9
14-Jul-12	1 2 1 1 2 3 5 5	17	20
15-Jul-12	4 5 5 5 3 5 6 5	45	38
16-Jul-12	4 4 3 3 3 3 2 2	16	24
17-Jul-12	3 3 3 1 1 3 2 2	10	18
18-Jul-12	2 2 1 1 1 1 2 1	5	11
19-Jul-12	1 2 2 2 2 1 1 1	5	12
20-Jul-12	1 3 2 3 2 3 3 3	12	20
21-Jul-12	2 2 2 2 2 3 3 2	9	18
22-Jul-12	2 2 3 3 1 1 2 2	8	16
23-Jul-12	2 2 2 1 3 3 3 3	11	19
24-Jul-12	2 2 2 2 2 1 2 1	6	14
25-Jul-12	2 2 2 1 1 1 1 1	5	11
26-Jul-12	1 1 1 0 1 1 0 0	2	5
27-Jul-12	1 2 2 2 1 1 1 2	5	12
28-Jul-12	1 2 2 2 2 2 4 4	12	19
29-Jul-12	2 3 2 2 1 1 1 1	6	13
30-Jul-12	2 2 2 3 3 4 4 2	14	22
31-Jul-12	2 2 1 2 2 2 1 2	6	14

Table 8. Local geomagnetic indices (K , A_K , ΣK) calculated at PAG observatory in August 2012.

Activity indices			
PAG Observatory		August 2012	
Day	K	A _k [nT]	ΣK
1-Aug-12	1 2 2 2 2 2 1 2	6	14
2-Aug-12	1 2 1 3 5 5 4 3	21	24
3-Aug-12	2 2 1 2 1 2 1 0	5	11
4-Aug-12	1 2 1 1 2 2 1 2	5	12
5-Aug-12	1 1 1 2 1 2 1 2	5	11
6-Aug-12	2 2 2 3 2 3 3 3	11	20
7-Aug-12	2 2 2 1 1 1 2 3	7	14
8-Aug-12	5 3 2 2 2 3 2 2	14	21
9-Aug-12	3 2 1 1 1 1 1 1	5	11
10-Aug-12	0 2 1 0 1 1 1 1	3	7
11-Aug-12	0 1 1 2 1 1 2 3	5	11
12-Aug-12	2 2 2 2 3 3 3 3	11	20
13-Aug-12	1 2 2 2 2 3 3 2	9	17
14-Aug-12	2 2 2 2 2 2 1 3	8	16
15-Aug-12	2 1 1 1 2 2 2 3	7	14
16-Aug-12	2 2 2 2 3 4 3 4	14	22
17-Aug-12	4 2 2 1 1 1 2 3	9	16
18-Aug-12	1 2 2 2 2 2 4 3	10	18
19-Aug-12	2 2 2 4 3 2 2 4	13	21
20-Aug-12	3 2 2 2 4 2 3 2	12	20
21-Aug-12	2 1 1 2 1 2 1 3	6	13
22-Aug-12	1 1 1 2 2 2 2 3	7	14
23-Aug-12	3 2 2 2 2 2 3 2	9	18
24-Aug-12	2 2 2 2 2 2 3 3	9	18
25-Aug-12	2 2 3 3 2 2 3 4	13	21
26-Aug-12	2 2 2 3 3 2 3 2	10	19
27-Aug-12	2 3 2 2 1 1 1 2	7	14
28-Aug-12	1 0 0 2 1 0 0 1	2	5
29-Aug-12	1 1 1 1 1 1 1 1	3	8
30-Aug-12	1 1 1 1 1 1 2 1	4	9
31-Aug-12	0 1 1 1 1 0 0 1	2	5

Table 9. Local geomagnetic indices (K , A_K , ΣK) calculated at PAG observatory in September 2012.

Activity indices			
PAG Observatory		September 2012	
Day	K	A _k [nT]	ΣK
1-Sep-12	2 1 2 2 1 2 1 2	6	13
2-Sep-12	3 2 3 2 2 3 4 4	15	23
3-Sep-12	3 3 2 3 5 5 4 4	25	29
4-Sep-12	3 2 3 2 2 3 3 3	12	21
5-Sep-12	4 4 4 4 2 3 4 3	22	28
6-Sep-12	3 3 1 1 1 3 3 2	10	17
7-Sep-12	1 2 2 1 1 2 4 4	11	17
8-Sep-12	3 1 2 2 2 2 2 1	7	15
9-Sep-12	1 1 2 2 1 1 1 2	5	11
10-Sep-12	2 2 2 0 2 1 2 0	5	11
11-Sep-12	0 1 2 1 0 0 0 1	2	5
12-Sep-12	1 1 2 2 2 1 2 2	6	13
13-Sep-12	2 2 1 1 0 2 1 1	4	10
14-Sep-12	1 2 1 1 1 2 1 3	6	12
15-Sep-12	2 2 1 2 1 2 2 3	7	15
16-Sep-12	2 2 2 2 1 1 3 1	7	14
17-Sep-12	2 1 1 1 1 1 1 1	4	9
18-Sep-12	2 3 2 2 2 2 1 1	7	15
19-Sep-12	1 2 1 2 2 4 5 5	19	22
20-Sep-12	3 2 3 2 2 2 2 2	9	18
21-Sep-12	1 1 1 2 2 2 2 1	5	12
22-Sep-12	2 1 1 2 1 1 0 2	4	10
23-Sep-12	0 1 1 0 0 0 0 0	1	2
24-Sep-12	0 1 0 1 1 1 1 1	2	6
25-Sep-12	1 0 0 1 1 1 0 0	2	4
26-Sep-12	1 1 1 1 2 1 3 3	7	13
27-Sep-12	3 2 1 1 1 1 1 1	5	11
28-Sep-12	0 1 1 1 1 1 1 0	2	6
29-Sep-12	1 1 2 1 2 1 1 1	4	10
30-Sep-12	1 1 1 3 3 3 3 4	12	19

Table 10. Local geomagnetic indices (K , A_K , ΣK) calculated at PAG observatory in October 2012.

Activity indices			
PAG Observatory		October 2012	
Day	K	AK [nT]	ΣK
1-Oct-12	5 4 3 2 2 2 2 1	15	21
2-Oct-12	2 1 0 2 3 2 2 2	7	14
3-Oct-12	3 2 2 2 1 1 1 1	6	13
4-Oct-12	0 1 0 0 0 0 0 0	0	1
5-Oct-12	0 1 1 1 1 2 2 3	5	11
6-Oct-12	2 1 1 2 2 2 2 2	6	14
7-Oct-12	1 2 1 1 1 1 3 3	7	13
8-Oct-12	3 3 5 5 4 3 5 4	30	32
9-Oct-12	5 5 4 4 2 2 3 5	28	30
10-Oct-12	3 2 2 3 2 4 4 3	15	23
11-Oct-12	2 2 1 2 2 2 1 2	6	14
12-Oct-12	3 3 3 2 3 3 3 2	13	22
13-Oct-12	3 4 4 4 4 6 4 4	32	33
14-Oct-12	4 2 3 3 4 3 5 4	23	28
15-Oct-12	3 2 2 2 2 1 2 2	8	16
16-Oct-12	1 1 2 2 1 2 1 2	5	12
17-Oct-12	2 1 2 1 2 1 1 3	6	13
18-Oct-12	3 1 2 2 1 1 1 2	6	13
19-Oct-12	3 2 1 1 1 0 0 0	4	8
20-Oct-12	0 0 2 2 1 0 0 0	2	5
21-Oct-12	1 2 2 1 1 1 1 1	4	10
22-Oct-12	1 1 1 1 0 1 1 1	3	7
23-Oct-12	2 2 2 2 2 2 3 1	8	16
24-Oct-12	2 1 1 1 1 1 1 1	4	9
25-Oct-12	1 1 1 2 1 0 1 2	4	9
26-Oct-12	1 1 1 1 1 2 2 2	5	11
27-Oct-12	2 0 1 1 1 1 1 1	3	8
28-Oct-12	0 1 2 2 2 1 1 0	4	9
29-Oct-12	1 0 1 0 0 0 0 2	2	4
30-Oct-12	2 1 1 1 0 0 0 1	2	6
31-Oct-12	0 0 0 1 2 3 2 3	6	11

Table 11. Local geomagnetic indices (K , A_K , ΣK) calculated at PAG observatory in November 2012.

Activity indices			
PAG Observatory		November 2012	
Day	K	A_K [nT]	ΣK
1-Nov-12	3 2 2 3 3 4 5 4	20	26
2-Nov-12	2 3 2 2 1 1 1 2	7	14
3-Nov-12	1 1 2 1 2 1 1 1	4	10
4-Nov-12	0 1 1 1 1 1 0 0	2	5
5-Nov-12	0 0 2 2 1 2 1 1	4	9
6-Nov-12	1 1 0 1 1 2 2 2	4	10
7-Nov-12	3 3 2 1 3 4 5 4	20	25
8-Nov-12	1 1 1 1 0 0 0 2	2	6
9-Nov-12	1 1 1 0 0 0 1 0	2	4
10-Nov-12	0 0 0 0 0 0 1 3	2	4
11-Nov-12	0 0 1 1 1 1 0 1	2	5
12-Nov-12	2 1 0 1 0 2 3 5	10	14
13-Nov-12	4 4 3 3 3 3 5 4	24	29
14-Nov-12	5 5 4 3 4 2 1 2	23	26
15-Nov-12	1 0 1 2 1 1 1 2	4	9
16-Nov-12	2 1 1 1 1 3 3 3	8	15
17-Nov-12	2 2 2 3 2 2 3 3	10	19
18-Nov-12	1 1 2 1 1 2 0 3	5	11
19-Nov-12	1 1 2 2 2 2 1 2	6	13
20-Nov-12	2 2 2 2 3 3 4 3	13	21
21-Nov-12	3 2 2 2 1 2 3 1	8	16
22-Nov-12	1 1 1 1 1 0 0 1	2	6
23-Nov-12	0 0 1 1 1 1 3 4	7	11
24-Nov-12	4 3 2 2 3 3 2 2	13	21
25-Nov-12	1 2 1 1 1 2 1 2	5	11
26-Nov-12	2 2 2 2 0 1 1 1	5	11
27-Nov-12	1 1 1 1 1 1 2 1	4	9
28-Nov-12	1 1 0 0 0 0 1 2	2	5
29-Nov-12	1 0 1 2 0 2 1 1	3	8
30-Nov-12	0 1 1 1 1 1 0 1	2	6

Table 12. Local geomagnetic indices (K , A_K , ΣK) calculated at PAG observatory in December 2012.

Activity indices			
PAG Observatory		December 2012	
Day	K	A_K [nT]	ΣK
1-Dec-12	1 1 1 1 2 1 4 3	8	14
2-Dec-12	2 1 3 2 2 1 1 0	6	12
3-Dec-12	0 1 1 1 1 1 1 2	3	8
4-Dec-12	2 2 1 2 1 0 1 0	4	9
5-Dec-12	0 1 1 1 0 0 1 1	2	5
6-Dec-12	1 1 1 1 0 0 0 0	2	4
7-Dec-12	0 0 1 0 0 0 1 0	1	2
8-Dec-12	0 0 1 0 1 1 1 1	2	5
9-Dec-12	1 2 1 2 1 2 1 3	6	13
10-Dec-12	3 1 1 2 1 1 1 1	5	11
11-Dec-12	1 1 1 1 0 0 1 1	2	6
12-Dec-12	1 0 1 1 1 1 0 1	2	6
13-Dec-12	2 1 0 0 0 0 1 1	2	5
14-Dec-12	2 2 2 2 1 1 2 3	7	15
15-Dec-12	2 2 2 2 3 3 3 2	10	19
16-Dec-12	2 0 1 1 2 2 2 1	5	11
17-Dec-12	2 2 2 4 3 3 1 1	11	18
18-Dec-12	2 2 1 3 2 3 1 1	8	15
19-Dec-12	1 2 2 2 1 1 1 1	5	11
20-Dec-12	0 1 2 2 3 3 3 2	9	16
21-Dec-12	2 1 1 1 0 1 1 1	3	8
22-Dec-12	0 0 1 1 0 0 0 1	1	3
23-Dec-12	0 0 1 1 1 1 0 0	2	4
24-Dec-12	0 1 1 1 1 3 1 1	4	9
25-Dec-12	1 1 1 1 0 1 1 2	3	8
26-Dec-12	0 1 0 1 1 0 0 1	2	4
27-Dec-12	1 0 1 1 0 0 0 0	1	3
28-Dec-12	1 1 1 1 1 0 1 2	3	8
29-Dec-12	1 1 1 1 1 1 0 2	3	8
30-Dec-12	1 1 2 2 2 2 2 1	6	13
31-Dec-12	0 1 1 1 0 0 0 0	1	3

Quasi-definitive hourly mean values of the Declination (D), Horizontal (H), and Vertical (Z) field components.

Until the advent of digital recording systems hourly mean values (HMVs) were the primary data product from magnetic observatories. Both, the spot hourly values and the HMVs were usually compiled into monthly tables. These tables were published in observatory yearbooks as shown in Fig. 1 (see Buchvarov, 2006).

HOURLY MEANS OF HORIZONTAL COMPONENT OF MAGNETIC INTENSITY																															
23000 + TABULAR QUANTITY (IN NANOTESLAS)																															
JANUARY 1983																															
DATE U.T.	01	02	03	04	05	06	07	08	09	10	11	12	13	14	15	16	17	18	19	20	21	22	23	24	25	26	27	28	29	30	31
1	698	697	694	693	708	712	723	725	715	699	692	690	688	688	691	694	695	697	705	704	707	705	705	706	701						
2	710	707	706	708	707	710	715	722	713	711	723	721	714	693	695	702	698	701	705	705	708	704	707	708	708						
3	712	716	718	715	718	719	728	729	716	708	707	700	681	668	671	687	689	696	698	700	696	700	700	700	703						
4	702	706	708	706	709	714	719	717	700	690	700	705	700	683	687	680	678	686	692	699	703	703	701	702	700						
5	703	702	703	705	706	710	714	712	705	700	711	712	706	696	689	694	696	691	701	704	703	706	704	704	703						
6	704	706	706	707	709	710	706	698	691	694	705	711	712	707	706	705	704	699	698	703	705	709	710	710	705						
7	712	716	711	711	709	708	713	714	712	710	718	716	709	704	697	703	707	708	711	712	712	712	712	709	710						
8	706	711	715	710	713	717	711	699	695	701	704	695	694	710	719	719	714	702	682	690	699	704	716	706							
9	708	700	700	703	708	707	705	704	697	690	688	696	710	714	713	711	687	657	669	680	676	660	659	664	692						
10	695	736	679	639	633	661	661	629	597	579	590	607	614	628	635	638	648	654	657	658	657	657	662	664	645						
11	663	666	669	679	683	686	696	691	686	671	672	675	679	688	688	690	687	686	680	684	687	686	684	696	682						
12	676	686	685	685	701	700	709	714	698	674	688	671	665	669	675	685	682	684	687	688	696	692	690	691	686						
13	694	694	700	699	706	705	706	701	691	682	681	681	685	693	693	683	690	679	672	678	683	685	687	695	690						
14	693	693	692	693	699	702	705	700	695	688	689	690	686	679	680	686	688	692	692	699	698	695	699	690	693						
15	720	704	706	710	714	716	719	718	706	698	696	697	703	703	701	662	638	660	661	655	665	680	704	702	693						
16	691	690	697	703	706	703	711	713	703	694	672	650	652	654	657	653	653	643	673	673	684	687	687	688	681						
17	703	694	693	702	703	708	713	709	698	678	665	669	637	636	661	664	677	672	683	700	655	678	683	705	683						
18	701	686	681	688	689	702	698	704	707	709	687	657	658	660	661	668	671	685	687	681	687	685	687	687	685						
19	686	687	689	690	697	703	693	697	685	673	670	684	689	688	663	673	685	685	688	696	693	695	693	696	687						
20	702	707	702	693	700	702	696	686	682	665	670	680	686	690	693	691	687	690	696	709	717	701	691	693	693						
21	694	699	704	703	705	702	713	710	700	691	690	693	694	695	694	698	699	700	699	718	706	697	699	703	700						
22	722	704	704	706	710	711	706	698	690	683	687	688	680	676	692	698	701	699	697	696	696	705	706	702	691						
23	699	699	701	702	703	709	716	720	714	706	709	709	710	714	712	709	712	716	718	720	714	708	699	692	709						
24	692	690	695	695	696	699	713	716	712	715	716	715	714	710	700	697	686	688	681	692	712	700	695	731	702						
25	697	696	691	693	694	698	709	704	696	694	680	670	671	676	672	669	669	683	682	678	686	693	690	691	687						
26	691	696	696	697	700	701	702	697	688	681	688	684	689	680	688	685	682	686	681	684	694	699	699	699	691						
27	699	700	696	703	700	700	703	700	696	693	692	695	693	695	695	698	700	699	689	697	693	694	698	700	697						
28	701	702	702	703	706	709	711	700	691	695	703	709	707	703	699	683	668	680	698	688	685	689	695	684	696						
29	682	684	683	684	690	701	715	712	704	703	704	706	714	722	713	675	637	629	656	682	690	685	683	695	689						
30	693	694	694	698	706	712	711	702	694	694	694	658	665	671	677	688	688	685	699	704	701	699	706	723	694						
31	700	698	695	695	697	707	714	713	702	694	693	698	695	682	678	677	681	678	677	674	675	671	668	676	689						
MEAN	698	699	697	698	701	705	708	705	696	689	689	688	687	685	687	686	684	684	688	692	693	693	694	697	693						
MEAN Q	706	707	706	707	708	710	711	709	702	700	709	710	704	695	696	700	701	700	702	704	705	707	708	707	705						
MEAN D	702	702	691	688	689	698	700	695	682	672	662	656	653	656	663	657	663	672	673	670	679	685	689	677							

Fig. 1. Table of HMVs of Panagyurishte (PAG) observatory for the H component in January 1983

Presently, hourly mean values are based on the digital recordings of the three-component fluxgate magnetometer FGE. The baseline of this magnetometer is determined from absolute measurements with a DI-flux theodolite and an Overhauser proton magnetometer.

Before calculating the HMVs, inspection and verification of the reported data was performed. The reported data (available in near real time) are usually used in applications where the reliable representation of higher-frequency magnetic field variations is more important rather than absolute levels or secular variation. This concerns, e.g. the forecast of magnetic activity, radio-wave propagation, or space weather. In the case of reported data it is not possible to verify them prior to dissemination. Careful monitoring of the automatically transmitted data and the present-day computer technologies enable us to improve the quality of data and reduce the number of gaps in the records. After the quality control procedures have been applied to the 2012 reported data, we obtained the quasi-definitive minute mean values and calculated the HMVs.

Monthly elements' plot of the hourly mean values of the Declination (D), Horizontal (H), and Vertical (Z) field components for 2012 are shown in next figures:

Definitive Hourly Mean Values

January 2012

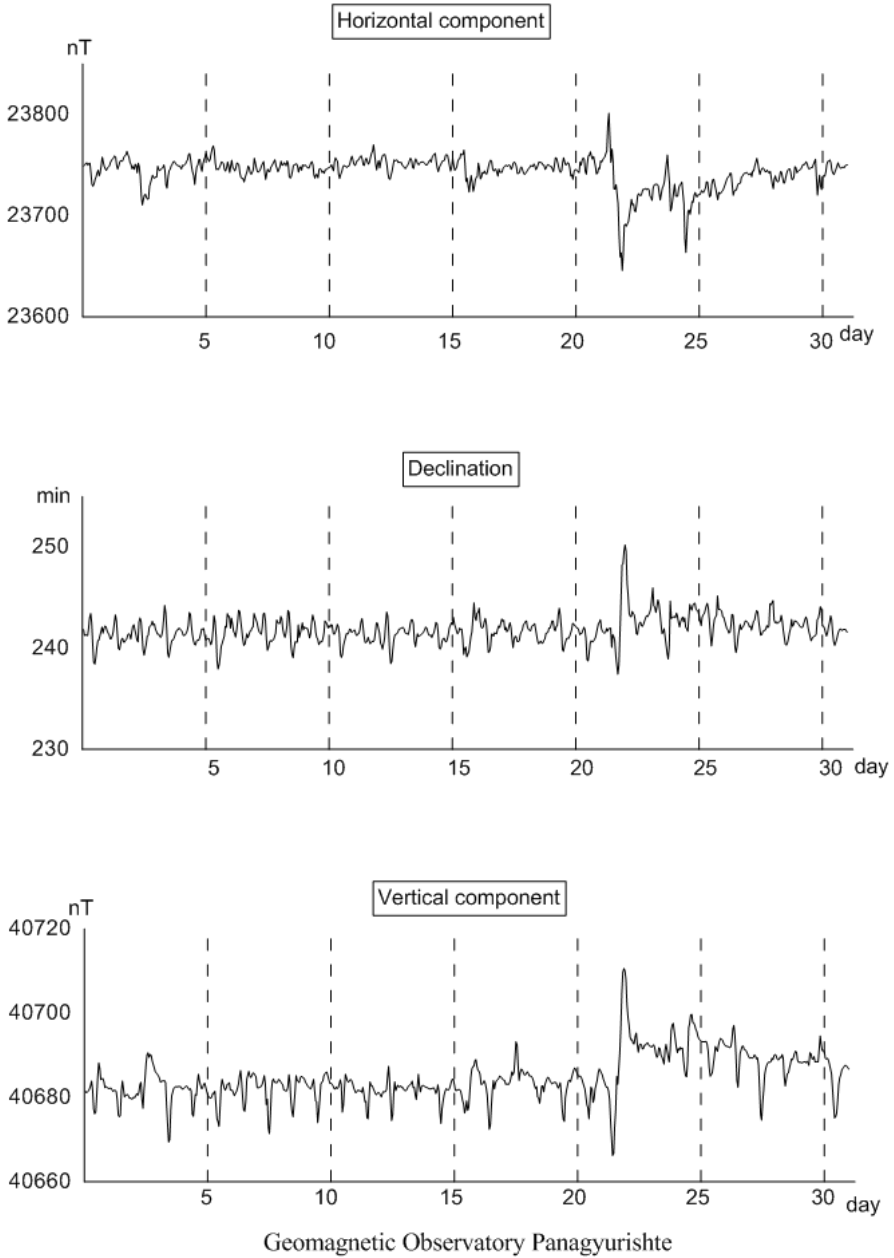


Fig. 2. Plot of the hourly mean values of the geomagnetic field components registered in PAG observatory for January 2012.

Quasi-Definitive Hourly Mean Values

February 2012

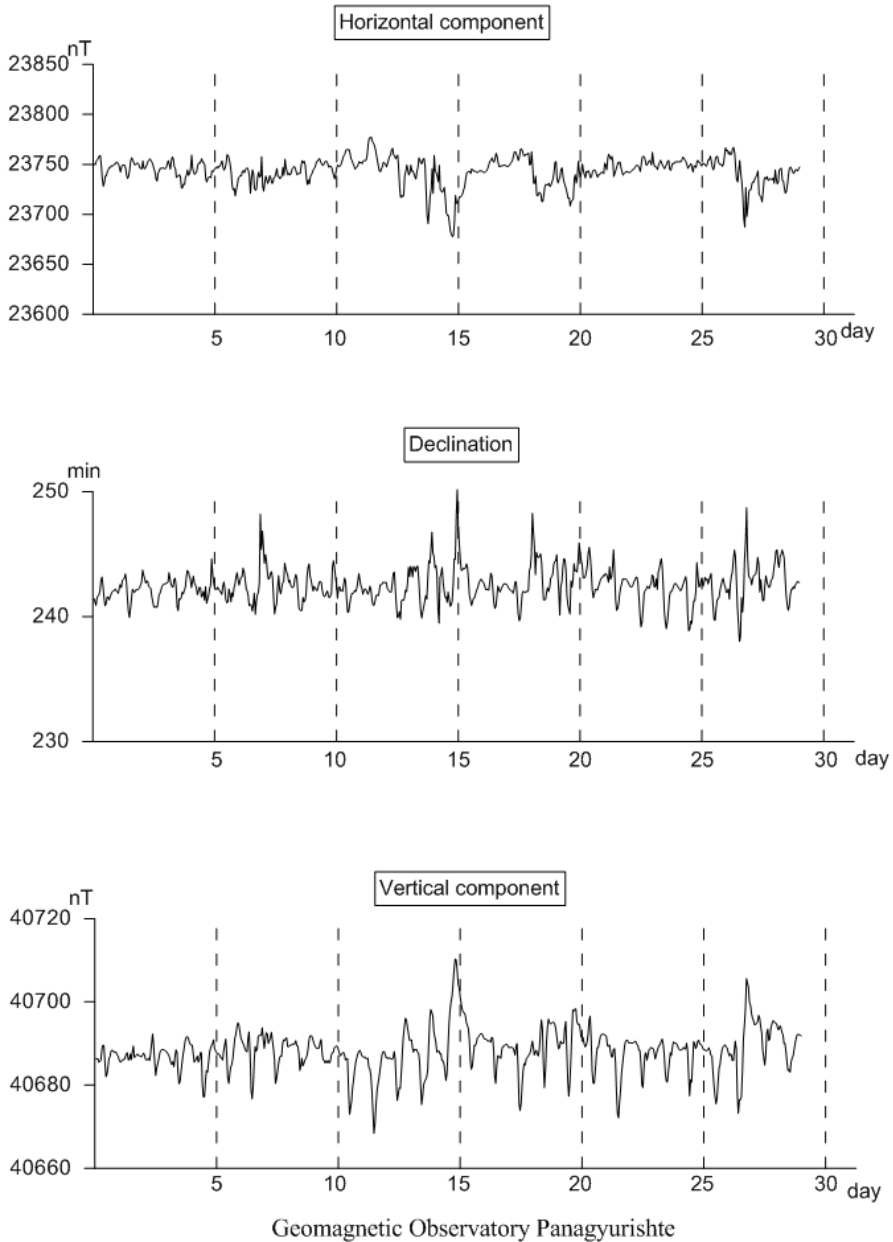


Fig. 3. Plot of the hourly mean values of the geomagnetic field components registered in PAG observatory for February 2012.

Quasi-Definitive Hourly Mean Values

March 2012

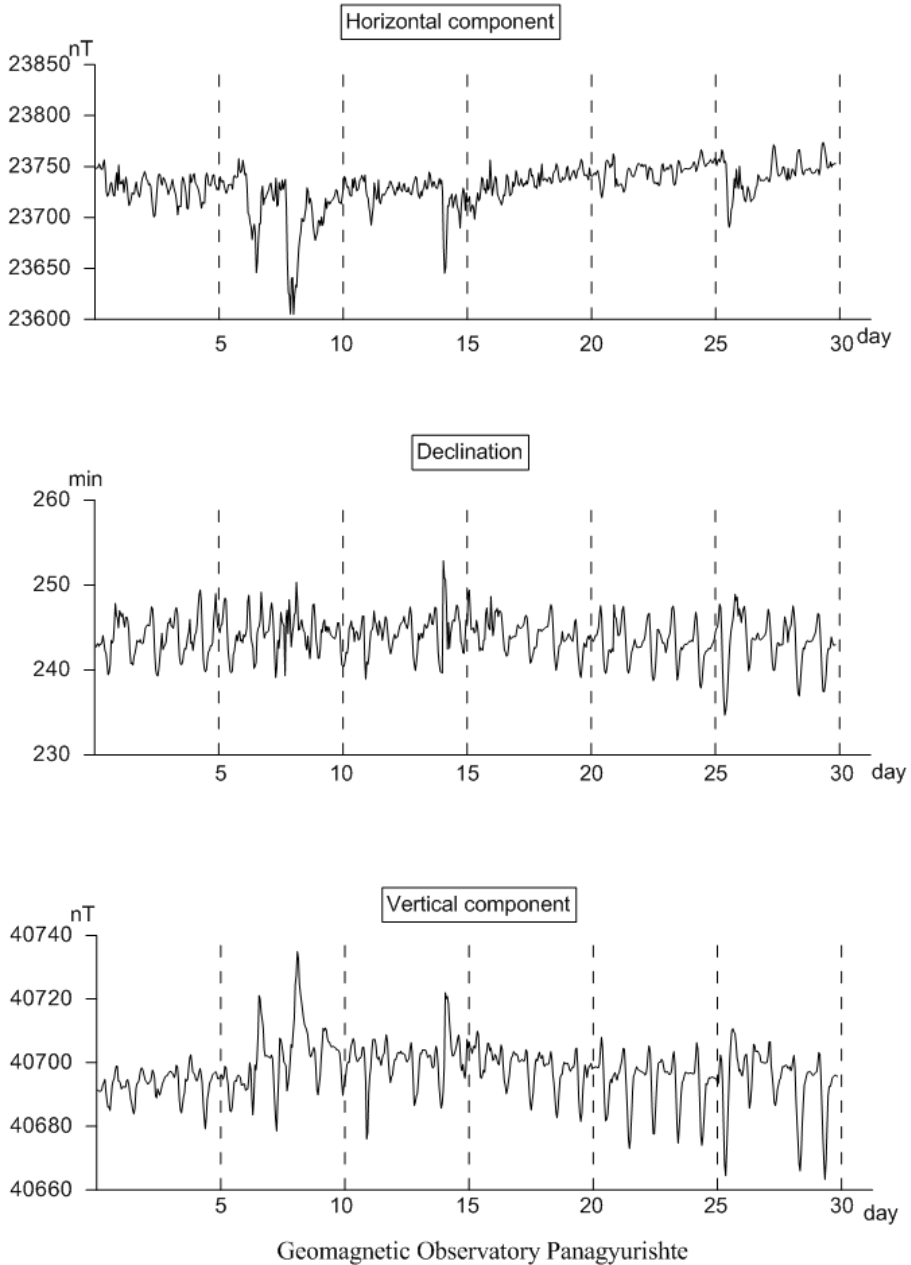


Fig. 4. Plot of the hourly mean values of the geomagnetic field components registered in PAG observatory for March 2012.

Quasi-Definitive Hourly Mean Values

April 2012

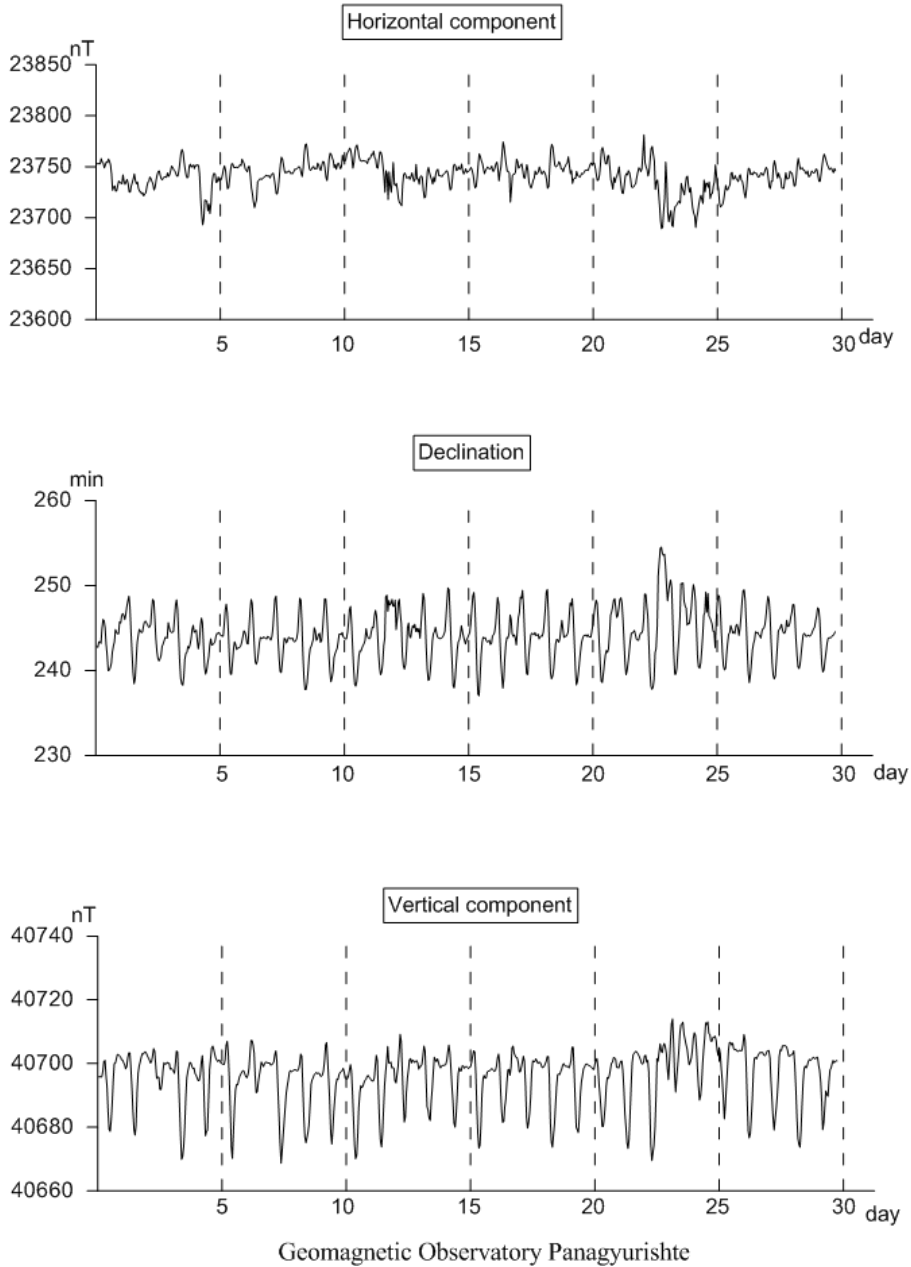


Fig. 5. Plot of the hourly mean values of the geomagnetic field components registered in PAG observatory for April 2012.

Quasi-Definitive Hourly Mean Values

May 2012

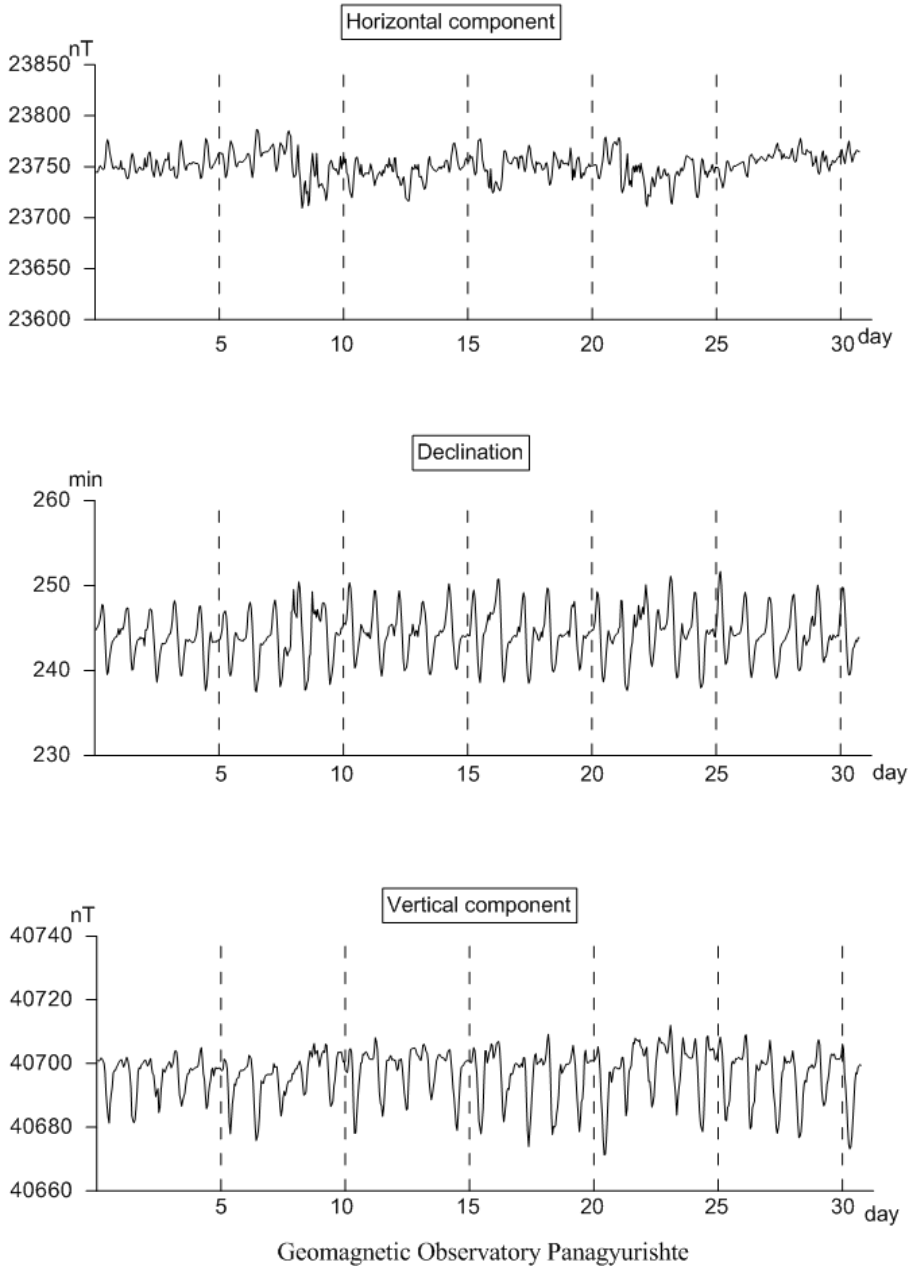


Fig. 6. Plot of the hourly mean values of the geomagnetic field components registered in PAG observatory for May 2012.

Quasi-Definitive Hourly Mean Values

June 2012

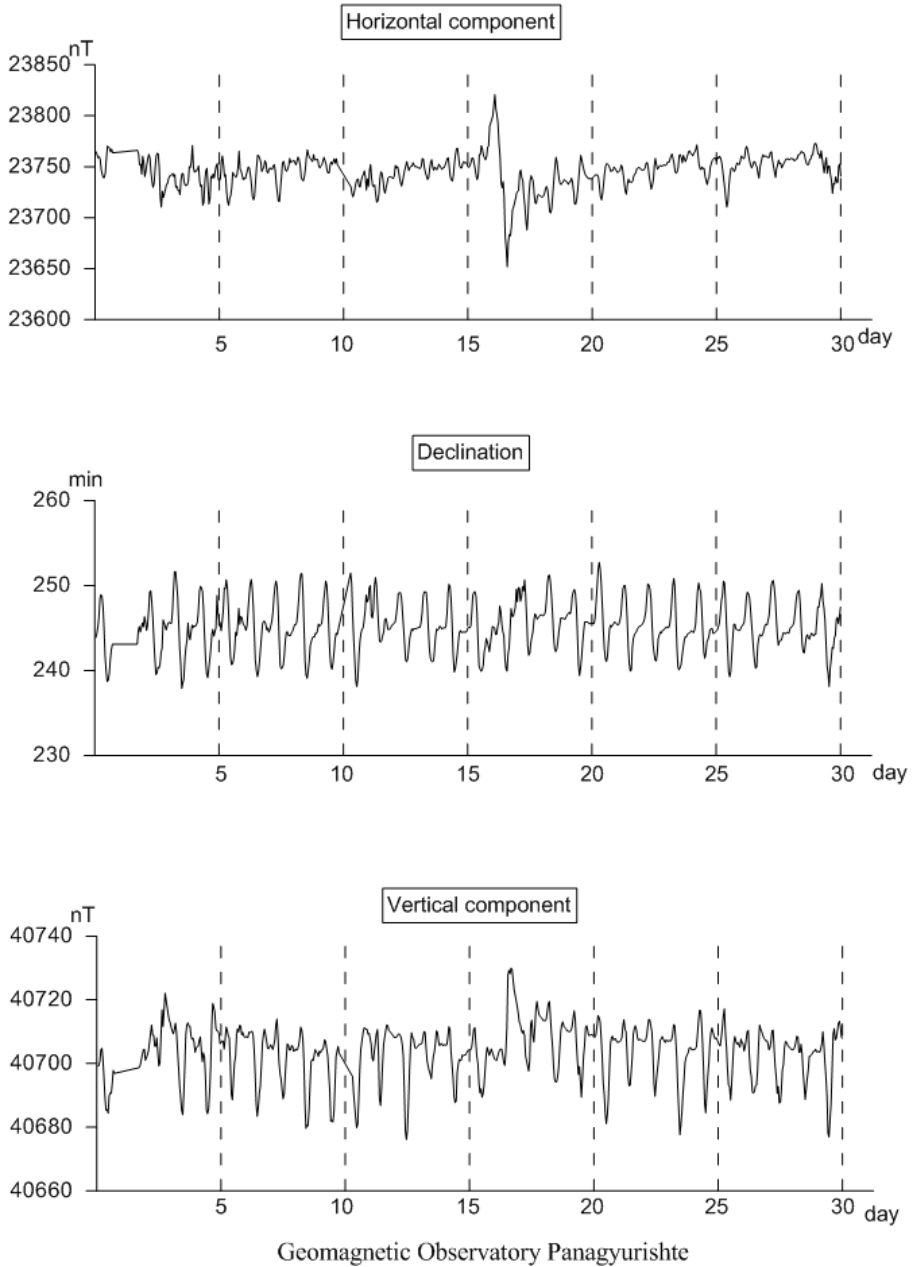


Fig. 7. Plot of the hourly mean values of the geomagnetic field components registered in PAG observatory for June 2012.

Quasi-Definitive Hourly Mean Values

July 2012

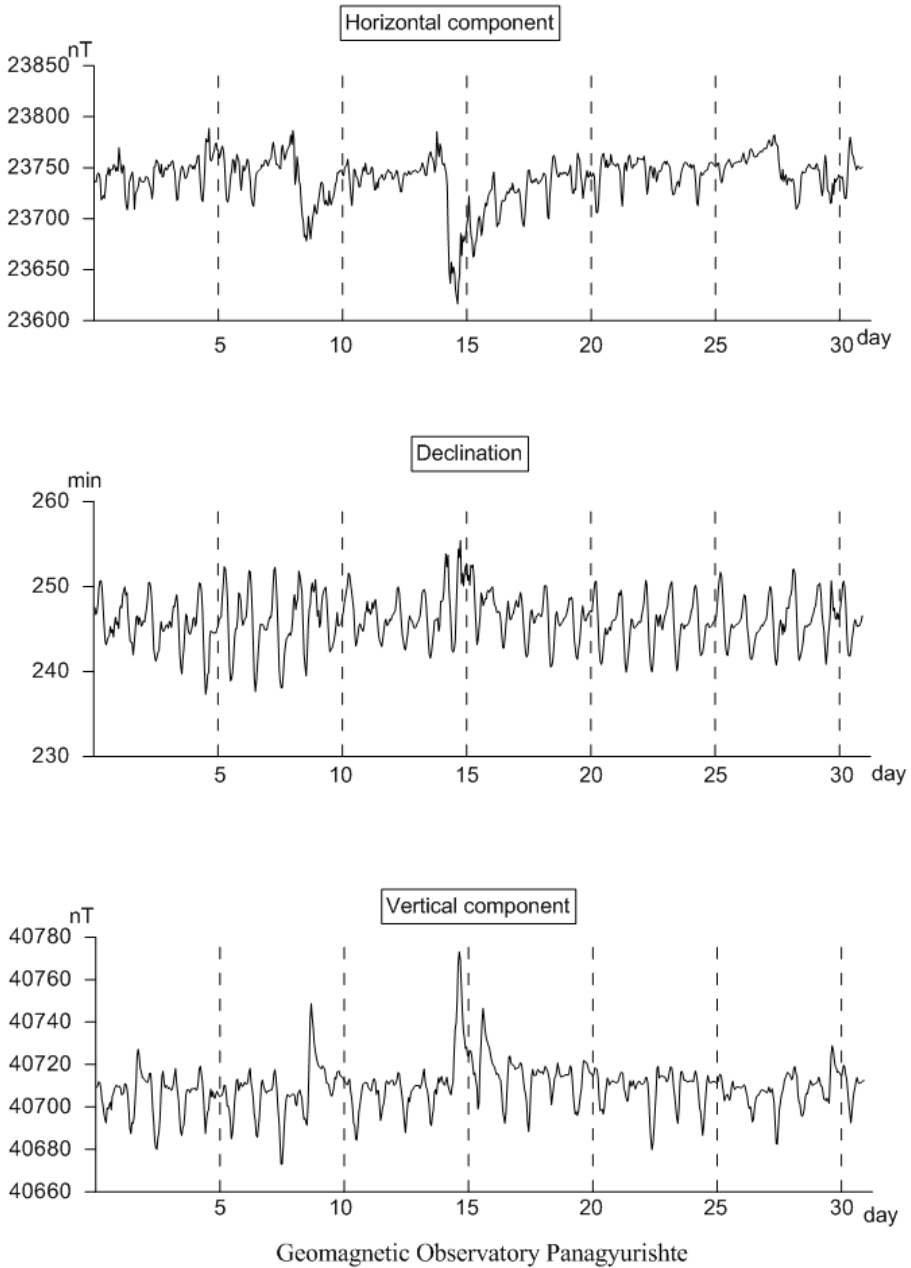


Fig. 8. Plot of the hourly mean values of the geomagnetic field components registered in PAG observatory for July 2012.

Quasi-Definitive Hourly Mean Values

August 2012

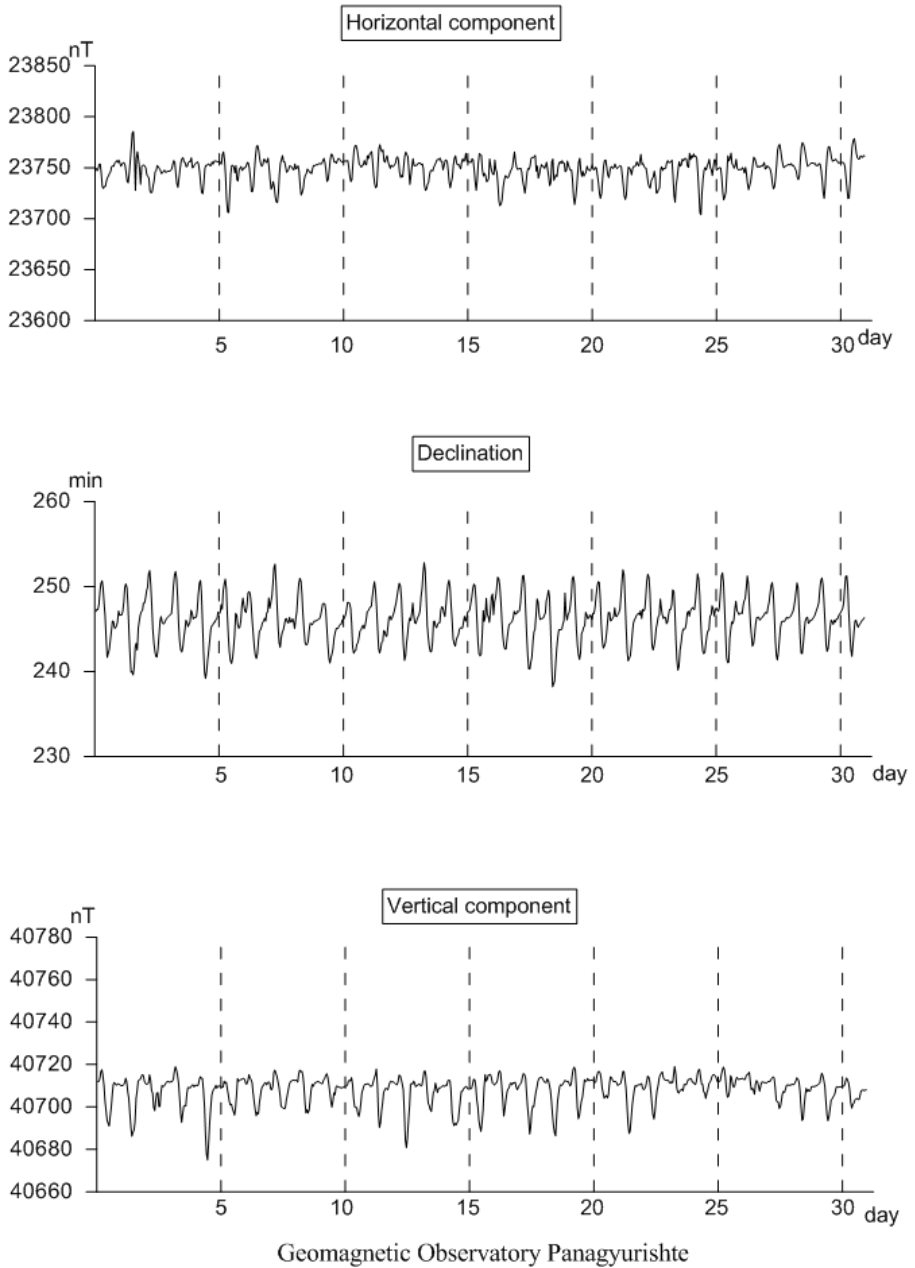


Fig. 9. Plot of the hourly mean values of the geomagnetic field components registered in PAG observatory for August 2012.

Quasi-Definitive Hourly Mean Values

September 2012

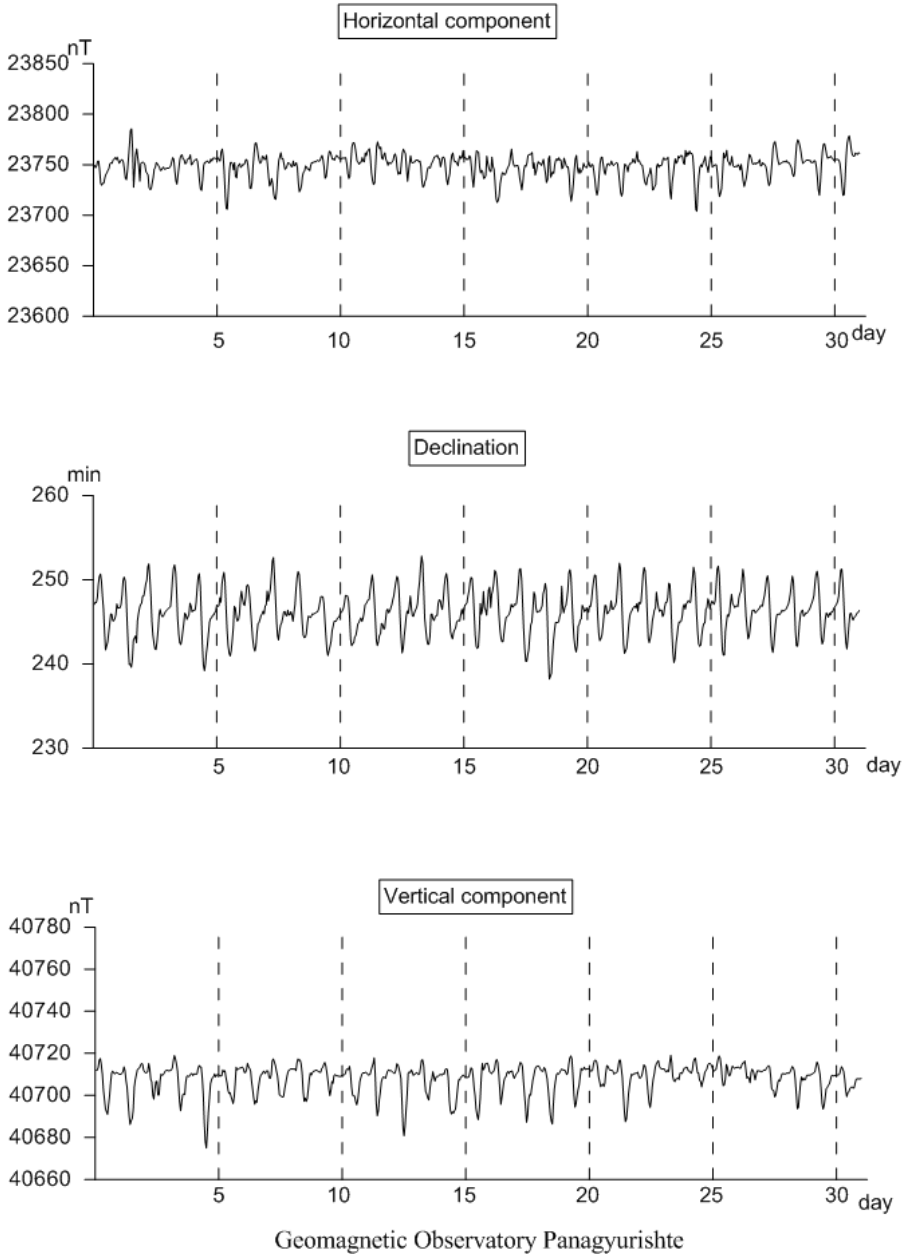


Fig. 10. Plot of the hourly mean values of the geomagnetic field components registered in PAG observatory for September 2012.

Quasi-Definitive Hourly Mean Values

October 2012

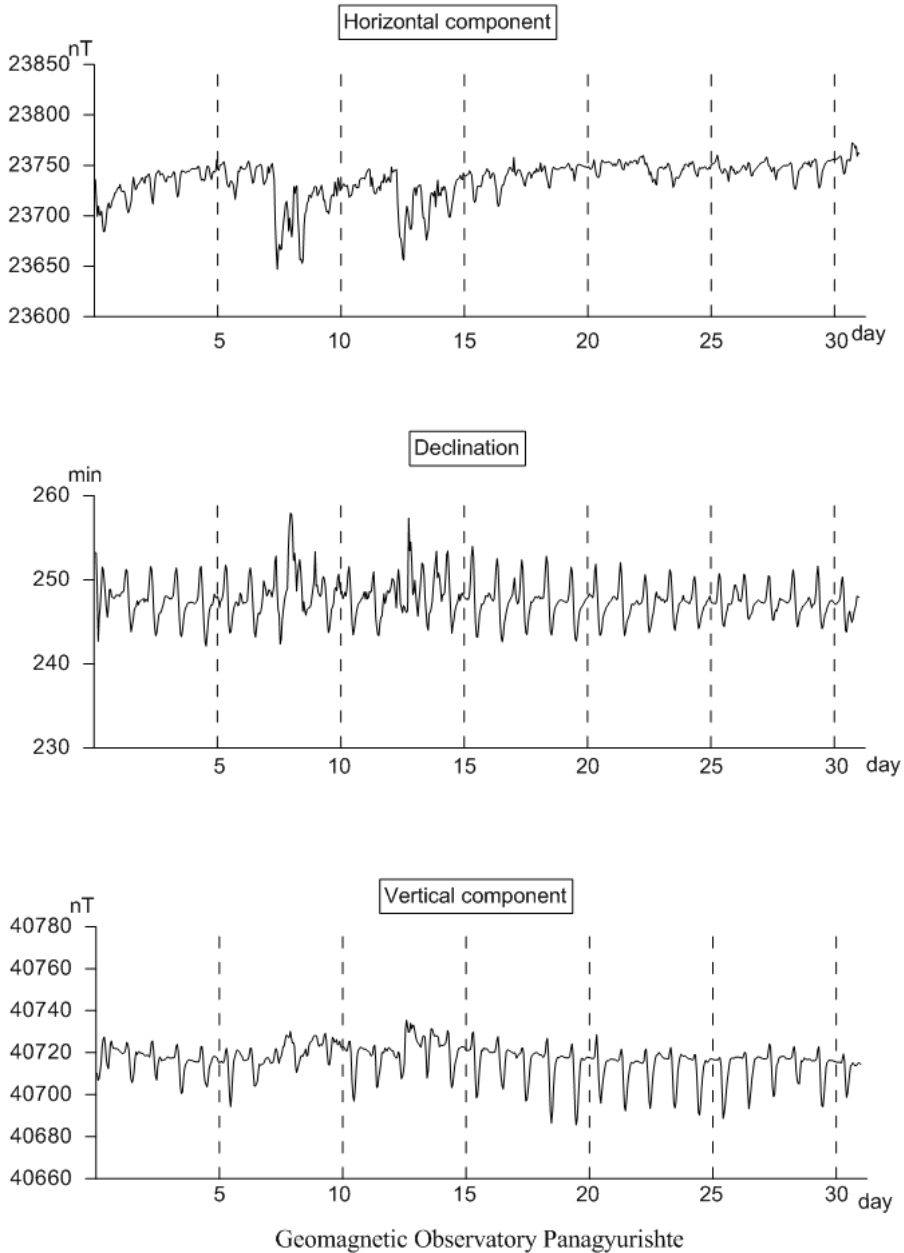


Fig. 11. Plot of the hourly mean values of the geomagnetic field components registered in PAG observatory for October 2012.

Quasi-Definitive Hourly Mean Values

November 2012

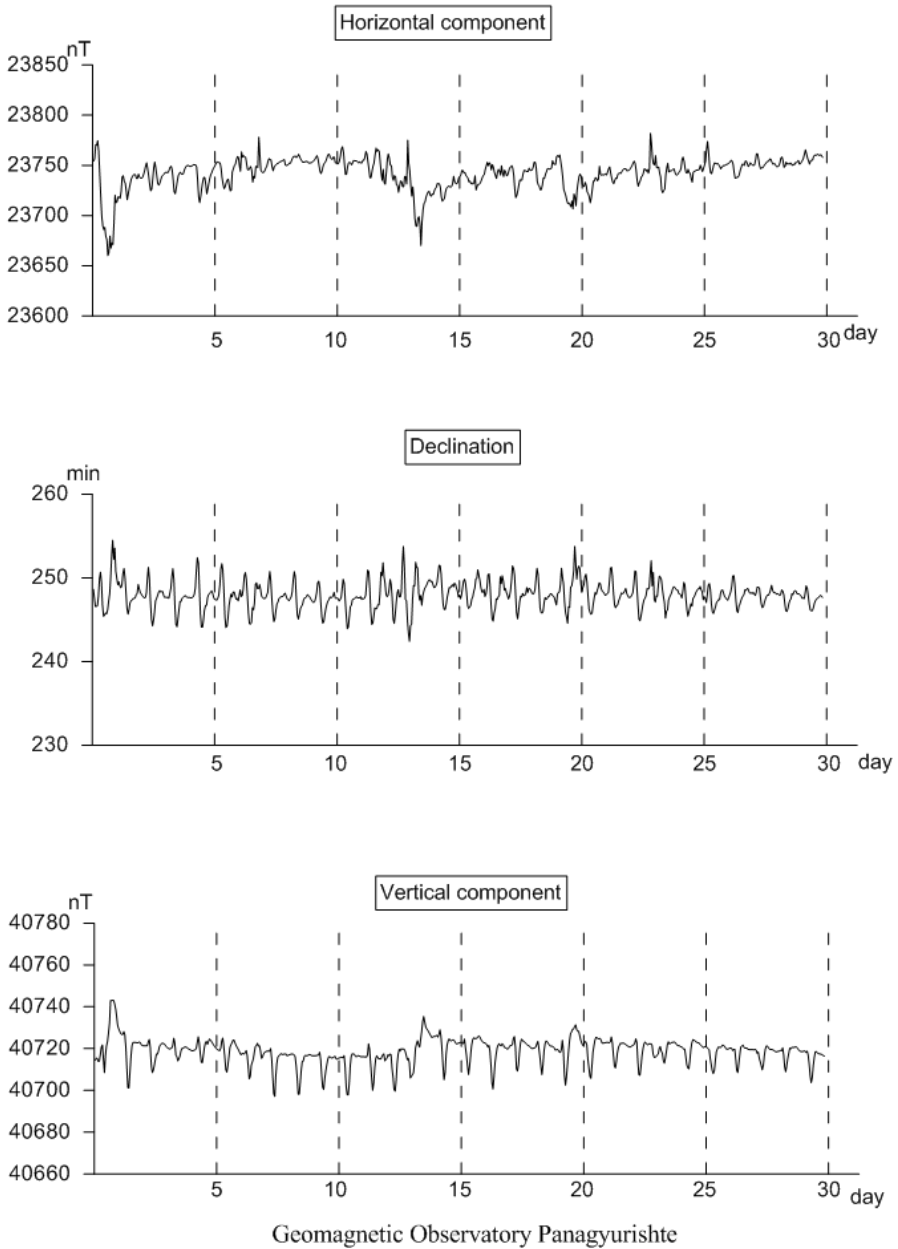


Fig. 12. Plot of the hourly mean values of the geomagnetic field components registered in PAG observatory for November 2012

Quasi-Definitive Hourly Mean Values

December 2012

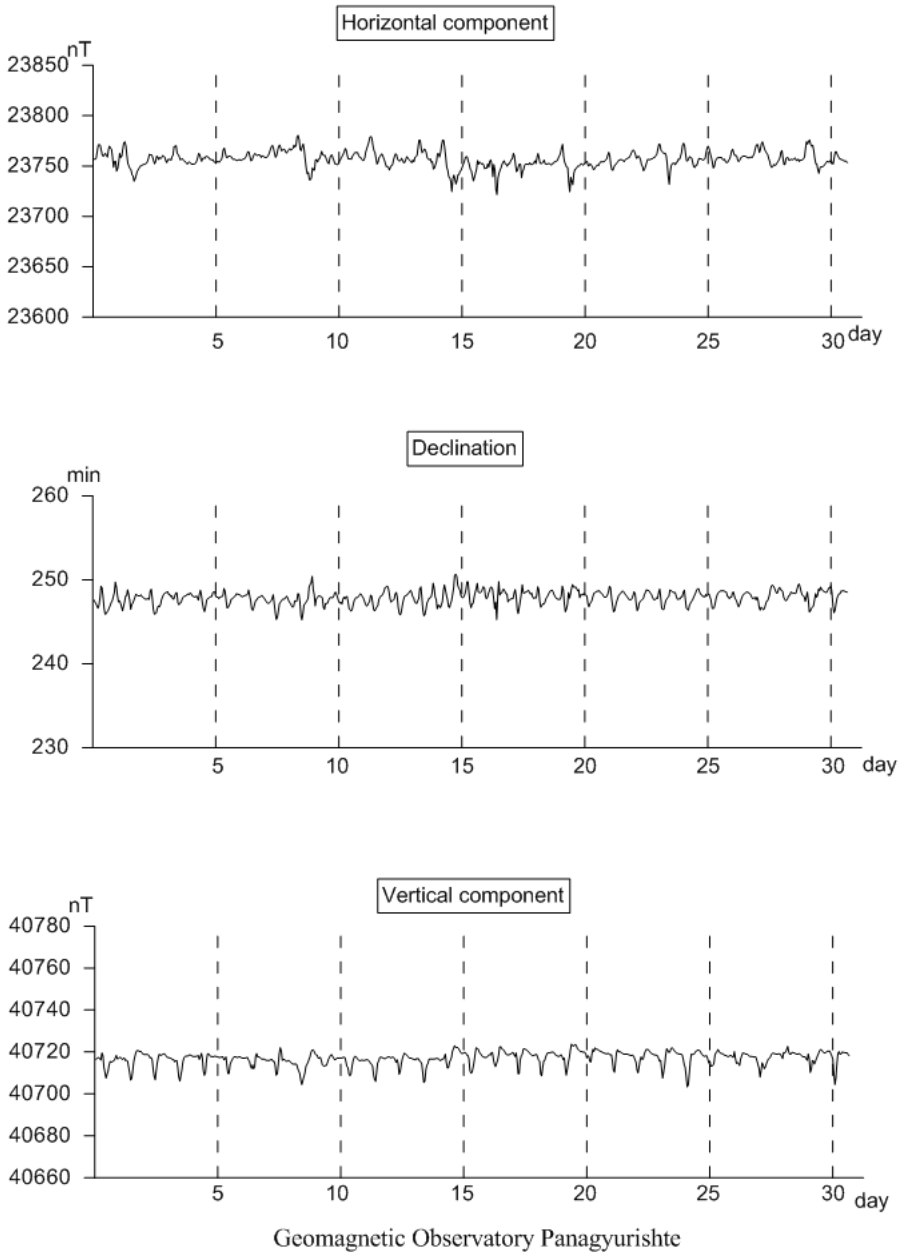


Fig. 13. Plot of the hourly mean values of the geomagnetic field components registered in PAG observatory for December 2012.

Conclusions

Continuous registration of the geomagnetic field components gives the sum of all field contributions from the sources internal and external to the Earth. A straightforward separation of the the individual contributions is impossible and many scientific studies deal with different aspects of this problem (Mandea nad Korte, 2010). Approximate description of the strength of different external variations , however, are provided by geomagnetic indices. A quantitative measure of the 2012 local geomagnetic activity in the form of 3 hour *K*-index is published here, based upon the range of fluctuations in the PAG observatory traces over 3 h. intervals. Tables shows that 2012 has relatively quiet geomagnetic field. Monthly variations of the geomagnetic field components are plotted by means of hourly mean values. Data are checked and verified according to IAGA requirements (Jankowski and Sucksdorff, 1996).

Acknowledgments. We would like to thank Dr. Hans-Joachim Linthe and all the experts from Adolf-Schmidt Observatory in Niemegk and Section 2.3 "Earth's Magnetic Field" of GFZ-Potsdam for the scientific and technical support which they provide to PAG Observatory.

References

- Buchvarov I., 2006. Field and observatory geomagnetic measurements in Bulgaria. in Rasson and Delipetrov (*eds.*) *Geomagnetics for Aeronautical Safety*, Springer, p.61-62
- Jankowski J., Sucksdorff C., 1996. *Guide for magnetic measurements and observatory practic.*, International Association of Geomagnetism and Aeronomy, Warsaw, Poland.
- Mandea M., Korte M. (*eds.*), 2010 *Geomagnetic observation and models*, IAGA Special Sopron Book Series 5, Springer.

Годишен доклад за наблюдаваната геомагнитна активност в Обсерватория Панагюрище

П. Трифонова, М. Методиев

Резюме: Понастоящем, в ерата на интернет комуникациите, записите от геомагнитните обсерватории се предоставят на заинтересованите потребители почти в реално време, докато обработените времеви серии (окончателни данни) са обект н амного проверки и се разпространяват с месеци закъснение. Настоящият доклад представя квази-окончателни геомагнитни данни, получени в Обсерватория Панагюрище през 2012 г., изготвени под формата на локални геомагнитни индекси и графики на средночасовите стойности на компонентите на магнитното поле. Верификацията на данните е извършена в съответствие с изискванията на IAGA.

LIDAR INVESTIGATIONS OF THE TROPOSPHERE PERFORMED DURING SUMMER 2011 MEASUREMENT CAMPAIGN

A. Deleva

Institute of Electronics, 72 Tsarigradsko Chaussee Blvd., 1784 Sofia, Bulgaria, e-mail: adeleva@ie.bas.bg

Abstract. Lidar investigations of the troposphere, made over the city of Sofia from May to August 2011, are described. Regular EARLINET weekly measurements were performed in that period as well as everyday lidar observations of the atmosphere during the eruption of the Grimsvötn Island volcano and during Saharan dust incursion. Lidar measurements are performed with an aerosol lidar equipped with Nd:YAG laser. Lidar data are presented in terms of vertical atmospheric backscatter coefficient profiles and color maps of the aerosol stratification time evolution. HYSPLIT (HYbrid Single-Particle Lagrangian Integrated Trajectory) backward trajectories and DREAM (Dust REgional Atmospheric Model) forecasts are employed to make conclusions about atmospheric aerosol's origin. It was concluded that the atmosphere above Sofia was not polluted with volcanic aerosols ejected during the Grimsvötn volcano eruptions from 21-28 May 2011. However, thick urban aerosol layers over Sofia have been registered during the summer months. Reported experimental examples are extracted from regular lidar investigations of the atmosphere within the frame of European project EARLINET.

Key words: lidar, aerosols, clouds, Saharan dust, troposphere.

Introduction

Aerosols, very small particles in the air, play an important role in the global climate changes and influence on the ecological state of the environment. They are a significant source of direct and indirect effects on the planetary radiative budget. Atmospheric particles determine the positive or negative radiative forcing in function of its size, chemical composition, spatial and temporal distribution. The height and size distributions of aerosols are critical to all climate influences. Atmospheric particles have a direct radiative forcing because they scatter and absorb solar and infrared radiation in the

atmosphere. They also alter the formation and precipitation efficiency of liquid-water, ice and mixed-phase clouds, thereby causing an indirect radiative forcing associated with these changes in cloud properties. Aerosol-cloud interaction is recognized as one of the key factors influencing cloud properties and precipitation regimes across local, regional, and global scales and remains one of the largest uncertainties in understanding and projecting future changes (J.E. Penner et al., 2001; Guibert, S. et al., 2005; Solomon, S. et al., 2007).

There is a natural aerosol component consisting mostly of soil dust, sea salt, biogenic and organic matter that is geographically and seasonally variable. Among the different types of aerosols, Saharan dust is the dominant natural components in the troposphere (Gian Paolo Gobbi et al., 2000; Perez L. et al., 2008, Sassen K. et al., 2003, U. Pöschl, 2005). Similarly, major volcanic eruptions, which occur infrequently and presumably randomly, inject large quantities of volcano ash and gases into the atmosphere at significant heights. Winds can transport the ash and gases rapidly and in multiple directions which depend on the wind speed and wind direction so that transport is possible over long distance in just a few hours (Ansman A. et al., 1997; Hansell A. L. et al., 2006; A. Schreiner et al., 2004; Kelly P. M. et al., 1996). There is also an anthropogenic component that is linked to fossil-fuel and biomass burning, as well as other human activity. This component has been steadily increasing with global industrialization and urbanization. In highly populated and industrialized regions and in areas of intense agricultural burning the aerosol forcing is much stronger than the globally averaged one, contributing to the global warming. Aerosols, when concentrated near the surface, have long been recognized as affecting pulmonary function and other aspects of human health (N. Sabbagh-Kupelwieser et al., 2010; E. Katragkou et al., 2009; Tasić M. et al., 2006). Urban air consists of a significant fraction of sub micrometer and ultra fine particles (urban aerosols, smog), which give a small contribution to the particulate mass, but are said to be associated with a number of significant negative influences on human health. Smog is a type of air pollution derived from vehicular emission, internal combustion engines and industrial fumes. It can be formed in almost any climate where industries or cities release large amounts of air pollutions. During periods of sunny weather, when the upper air is warm enough to inhibit vertical circulation in the atmosphere, the smog resides for a longtime near the ground, over densely populated cities or urban areas and can reach dangerous levels. Such event is often observed in geologic basins encircled by hills or mountains.

Aerosol effects on the environment are very hard to quantify due to the fact that the amount and origin of atmospheric particles vary substantially with location and from year to years, and in many cases exhibit strong seasonal variations. Extending the principle of radar to the optical range, lidar (**L**ight **D**etection **A**nd **R**anging) technology has found use in many of today's aerosol investigations. The fast spread of lidars contributes to their organizing in lidar networks as EARLINET (European Aerosol Research Lidar Network) (EARLINET:<http://www.earlinet.org>). At present, 27 lidar stations distributed over Europe are part of the network. Main result of such cooperation is the establishment of a quantitative lidar dataset describing the aerosol vertical, horizontal, and temporal distribution, including its variability on a continental scale. Additional more specific measurements (on Saharan dust, volcanic ash, forest fire) are also included in the project work program (Papayannis A. et al., 2008). The joint analysis of lidar observations in

different locations is a useful approach for better understanding and interpretation of some regional aerosol events and their influence on the environmental conditions. Bulgarian lidar station at Sofia (Laser Radar Laboratory of the Institute of electronics, BAS) has been involved in coordinate regular measurements according to the schedule of the EARLINET project. Under appropriate weather conditions, we carry out measurements twice a week. Two night time measurements are performed every Monday and Thursday after sunset, while daytime measurements are performed every Monday at noon when the Sun is in its zenith. These times are selected in order to have one daytime measurement at a well-developed atmospheric planetary boundary layer (PBL) condition, and two observations with low-background light to monitor the aerosol layer developed during the day. When special aerosol loading is forecast, the regular schedule of measurements is altered and more observations are conducted in view of obtaining as full as possible an image of the vertical distribution and temporal changes of the aerosol field over lidar station. Usually each lidar measurement lasts for 1-3 hours. The lidar signal is accumulated for 5-10 min (corresponding to data accumulation of 600-1200 different raw profiles received at each laser pulse). These profiles are subsequently summarized to cover 30-min time of observation in conformity with the EARLINET work protocol. During the EARLINET project, DREAM (Dust REgional Atmospheric Model) is used as one of the forecasting models to issue early warning of Saharan dust events over Europe (DREAM:<http://www.bsc.es/projects/earthscience/DREAM>). DREAM- weather forecast maps elaborated by Barcelona Supercomputing Senter gives an image of the wind direction and speed, position of cloud fields and magnitude of dust load in the atmosphere above North Africa and Europe. Also, information about the origin and path that the air-mass passed before their arrival over the lidar site we obtain from the HYSPLIT (HYbrid Single-Particle Lagrangian Integrated Trajectory) model (Draxler R. et al., 2003; Rolph G., 2011). It represents a complete system for computing simple air parcel trajectories to complex dispersion and deposition simulations. The calculations of backward air mass trajectories give a plot of the road that the air mass traversed for a chosen time period before to arrive to the location of lidar observations. Both DREAM and HYSPLIT models are freely available on the Web.

Lidar system and data processing

The Nd:YAG lidar used in the experiments was developed in the Laser Radar Laboratory (Atanaska D. Deleva et al., 2008; A. Deleva et al., 2010). The radiation source is a Q-switched frequency-doubled Nd:YAG laser (pulse energy up to 600 mJ at 1064 nm, 80 mJ at 532 nm; pulse duration 15 ns FWHM; fixed repetition rate 2 Hz; beam divergence 2 mrad). The lidar is mounted on a stable metal coaxial construction allowing reliable fixing and precise synchronized mutual motion (horizontal and vertical) of both the telescope and the output laser beam. The radiation backscattered by atmospheric molecules and aerosols is received by a Cassegrain-type telescope (aperture 35 cm; focal distance 200 cm). The parallel output beam formed by the telescope output optics is passed to a spectrum analyzer for separation of the incoming optical signals. The main lidar elements defining the measurement quality of the system are the photo-receiving modules and the unit

recording the sounding pulses. Each module of Nd:YAG lidar comprises a photo-receiving sensor, an amplifier, a high-voltage power supply, a 14-bit analog-digital converter (ADC), and a Hi-Speed 480 MHz USB 2.0 interface for computer connection. Received signals from the atmosphere are digitized every 100 ns with an ADC, resulting in a 15 m range resolution (about 7.5 m altitude resolution). Thus, the Nd:YAG lidar measures the temporal evolution of the aerosol field with high time and height resolution. The data acquisition software for calculating the atmospheric backscatter coefficient profiles is based on the widely used Klett-Fernald-Sasano algorithm (J. D. Klett, 1981; F. G. Fernald, 1984; Ya Sasano et al., 1985). The magnitude of this coefficient value is proportional to the aerosol density so the retrieved lidar vertical profile illustrates the stratification of the aerosol loading over the lidar station. We present here the results mainly in terms of vertical atmospheric backscatter profiles (x-axis represents the value of the calculated atmospheric backscatter coefficient; y-axis – the altitude above sea level, ASL). The measurement date and laser sounding wavelength are written over the lidar profile plot. Also in the paper we include the range-corrected signals (RCS) maps in order to display the temporal evolution of the aerosol loading of the atmosphere. RCS is produced by subtracting the estimated background noise from the raw lidar signal and multiplying by the square of the distance to the backscattering atmospheric sample.

The Nd:YAG lidar is configured in a mono-static biaxial alignment pointing at a slope angle of 32° with respect to the horizon, as determined by its position in the laboratory. Thus, although signals from as far as 30 km are being recorded, the maximum sounding height is limited to 16.4 km. The good parameters of all the laser, telescope, photo-receiving modules and software make it possible for the Nd:YAG lidar to be utilized for carrying out fast remote measurements of the atmosphere from 130 m above ground level (AGL) (approximately 700 m ASL) to the tropopause.

Lidar observations and discussions

In the end of May an alert was distributed to all EARLINET stations because on 21 May 2011 the Iceland's most active volcano, Grimsvötn, erupted, sending a plume of ash and steam to about 12-14 km high into the atmosphere and causing disruption to air travel in North-Western Europe. The eruptions ceased on 28 May 2011. The volcanic ash propagated quickly in the atmosphere traversing most of European countries. Its trajectories were forecasted by Navy Aerosol Analysis and Prediction System (NAAPS) (NAAP: <http://www.nrlmry.navy.mil/aerosol>) and observed by many meteorological stations, to prevent unintended consequences of the airplane transport. During Grimsvötn eruption all lidar stations of the EARLINET network performed a large campaign of observations to identify the location, height and thickness of volcanic aerosols transported in the air over Europe. As a partner in EARLINET project, Sofia lidar station accomplished monitoring of the atmosphere in the period 26-30 May, regardless that NAAPS didn't forecast that the atmosphere over Bulgaria will be polluted by volcanic aerosols. The experimental results from those investigations we describe by the vertical profiles of the atmospheric backscatter coefficient in Fig.1 and Fig.3. The height of the profiles on Fig.1 was limited to 5-6 km. because the atmosphere remained clear at higher altitudes and we didn't register neither

clouds nor aerosol layers. The decrease of the profile height makes it easier to visualize the mass stratification of the boundary aerosol layer with thickness of 3-4 km. The aerosol profiles show relatively large values of the atmospheric backscatter coefficient in the range of $2-3 \cdot 10^{-6} \text{ m}^{-1} \text{ sr}^{-1}$ for altitude 1.5-2.5 km. It can be assumed that the reason for this is not only the higher density of the aerosol particles at that altitude, but also the higher humidity of the air, as for the days of the investigations Barcelona Supercomputing Center (BSC) forecasted cloud cover over Bulgaria (the upper part of DREAM maps on Fig.2).

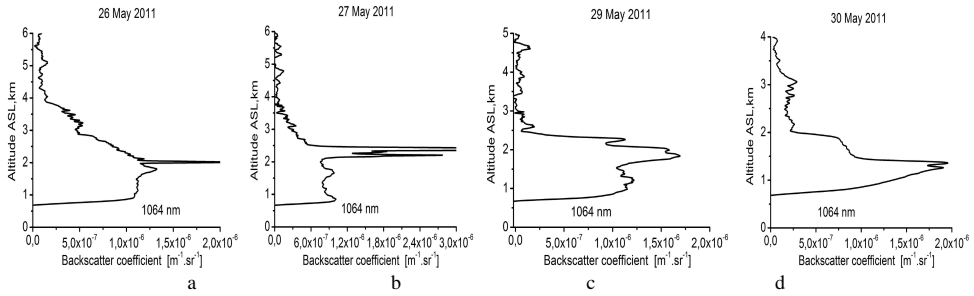


Fig.1. Lidar monitoring of the atmosphere performed on 26, 27, 29 and 30 June 2011. Atmospheric backscatter coefficient profiles retrieved on the basis of the lidar measurement data.

Regarding the nature of the particles in the observed thick aerosol layer immediately above the earth surface we could assume that they are either Saharan dust or have anthropogenic origin. The Balkans are located in the south-east part of Europe, thus continental type aerosols are dominant with industrial or transport influences. However, because they are situated in the eastern Mediterranean basin, the most relevant in the characterization of aerosol properties is the African-desert dust which distorts the atmospheric composition. We have to discard the possibility that in the end of May 2011 in the atmosphere over Sofia there were desert aerosols, because the lower part of the DREAM maps on Fig.2 and Fig.3 shows that Saharan-dust transport over Bulgaria is not expected for the measurement period 26-30 May.

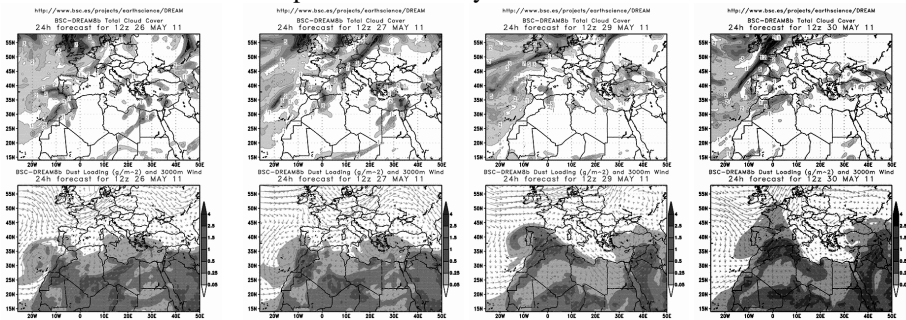


Fig.2. Forecast maps provided by Barcelona Supercomputing Center (BSC) showing no-Saharan-dust transport over Bulgaria for the days of lidar observations (26, 27, 29 and 30 June 2011).

The results of the investigation on 28 May are shown on a separate figure (Fig.3). In that day except for the low-situated stable aerosol layer, observed the whole week above the city, for a short period (about 1 hour) we registered additionally Cirrus cloud in the

altitude range 9-11 km. Cirrus clouds are formed in the upper levels of the troposphere at heights greater than 6 km. As a general rule, Cirrus clouds are thin enough to be transparent or very close to it, because humidity is low at such high altitudes (Prabhakara C., 1993, S. Veerabuthiran, 2004; Satyanarayana, M., 2008). Also, Cirrus clouds sometimes have a short lifetime. The RCS-map (Fig.3.c) illustrates that natural characteristic of theirs. It is observed that in the beginning of the monitoring Cirrus cloud was practically transparent, then it became denser, cloud's base lowered to about 9 km and after that Cirrus cloud got totally dissolved.

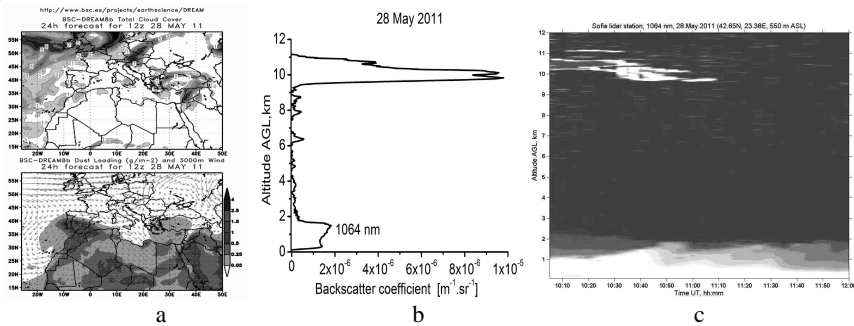


Fig.3. Lidar measurement performed on 28 May 2011. Forecast map provided by Barcelona Supercomputing Center (BCS) showing no-Saharan-dust transport over Bulgaria (a). Backscatter coefficient profile and RCS-map of the time evolution of the aerosol load (b, c).

The most important conclusion from the described investigations is that the atmosphere above Sofia was not polluted with volcanic aerosols ejected during the Grimsvötn eruptions from 21-28 May 2011. However for the whole week of the lidar investigations the air above the city up to altitude of 3-4 km was continuously loaded with aerosols. Those altitudes exceed the maximum top limit of the well developed planetary boundary layer over Sofia which for summer is estimated to be 1800 m (Ts. T. Evgenieva et al., 2009). The planetary boundary layer (PBL) is the lowest layer of the atmosphere, where practically most of the aerosols originating from human activities are situated. Its top limit marks the height of the convection process due to the diurnal cycle of warming and cooling of the Earth surface. The air quality over an urban area depends on the solar radiation reaching the PBL, local pollution sources and processes of vertical mixing and advection. Sofia is situated in a valley surrounded by mountains. Sometimes local meteorological conditions create inversion of the temperature in altitude, which on the other hand suppresses the air circulation. As neither other source of aerosols, nor dust transport from Sahara over the Balkans was forecasted in the end of May 2011, our conclusion was that the smog of human activities and traffic in town caused the observed relatively thick aerosol aggregation.

Barcelona Supercomputing Center forecasted Saharan dust transport above Bulgaria for the period 7-9 June, 2011. We performed lidar measurements every day and we show the results by the atmospheric backscatter profiles on Fig.4. Three profiles are retrieved each averaged for 30 min interval (corresponding to data accumulation of 3600 different raw profiles received at each laser pulse).

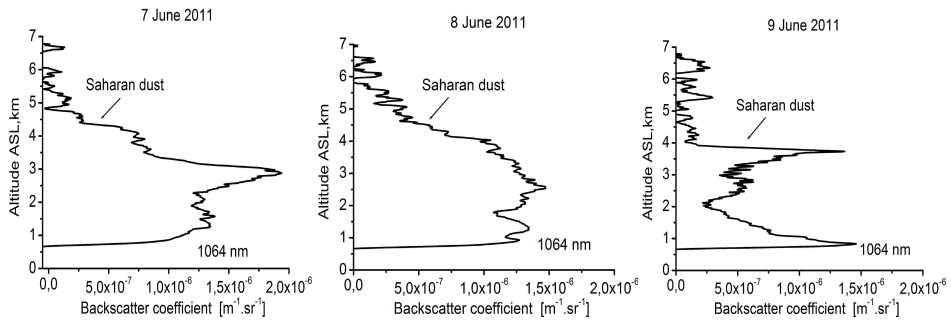


Fig.4. Atmospheric backscatter coefficient profiles, retrieved on the base of the lidar measurement data, obtained during Saharan dust incursion above Sofia, 7-9 June, 2011.

We were performing the investigations in the three days at time interval 9-12 AM. At that time we have registered the stable persistence of aerosol layers above PBL. During the first two days the layers had a top limit 5-6 km, the center of their mass was about 2.5 km, the concentration of particles above it gradually decreased with altitude increase and the border of layers with PBL (about 1.5 km) was expressed mildly. On 9 June we registered change in the aerosol stratification above PBL. The top limit had lowered to 4 km and at that altitude the layer was most dense.

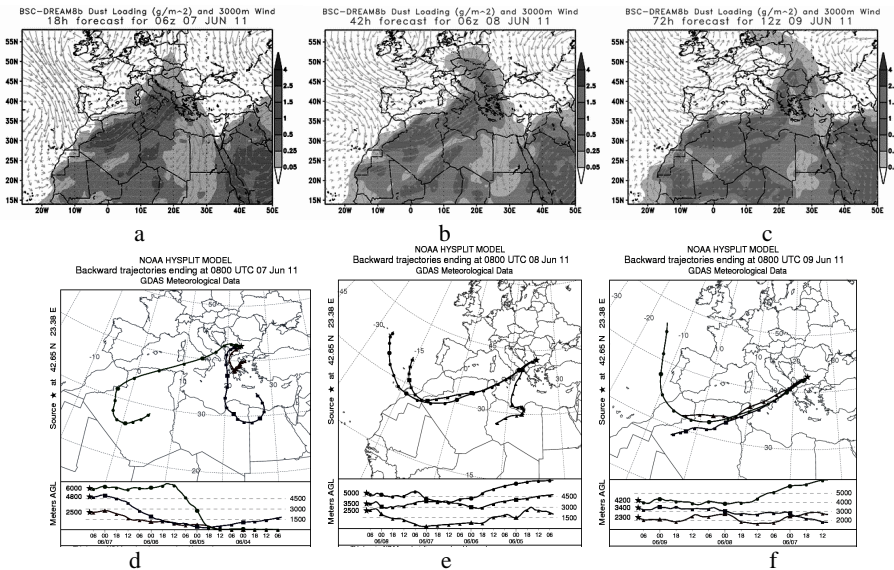


Fig.5. DREAM-forecast maps (a-c), provided by Barcelona Supercomputing Center (BCS) showing Saharan-dust incursion over Bulgaria, 7-9 June, 2011. HYSPLIT-model backward trajectories (d-f) for the days of lidar observations.

With decrease of altitude the concentration of particles decreased sharply and reached its lowest value just above PBL, where the border between the two layers (at altitude 2 km) is highly pronounced. We used information provided by DREAM and HYSPLIT models in order to make conclusions about the origin of the aerosols observed by the lidar. The

corresponding forecast maps are shown on Fig.5. The DREAM maps (Fig.5.a-c) show that dense Saharan dust covered the area of Bulgaria. For the measurement days we calculated HYSPLIT backward trajectories for 100 hrs duration in the altitude range 1.5-6 km. The black-and-white image makes hard distinguishing the trajectories in altitude, so we will clarify it in more detail. It is necessary especially for 7 June (Fig.5 d). The trajectories in the altitude range 1.5-2.5 km (on Fig.5.d is include one of them at 2.5 km only) start over close to Bulgaria regions, which atmosphere was loaded with Saharan dust. It is visible on the lower part of the HYSPLIT map that the air masses which during the measurement were above Sofia at altitude 2.5 km before have moved directly above the Earth surface. Therefore we infer that the air above Sofia up to height of 2.5 km contained substantial amount of anthropogenic aerosol and ones emitted by the Earth surface. The higher calculated trajectories up to 6 km start over African desert regions or near the Sahara surface, illustrated by the included trajectories at 4.8 and 6 km (Fig.5 d). The HYSPLIT information leads us to the conclusion that the air masses in the upper part (3-5 km) of the registered aerosol layer consisted mainly of desert aerosols. For the remaining two days (8 and 9 June) it is not necessary to describe the backward trajectories in the altitude range 2.3-5 km because it is obvious that they pass over Sahara desert and across the highly dusted space over Mediterranean Sea before the end point above Sofia. All information about aerosol layer origin, its altitude above ground, persistence during lidar observations, confirmed the conclusion of a long-distance Sahara dust transport above Sofia from 7 to 9 June 2011 in the altitude range 2-5 km, where we most often register desert aerosols

Up to the end of June Barcelona Supercomputing Center didn't forecast other Saharan dust outbreaks over Bulgaria. But EARLINET community was again mobilized in the last days of the month because in some lidar stations in Italy and Germany were registered a layer at 16 km and a weaker layer at about 12 km.

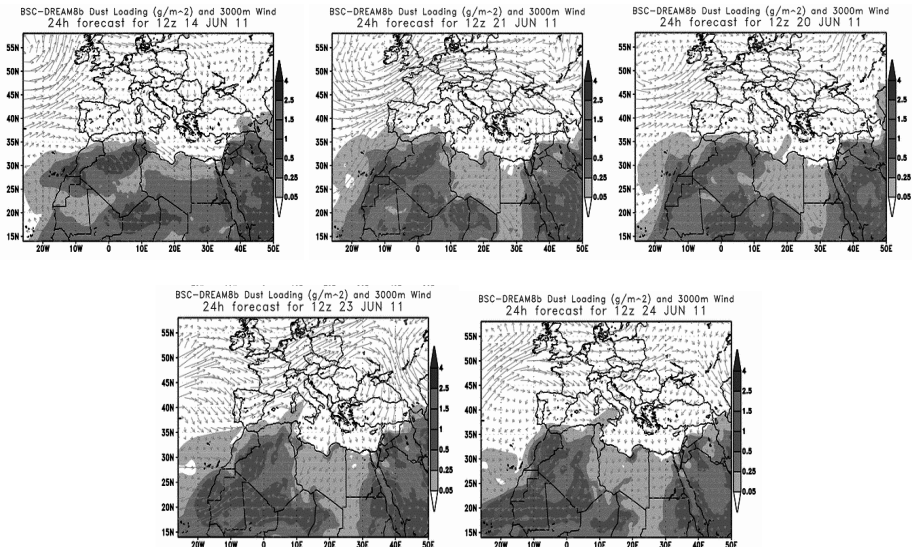


Fig.6. Forecast maps provided by Barcelona Supercomputing Center (BSC) showing no-Saharan-dust transport over Bulgaria for 14, 20, 21, 23 and 24 June 2011.

It was suspected that it is expected development of sulphate particles 3-4 weeks after the injection of sulphur dioxide from Grimsvötn volcano. The Sofia lidar station performed monitoring of the atmosphere for the period 20-24 June due to the same reason. We can say beforehand that those days we didn't register any layers in the upper troposphere, until again in the end of May we observed exceptionally rare aerosol load of the air above Sofia. We could conclude that it has anthropogenic origin because there is no information for other sources of aerosols like fires, volcano eruption or desert dust transport for the end of June. DREAM forecasts (Fig.6) for the days of the lidar monitoring show an atmosphere free of desert dust over Balkans. On Fig.7 are shown lidar results obtained on 14, 20, 23 and 24 June 2011. We have observed during these days aerosol load above Sofia up to 3-6 km heights. All the measurements were performed in the interval around noon (9 AM – 13 PM) and only on 23 June there is additional one around Sunset. For that day we present profiles from the daily as well as from the evening monitoring, because they show the daily cycle in urban aerosols caused by warming the ground (Massimo Del Guasta, 2002). The solar radiation reaching PBL is the reason for its daily changes from the state of stable residual layer (about Sunrise) to well developed mixing layer (during noon and shortly after). When look at Fig.7 it becomes visible that the profiles from the daily measurements from 20-th (Fig.7.b) and 23-th (Fig.7.d) June have quite similar contours.

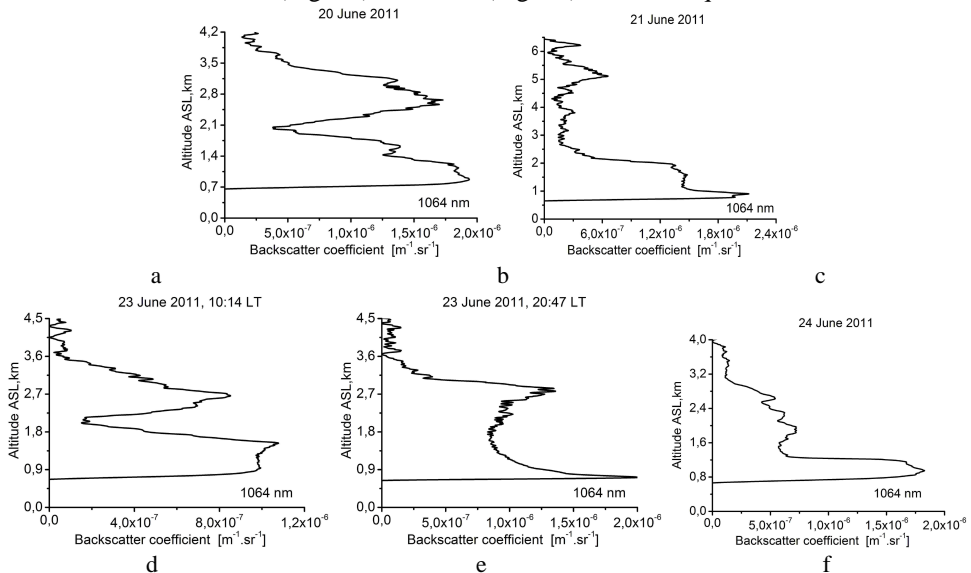


Fig.7. Atmospheric backscatter coefficient profiles retrieved on the basis of the lidar measurement data obtained on 14, 20, 21, 23 and 24 June 2011.

That leads to the conclusion that the aerosol layers registered during the two days have had slightly different mass altitude stratification. Taking into consideration that during Summer both the residual layer as well as the mixing layer over Sofia could raise to 1800 m height (Ts. T. Evgenieva et al., 2009), then our explanation of the received results is that for both days we have observed typical for the Summer residual layer with thickness about 1800 m and above it another one with top limit 4 km and 3.6 km, respectively. As a result of the hot

weather the fine aerosols could possibly have risen high above PBL the day before and have stayed there longer as a result of the weaker gravity and the absence of wind.

The comparison of the profiles from the daily (Fig.7.d) and the evening (Fig.7.e) measurement on 23th June shows that the registered in the morning two clearly defined layers completely merged, but the top limit of the aerosol load remains constant with value of 3.6 km. The merging of the layers is caused mainly by the convective processes in PBL. Every day they start before the Sunset and their intensity during the day depends on the change of the temperature of the air. The convective and adjective processes in PBL lead to the mixing of the particles in the layer close to the Earth surface and to the formation of well defined mixing layer during noon. The remaining profiles on Fig.7 show that on 20, 21 and 24 June we have registered aerosols up to 4-6 km. Besides that in the lower part of the layers we have calculated high values for the atmospheric backscatter coefficient reaching $2 \cdot 10^{-6} \text{ m}^{-1} \text{ sr}^{-1}$. We assumed that it is caused by water vapor flooding of small anthropogenic particles during sunrise.

It is disturbing that, similarly to May and June, the thick urban aerosol layers over Sofia have been also registered during the next warm/hot months. It was imperceptible by eye, but clearly noticeable for the laser light at 1064 nm wavelength. Some atmospheric backscatter profiles retrieved from the measurement data obtained in July and August 2011 we present on Fig.9. The investigations were carried out in the morning. The DREAM maps (Fig.8) show that for the corresponding days there was no Saharan dust transport over Bulgaria.

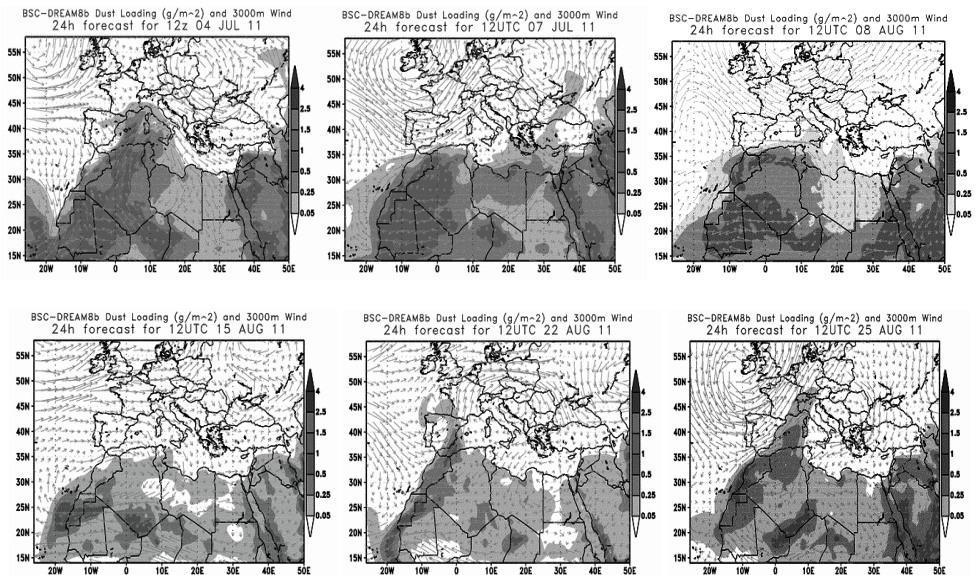


Fig.8. Forecast maps provided by Barcelona Supercomputing Center (BCS) showing no-Saharan-dust transport over Bulgaria for 14, 20-the days of lidar observations.

The lidar profiles on Fig.9 show the unsubstantial difference in the mass stratification of the registered aerosol layers. The main result of the measurements is that the atmosphere over Sofia in heights 3.5-4 km have been again loaded with urban aerosols.

The heat and the lack of winds in the valley, where Sofia is located, caused elevation of the city smog to such unusual heights.

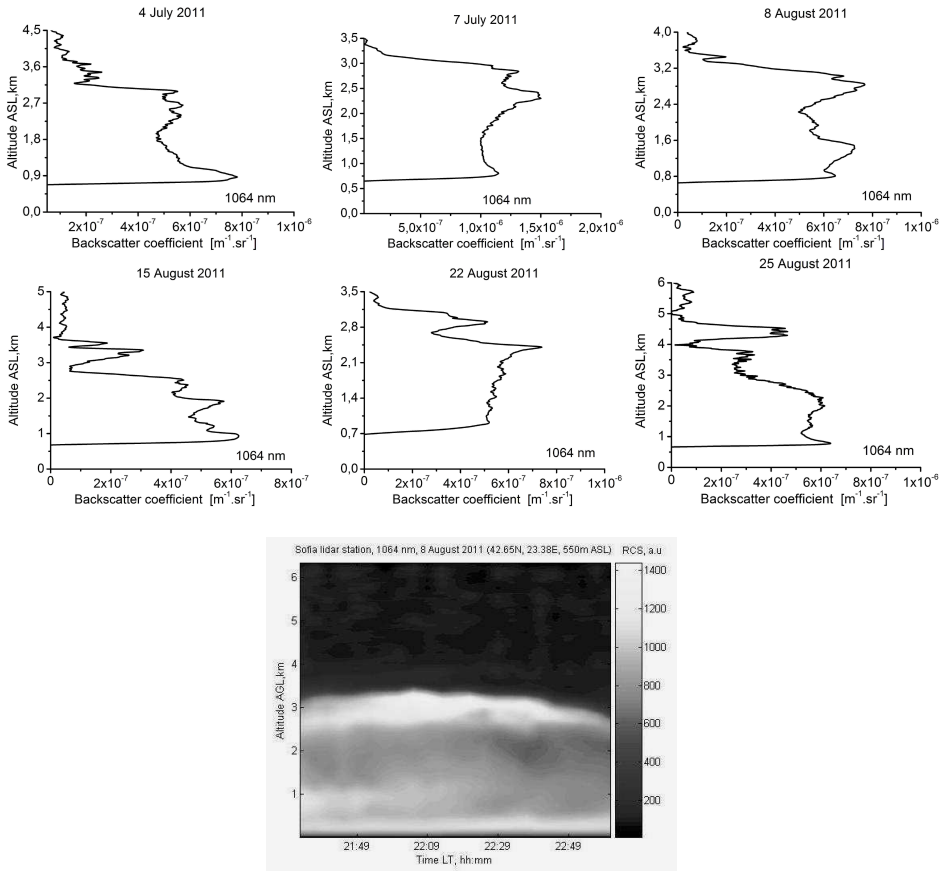


Fig.9. Atmospheric backscatter coefficient profiles retrieved on the basis of the lidar measurement data obtained in July and August 2011. RCS-map of the time evolution of the aerosol load up to 3.5 km observed on 8 August 2011.

The analysis of the data from the separate measurements shows that pollution is permanently present in the air above the city. As an example of this on Fig.9 we present RCS-map of the time evolution of the urban load observed on 8 August 2011. RCS-map illustrates relatively stable atmospheric aerosol stratification and its invariability during the lidar observation.

Conclusions

Lidar investigations of the atmosphere, performed in the period May-August 2011 are described. The experimental results could be summarized as follows. In the end of May the air above Sofia was not polluted by volcanic ash ejected during the Grimsvötn eruptions

(21-28 May 2011). In the period 7-9 June a long-distance Sahara dust transport above Sofia was detected. The most important conclusion concerning the air quality is that during most of the hot-month days in 2011 the atmosphere had been persistently loaded by anthropogenic aerosols at a height of 3.5-4.5 km above the city.

Acknowledgments. The research leading to these results has received funding from the European Union Seventh Framework Programme (FP7/2007-2013) under grant agreement n° 262254". The financial support for EARLINET by the European Commission under grant RICA-025991 is also gratefully acknowledged.

The authors gratefully acknowledge the NOAA Air Resources Laboratory (ARL) for the provision of the HYSPLIT model for air mass transport and dispersion and/or READY website used in this publication.

The authors would like also to express their gratitude to the Earth Sciences Division, Barcelona Supercomputing Center, Spain, for the provision of the DREAM model aerosol dust data used in this publication.

References

- Ansmann A., I. Mattis, U. Wandinger, F. Wagner, J. Reichardt, and T. Deshler, 1997. Evolution of the Pinatubo aerosol: Raman lidar observations of particle optical depth, effective radius, mass, and surface area over Central Europe at 53.48N, *J. Atmospheric Sciences*, 54, 2630-2641.
- A. Schreiner, T. J. Schmit, and G. P. Ellrod, 2004. First measurements of volcanic sulfur dioxide from the GOES Sounder: Implications for improved aviation safety, *Proceedings, 2nd Intl. Conf. on Volcanic Ash and Aviation Safety*, 21-24 June 2004, Alexandria, Virginia, Paper number 3.7.
- Atanaska D. Deleva, Ivan V. Grigorov, Lachesar A. Avramov, Vladimir A. Mitev, Alexander S. Slesar, and Sergey Denisov, 2008. Raman-elastic-backscatter lidar for observations of tropospheric aerosol, *Proc. SPIE 7027*, 70270Y-1÷70270Y-8
- A. Deleva, A. Slesar, and S. Denisov, 2010. Investigations of the aerosol fields and clouds in the troposphere with Raman-aerosol lidar, *Bulgarian Geophysical Journal*, 36, 26-39
- DREAM: <http://www.bsc.es/projects/earthscience/DREAM/>
- Draxler, R., and Rolph G., 2003. HYSPLIT (HYbrid Single-Particle Lagrangian Integrated Trajectory), Model access via NOAA ARL (READY) Website (<http://www.arl.noaa.gov/ready/hysplit4.html>), NOAA Air Resources Laboratory, Silver Spring, MD, (2003).
- EARLINET; <http://www.earlinet.org>
- E. Katragkou, S. Kazadzis, V. Amiridis, et al., 2009. PM10 regional transport pathways in Thessaloniki, Greece, *Atmospheric Environment*, 43, 1079-1085
- F. G. Fernald, 1984. Analysis of atmospheric lidar observations: some comments, *Appl. Opt.*, 23, 652-653
- Gian Paolo Gobbi, Francesca Barnaba, Riccardo Giorgi, Alessandra Santacasa, 2000. Altitude-resolved properties of a Saharan dust event over the Mediterranean, *Atmospheric Environment*, 34, 5119-5127
- Guibert, S., Matthias V., and Schulz M., 2005. The vertical distribution of aerosol over Europe - synthesis of one year of EARLINET aerosol lidar measurements and aerosol transport modeling with LMDZT-INCA, *Atmospheric Environment*, 39, 2933-2943

- Hansell, A.L., Horwell, C.J. and Oppenheimer, C., 2006. The health hazards of volcanoes and geothermal areas, *Occupational Environmental Medicine*, 63: 149-156.
- J. E. Penner, M. Andreae, H. Annegarn, L. Barrie, J. Feichter, D. Hegg, A. Jayaraman, R. Keaitch, D. Murphy, J. Nganga, and G. Pitari, 2001: in *Climate Change 2001: The Physical Scientific Basis, Contribution of Working Group I to the Third Assessment Report of the Intergovernmental Panel on Climate Change*, B. Nyenzi and J. Prospero, Eds., http://unfccc.int/resource/cd_roms/na1/mitigation/Resource_materials/IPCC_TAR_Climate_Change_2001_Scientific_Basis/TAR-05.pdf
- J. D. Klett, 1981. Stable analytical inversion solution for processing lidar returns, *Appl. Opt.*, 20, 211-220
- Kelly, P.M., Jones, P.D. and Pengqun, J., 1996. The spatial response of the climate system to explosive volcanic eruptions, *International Journal of Climatology* 16, 537-50.
- Massimo Del Guasta, 2002. Daily cycles in urban aerosols observed in Florence (Italy) by means of an automatic 532-1064nm LIDAR, *Atmospheric Environmental*, 36, 2853-2865
- NAAP: <http://www.nrlmry.navy.mil/aerosol/>
- N. Sabbagh-Kupelwieser, H. Horvath, and W. Szymanski, 2010. Urban Aerosol Studies of PM10 Size Fraction with Reference to Ambient Condition and Visibility, *Aerosol and Air Quality Research*, 10, 425-432
- Papayannis, A., Amiridis V., Mona L., Tsaknakis G., Balis D., Bösenberg J., Chaikovski A., De Tomasi F., Grigorov I., Mattis I., Mitev V., Müller D., Nickovic S., Pérez C., Pietruczuk A., Pisani G., Ravetta F., Rizi V., Sicard M., Trickl T., Wiegner M., Gerding M., Mamouri R.E., D'Amico G., and Pappalardo G., 2008. Systematic lidar observations of Saharan dust over Europe in the frame of EARLINET (2000-2002), *Journal of Geophysical Research D: Atmospheres*, 113 (10), art. no. D10204.
- Perez L., Tobias A., Querol X., Künzli N., Pey J., Alastuey A., Viana M., Valero N., González-Cabré N., Sunyer J., 2008. Coarse particles from Saharan dust and daily mortality, *Epidemiology*, 19 (6), 800-807
- Prabhakara, C., Kratz, D., P., Yoo, J.-M., et al., 1993. Optically thin cirrus clouds: radiative impact on the warm pool, *Journal of Quantitative Spectroscopy and Radiative Transfer*, 49 (5), 467-483
- Sassen, K., DeMott, P., Joseph J. Prospero, J., J., et al., 2003. Saharan dust storms and indirect aerosol effects on clouds: CRYSTAL-FACE results, *Geophysical Research Letters*, 30 (12), 1633, doi:10.1029/2003GL017371
- Satyanarayana, M., Radhakrishnan, S., R., V. Kakumar, V., et al., 2008. Microphysical parameters of cirrus clouds using lidar at a Tropical station, Gadanki, Tirupati (13.5°N, 79.2°E), India, *Proc. SPIE* 7153, 71530Y-71530Y-12
- Solomon, S., D. Qin, M. Manning, Z. Chen, M. Marquis, K.B. Averyt, M. Tignor, and H.L. Miller (eds.), 2007: in *Climate Change 2007: The Physical Science Basis, Contribution of Working Group I to the Fourth Assessment Report of the Intergovernmental Panel on Climate Change*, Cambridge Univ. Press (http://www.ipcc.ch/publications_and_data/ar4/wg1/en/contents.html), New York
- S. Veerabuthiran, 2004. High-altitude cirrus clouds and climate, *Resonance*, 9, no. 3, pp. 23-32, 2004
- Rolph, G. D., 2011. Real-time Environmental Applications and Display sYstem (READY) Website (<http://ready.arl.noaa.gov>). NOAA Air Resources Laboratory, Silver Spring, MD.
- Tasić M., Rajšić S., and Mijić Z., 2006. Atmospheric aerosols and their influence on air quality in urban areas, *Facta Universitatis*, 4, 83-90
- Ts. T. Evgenieva, N. I. Kolev, I. Ts. Iliev, Pl. B. Savov, B. K. Kaprielov, P. C. S. Devara, and I. N. Kolev, 2009. Lidar and spectroradiometer measurements of atmospheric aerosol optical

characteristics over an urban area in Sofia, Bulgaria, *International Journal of Remote Sensing*, 30, no. 24, 6381-6401

U. Pöschl, 2005. Atmospheric Aerosols: Composition, Transformation, Climate and Health Effects, *Atmospheric chemistry*, 44, 7522-7540

Ya Sasano, E. Browell, and S. Ismail, 1985. Error caused by using constant extinction/backscattering ratio in the lidar solution, *Appl. Opt.*, 24, 3929-3932

Лидарни изследвания на тропосферата, направени през лятната 2011 измерителна кампания

А. Делева

Резюме. В тази работа ние описваме лидарни изследвания на тропосферата, направени от май до август месец на 2011. През този период са извършвани както регулярни седмични EARLINET измервания така и всекидневни лидарни наблюдения на атмосферата по време на избухванията на Grimsvötn вулкана в Исландия и при пренос на прах от пустинята Сахара. Лидарният мониторинг е направен с аерозолен лидар с Nd:YAG лазер. Експерименталните резултати са представени чрез вертикални профили на коефициента на обратно разсейване на атмосферата и цветни карти на времевата еволюция на аерозолната стратификация. За да направим изводи за произхода на частиците в регистрираните аерозолни слоеве ние изчислявахме HYSPLIT (HYbrid Single-Particle Lagrangian Integrated Trajectory) обратни траектории и използвахме DREAM (Dust REgional Atmospheric Model) прогнозите за дните на измерванията. Бяха направени изводи, че атмосферата над София не е била замърсена с вулканична пепел по време на избухванията на Grimsvötn вулкана (21-28 май 2011). Най-важното заключение, което е от значение за качеството на въздуха над София, е, че през преобладаваща част от дните на горещите месеци през 2011г. над града до височина 3.5-4.5 км атмосферата е била трайно натоварена с антропогенни аерозоли. Описаните експерименти са част от регулярните лидарни изследвания на атмосферата, които извършваме в рамките на Европейския проект EARLINET.

DATA AND ANALYSIS OF THE EVENTS RECORDED BY NOTSSI IN 2012

E.Botev, V.Protopopova, I.Popova, Bl.Babachkova, S.Velichkova, I.Tzoncheva, Pl.Raykova, Vl.Boychev, D.Lazarov

Geophysical Institute, BAS, Akad. G. Bonchev street, bl.3, Sofia, Bulgaria, e-mail: ebotev@geophys.bas.bg

Abstract. A map of epicenters of 1508 earthquakes that occurred during 2012 in the Balkan Peninsula (sector outlined by latitude $\varphi = 37^{\circ} - 47^{\circ}\text{N}$ and longitude $\lambda = 19^{\circ} - 30^{\circ}\text{E}$) is presented. Expert generalized analysis of the seismicity over the territory of Bulgaria and its very adjacent lands (with more than 930 localized events) is proposed. Catalog of earthquakes with magnitude $M > 2.5$ is applied.

Key words: Balkan Peninsula, Bulgaria, seismicity

The present scientific communication contains generalized information on the results of collection, processing and analysis of the data about the seismic events recorded by the National Operative Telemetric System for Seismological Information (NOTSSI) in 2012. The expanded information about the realized seismicity is suggested as a natural generalization and supplementation of the monthly compilations of the preliminary seismological bulletin of NOTSSI. The analysis and evaluation of the space, time and energy distribution of the seismicity, periodically been made, open up possibilities for searching for time correlations with the parameters of different geophysical fields aiming to find out eventual precursor anomalies.

The recording and space localization of the seismic events in NOTSSI during 2012 is realized by means of the new digital network (Solakov et al., 2005). The routine processing and acquisition of the initial data is organized in a real time duty regime. The operations are fulfilled by the authors of this communication. In such a way the main goal of NOTSSI, namely the seismicity monitoring in order to help the authorities' and social reaction in case of earthquakes felt on the territory of the country, is realized. The computing procedure for determining the parameters of the seismic events is an adaptation of the widespread product HYPO71 (Solakov, 1993). The energy parameters of the events are presented mainly by the magnitude M calculated according to the record's duration by the formula (Christoskov and Samardjieva, 1983)

$$M = 1.92 + 2.72\log\tau - 0.026\Delta$$

The focal mechanism parameters are obtained by means of a program FOCMEC (Snoke,2009). The high sensitivity of the seismographs allows recording and processing of a great number of long distance earthquakes. As a result of the achieved experience in the authors interpretation work, different magnitude's lower threshold for successful determination of local, regional and long distance earthquakes is established: $M=1.5$ for the territory of Bulgaria, $M=3.0$ for the central part of the Balkans, $M=5.0$ for long distance events. The precision of the epicenter's determination is different; except on the distance it depends also on the specific position of the epicenter in relation to the recording network. The parameters of seismic events occurring at a distance more than 100-150 km outside the territory of Bulgaria should be accepted only informatively and cannot be used for responsible seismotectonic investigation.

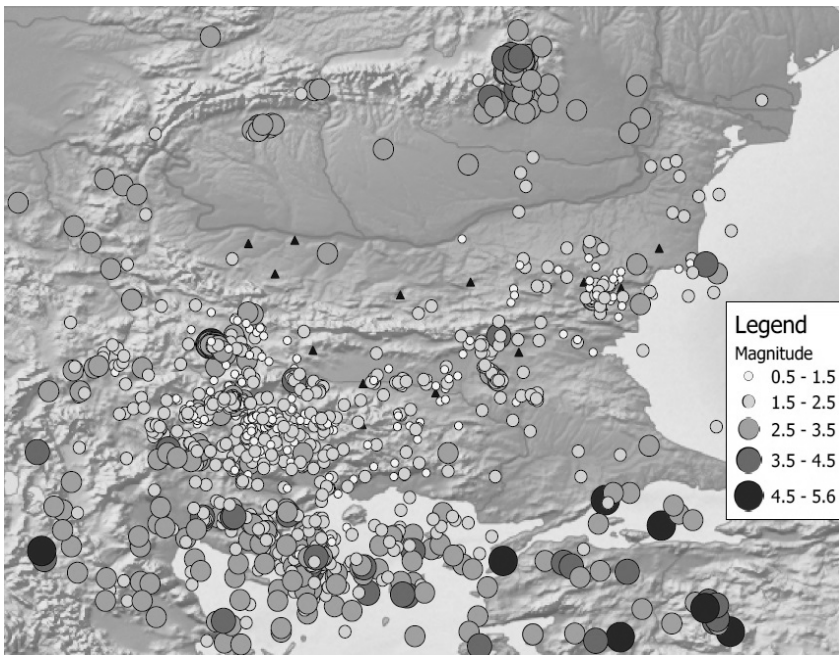


Fig.1. Map of epicenters in Central Balkans during 2012.

For the period of observations presented in this communication, the primary data about 2000 local, regional, distant earthquakes and industrial explosions on the territory of Bulgaria are recorded, classified and processed (as a work bulletin) in NOTSSI. After comprehensive analysis of the records and application of the above mentioned calculation procedures it is established that 1508 of all registered earthquakes are in the Balkan Peninsula region outlined by geographic latitude $37^{\circ} - 47^{\circ}$ N and longitude $19^{\circ} - 30^{\circ}$ E. The epicenters of the earthquakes differentiated by magnitude levels are plotted on Fig.1. The number of the events in the magnitude interval $M=0.5-1.9$ is 744, in $M=2-2.9 - 576$, in

M=3-3.9 - 155, in M=4-4.9 – 33 earthquakes. During this not so active period there are 2 events with magnitude $M > 5$. The maximum magnitude value is $M=5.6$.

As a whole, the seismic situation in the study part of the Balkans during 2012 is characterized by not so high activity - 1508 events against 1829 in 2011, 2401 in 2010, 2744 in 2009, 1775 in 2008, and around 1100- 1400 for most of the previous years. The maximum realized earthquake is with magnitude $M_s=5.8$ while this value for the previous years is lower than five, as a rule, except 2011 – $M=5.8$. It can be noted that the observed tendency of high increase of the activity compared with the former years is partly due to the high level of earthquake activation in Marmara sea, Central Greece, Serbia, Romania, and also due to increase of number of microearthquakes in the territory of Bulgaria.

The strongest event outside Bulgaria during the study period occurred in the region situated to the south of Marmara sea (Turkey) with magnitude $M=5.3$. Shakable effects because of outside attack (Vrancea source zone in Romania) during the study period occurred 3 times in north-eastern Bulgaria (intensity III in towns of Ruse, Tutrakan and Silistra).

As a whole, events with $M < 3.0$ which occur outside Bulgaria are difficult to be localized by the national seismological system; consequently, not all of them have been marked on the scheme in Fig.1.

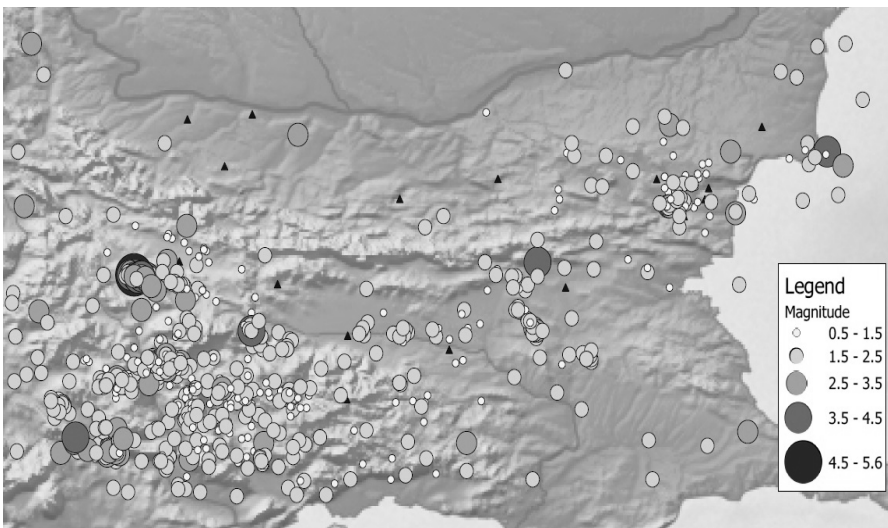


Fig.2. Map of epicenters in Bulgaria and adjacent lands during 2012

Fig.2 illustrates the seismicity just in the territory of Bulgaria and nearby lands ($\varphi = 41^{\circ} - 44.5^{\circ}N$, $\lambda = 22^{\circ} - 29^{\circ}E$). The earthquakes are differentiated by magnitude intervals. The seismic stations are also noted in the same figure by triangles. The parameters of relatively stronger earthquakes are presented in Table 1.

Table 1. List of earthquakes with $M \geq 2.5$ in Bulgaria and adjacent lands during 2012

Date			Time	Coordinates		H,km	M
2012/	1/	12	5:37:21.3	41.85	22.86	13	3.0
2012/	1/	19	13:41:34.4	41.26	23.45	5	2.6
2012/	1/	20	22:58:42.0	41.96	23.38	5	3.5
2012/	1/	24	5:25:45.7	41.72	24.26	8	3.0
2012/	2/	9	22:34:40.5	42.20	26.27	10	3.2
2012/	2/	9	22:37:20.6	42.18	26.29	8	2.6
2012/	2/	12	23: 8:46.9	42.68	23.27	15	2.6
2012/	2/	29	15: 1:48.2	43.65	27.38	12	2.8
2012/	3/	23	11: 2:34.9	41.34	22.83	7	2.6
2012/	3/	30	20:48:33.6	42.67	26.30	4	3.9
2012/	4/	8	15:27:12.7	42.19	25.22	2	2.5
2012/	5/	1	19:11:23.0	41.91	23.28	2	2.8
2012/	5/	4	13:20: 0.1	43.07	22.10	1	3.2
2012/	5/	7	12:44:14.2	41.82	22.02	15	2.5
2012/	5/	10	22:40:29.1	41.38	25.72	9	3.1
2012/	5/	12	7:32: 4.0	41.36	22.81	2	2.7
2012/	5/	15	17:30: 1.2	41.46	28.02	2	3.2
2012/	5/	18	2:50:14.4	41.92	23.26	2	2.6
2012/	5/	20	0: 0:32.5	42.58	23.00	9	5.6
2012/	5/	22	0: 4:52.6	42.58	22.97	8	3.9
2012/	5/	22	0:15: 5.0	42.55	23.15	13	2.5
2012/	5/	22	0:16:53.1	42.56	23.09	13	3.0
2012/	5/	22	0:23:35.4	42.56	23.06	11	2.9
2012/	5/	22	0:43:47.3	42.58	23.05	10	3.4
2012/	5/	22	0:49:24.5	42.57	23.04	9	2.7
2012/	5/	22	0:55:57.5	42.56	23.07	10	2.9
2012/	5/	22	1:30:50.6	42.58	23.01	9	4.4
2012/	5/	22	1:34:30.5	42.53	23.09	10	3.0
2012/	5/	22	1:37:21.9	42.54	23.12	12	2.9
2012/	5/	22	12: 4:59.1	42.33	23.06	2	2.8
2012/	5/	22	16:26:12.4	42.58	23.06	15	2.6
2012/	5/	22	17: 7:41.5	42.58	23.03	15	3.3
2012/	5/	22	19:52:35.2	42.59	23.03	15	2.9
2012/	5/	22	2:11: 6.3	42.60	22.97	12	3.2
2012/	5/	22	2:13:28.3	42.57	23.05	5	4.1
2012/	5/	22	3:23:26.9	42.40	23.42	2	2.9
2012/	5/	22	3:41:36.0	42.58	23.02	7	2.8
2012/	5/	22	4: 9:58.5	42.57	23.04	2	3.2
2012/	5/	22	4:29:11.5	42.58	23.08	15	3.1
2012/	5/	23	10:57:25.1	42.54	23.11	11	3.0
2012/	5/	23	11:41: 8.3	42.56	23.02	2	3.1
2012/	5/	23	13:31:32.4	42.58	23.03	15	2.6
2012/	5/	23	21:59:14.8	42.56	23.10	10	3.7
2012/	5/	24	22:49: 5.7	42.57	23.00	4	2.5

2012/	5/	25	15: 3: 3.5	41.49	22.76	2	2.5
2012/	5/	25	7: 8:40.1	42.59	23.01	9	2.8
2012/	5/	25	9:43: 5.9	42.53	23.07	7	2.8
2012/	5/	27	18:56:30.0	42.93	23.43	20	2.7
2012/	5/	29	7:23:31.7	42.56	23.03	6	3.8
2012/	5/	30	5:36:23.0	42.55	23.07	9	3.4
2012/	6/	3	20: 8:50.0	42.18	23.96	2	3.6
2012/	6/	5	0:43: 8.1	41.48	22.86	2	2.8
2012/	6/	16	4:51: 2.1	42.57	23.07	10	3.0
2012/	6/	17	4: 8: 6.3	41.38	22.87	8	2.5
2012/	6/	21	3:10:15.0	41.95	23.21	2	2.8
2012/	6/	23	8:58:48.4	41.90	23.27	2	3.4
2012/	6/	28	19:16:38.7	43.07	27.37	12	2.8
2012/	6/	29	1:27: 4.3	43.07	27.38	12	2.9
2012/	7/	2	13:26:32.2	41.80	23.12	3	2.9
2012/	7/	5	16:21:34.7	41.30	22.88	5	2.6
2012/	7/	5	6:43:44.8	41.31	22.85	1	2.6
2012/	7/	9	12:49:46.9	42.47	23.18	2	2.6
2012/	7/	14	12:52: 7.0	42.57	23.06	8	4.3
2012/	7/	22	22:10:51.4	41.32	22.80	2	3.5
2012/	7/	24	6:58:49.1	41.77	23.72	2	2.8
2012/	7/	31	0:10:21.4	42.54	23.10	7	3.3
2012/	8/	12	20:36:29.1	41.31	22.86	5	2.5
2012/	8/	16	2:11:54.4	42.57	23.06	10	3.0
2012/	8/	17	10:31:48.2	42.01	23.26	2	2.7
2012/	8/	17	19:54:44.5	42.01	23.26	2	2.5
2012/	8/	17	19:55:11.7	43.36	28.80	15	2.8
2012/	8/	19	6:36:13.7	42.32	22.22	1	3.0
2012/	8/	21	18:21:48.0	42.58	23.02	15	2.5
2012/	8/	25	12:31:33.8	43.09	27.30	8	2.5
2012/	8/	27	16:26:51.7	41.42	22.52	7	4.1
2012/	9/	3	16:54:32.4	41.41	22.91	4	3.0
2012/	9/	7	16:47:23.6	41.32	22.04	2	2.5
2012/	9/	14	11:32:37.0	42.57	23.00	2	2.7
2012/	9/	19	17: 0:48.6	42.56	23.09	15	2.7
2012/	9/	22	19:57:24.6	42.50	23.14	3	2.7
2012/	9/	27	19: 8:18.2	41.79	22.77	5	2.5
2012/	9/	28	9:47:45.4	44.23	22.16	2	2.6
2012/	10/	4	20:37:16.5	41.38	24.06	4	3.2
2012/	10/	12	7:59:53.4	41.06	22.83	2	2.5
2012/	10/	18	0:23:16.4	43.58	24.34	8	2.6
2012/	10/	24	1: 2: 6.7	41.36	23.70	2	2.5
2012/	11/	11	2:15: 5.7	41.31	22.83	10	2.5
2012/	11/	24	22:15:57.0	43.15	28.76	8	2.5
2012/	11/	25	5:58:54.5	41.12	27.24	10	2.5

2012/	11/	28	15:32:52.3	41.31	22.40	12	3.4
2012/	11/	29	23:52:21.7	41.91	23.25	6	2.5
2012/	12/	2	20:11:31.7	43.02	27.92	13	3.0
2012/	12/	3	18:58:39.4	43.46	28.67	15	4.1
2012/	12/	6	7:28:35.1	41.38	22.51	9	2.6
2012/	12/	10	16:58:29.0	43.46	27.88	15	2.7
2012/	12/	15	15:43:37.1	41.29	22.78	2	2.6
2012/	12/	23	20:31:16.4	41.33	22.62	2	2.6

On the territory of Bulgaria relatively low activity of earthquakes is observed during 2012: – only 932 events are observed, against 1205 in 2011, 1607 in 2010, 2017 in 2009 and 1079 in 2008. The earthquakes of a magnitude higher than 3.0 are in normal amount – 35 events compared with an averaged number of about 20-30 for most of the all previous years (exception is 2009 with 147 events because of the aftershocks of Valandovo $M=5.2$ earthquake.).

The maximum realized magnitude is $M_s=5.8$ ($M_w=5.6$) in the region of Pernik which is the highest earthquake, in comparison with the maximum magnitude in the course of previous years. The strongest Bulgarian event during 2012 occurs on 22 May and caused macroseismic effects with intensity of VII-VIII degree of MSC scale in the town of Pernik – close to Bulgarian capital Sofia. During the first day the main shock is followed by more than 30 events with maximum $M=4.4$, causing moderate damages in a wide area including the main city. According to the calculations of the national seismological centre the depth of the event is about 10 km. The epicentres of the shocks are in an area which was relatively silent for the last 100 years. The relatively short duration and low frequency of the aftershock sequence of this event does not increase significantly the relatively low number of all seismic events in Bulgarian territory during 2012.

As usual, the largest concentration of the epicenters in the other regions of Bulgarian territory during 2012 is marked in the southwestern part of the investigated region (presented in Fig.2). The Kroupnik seismic source is known with the strongest crustal earthquakes in Europe ($M=7.8, 7.1$) for the last 160 years. In 2012 about 50 events of $M<3.0$ and only 3 of $M\geq 3.0$ occurred in this region. The strongest felt earthquake for the south-western part of Bulgarian territory is with magnitude $M=3.5$, it is felt on 20 January in Razlog region (southern slopes of Rila mountain) by intensity of III - IV degree of MSC scale.

The other Bulgarian seismic sources in 2012 are relatively not so active than during the previous years. They produced not more than 15 earthquakes affecting different localities in this country by intensity of up to IV-V degrees of MSC scale. The maximum number of felt earthquakes is occurred around the Monastery uplift. About four cases of magnitudes less than 3.0 aroused shocks of intensity three or a bit more are felt in Monastery Highland territories. The maximum event with $M=4.1$ in Black sea caused V degree of MSC scale on 03 December in Shabla region (north-eastern Black sea coast). A strong event $M=3.9$ in the neighbor region of Sliven town caused effects of IV-V degree of MSC. A relatively so much significant seismic impact is associated with the Velingrad earthquake source zone in the Rhodopean region, where an event with magnitude $M=3.6$ shook the city of Velingrad with intensity of IV-V degree of MSC on 03 June. In the rest

part of the Bulgarian territory the felt events caused excitation of lesser intensity during 2012.

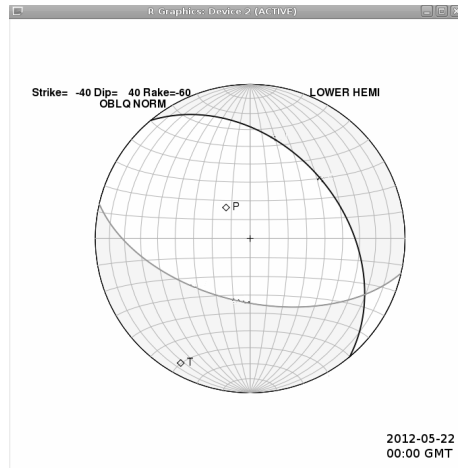


Fig.3. Focal plane solution of the strongest Pernik earthquake (22.05.2012, 00:00 GMT)

For the determination of the earthquake mechanism the program FOCMEC is used. Input data are the polarities of the P wave. Twenty three first motion polarities data from seismological stations in Bulgaria and surrounding area taken from NOTSSI and ISC database (<ftp://www.orfeus-eu.org/pub/data/continuous/2012/>) are included in the double - couple focal mechanism - Fig.3. The solution is displayed on lower hemisphere. The polarities from ISC are check as waveform. The strike, dip and rake are determined in accuracy up to 10 degree. The earthquake is characterized as a normal faulting, with very small strike-slip component. The fault plane solutions of the some other events are with very bad quality because of a low number of polarities.

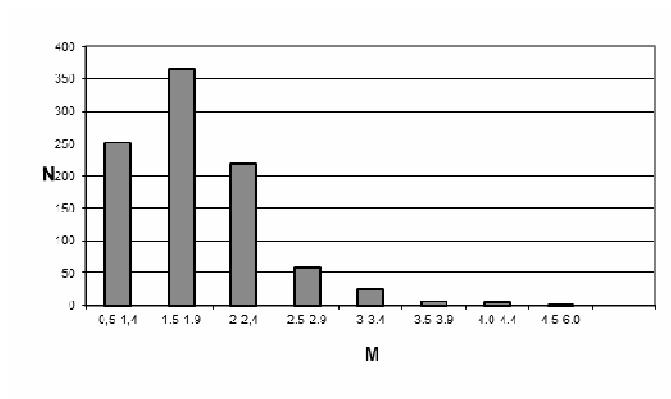


Fig.4. Magnitude - frequency distribution of the earthquakes

A detailed analysis of seismicity in the individual seismic zones is hard to be fulfilled because of the insufficient quantity of events and the narrow magnitude range of

the earthquakes. The joint statistics of all the events in Fig.2 characterize predominantly the seismicity parameters of the southwestern part of the territory under investigation.

The magnitude-frequency distribution for the entire data set is presented in Fig.4. The number of localized events increases with the magnitude decreasing: for $M > 5$ – 1 event, $M = 4.0-4.5$ is 5 events, $M = 3.5-3.9$ is 7 events, for $M = 3.0-3.4$ is 25 events, for $M = 2.5-2.9$ – 59, for $M = 2.0-2.4$ – 218 and so on. The abrupt diminishing of the number of earthquakes in the first two intervals ($M < 1.5$) in Fig.4 determines also the registration power of the seismic stations network.

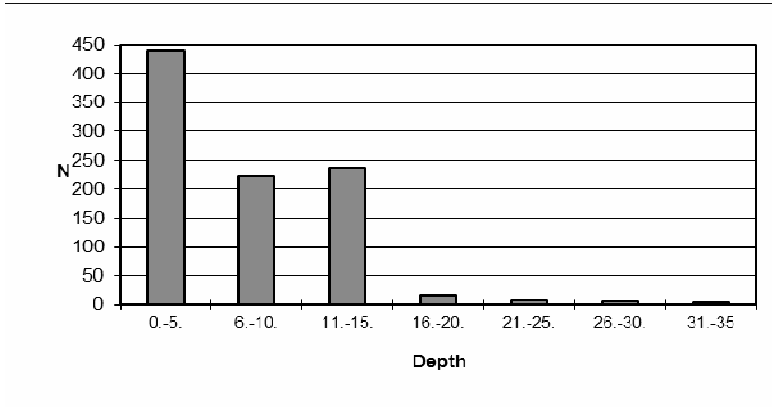


Fig.5. Depth - frequency distribution of the earthquakes

Taking the latter into account, it can be supposed that the magnitude sample for levels with $M > 1.5$ is comparatively closer to the reality for the bigger part of the Bulgarian territory.

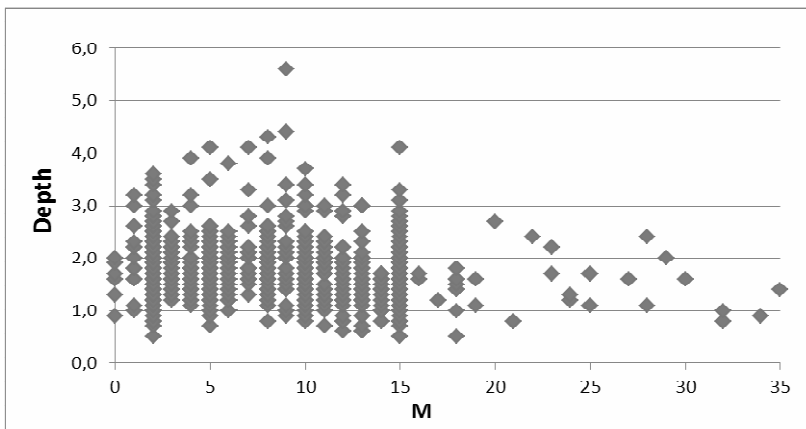


Fig.6. Magnitude - depth dependence

The picture of the depth distribution in Fig.5 shows that the majority of events occur down to 15 km depth. The number of events does not decrease smoothly with increase of the depth. It is possible the established predominating depth (from 0 to 5 km) to be also

due to the presence of small number of unidentified industrial explosions. In the same time the number of events in the interval 11-15 km is bigger. The magnitude distribution of the events in depth (Fig.6) permits to note some differentiation of depth "floors" with the increase of magnitude - the maximums can be traced out for the depth interval from 4 to 15 km. It is remarkable that the strongest events are not deep situated and the maximal event is associated with 9 km depth.

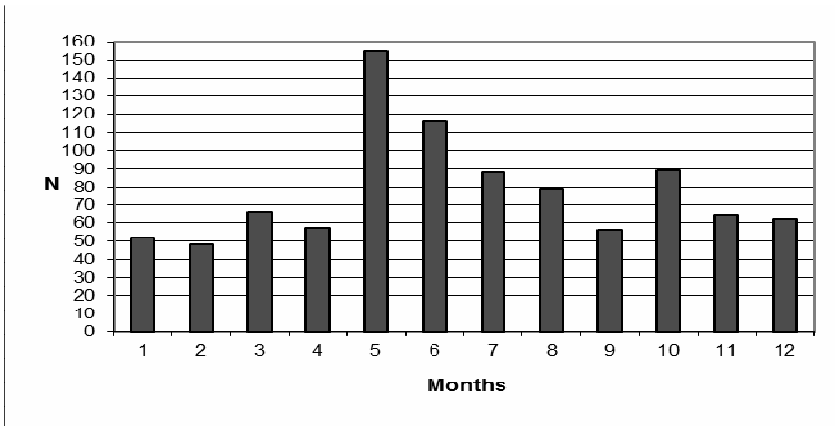


Fig.7. Time distribution of the earthquakes.

Fig.7 illustrates the distribution of seismicity in time according to the number of events per months. The biggest earthquake's amount is displayed in May, when more than 150 earthquakes occurred, and it is associated with aftershock activity of 22May maximal earthquake. The lowest earthquake quantity is in January - February, around 50 events. The energy release suggests that the period May - August, when the relatively short aftershock sequence in Pernik region occurred, is the time with maximum of energy release. Local maximum of events is observed in October, when about 90 earthquakes occurred.

Additionally, about 900 distant earthquakes have been recorded in the period under study, as well as more than 800 industrial explosions, processed and classified in the preliminary monthly bulletins. In order to identify the artificial seismic sources the methodical approach described by Deneva et al. (1988) and some information about the quarry sites in Bulgaria have been used.

Acknowledgements: The authors owe their gratitude to the engineering staff for the perfect software and hardware ensuring of NOTSSI.

References

- Christoskov L. and E. Grigorova, 1968. Energetic and space characteristics of the destructive earthquakes in Bulgaria since 1900. *Izv.BAS, vol XII*.
- Christoskov L. and E. Samardjieva, 1983. Investigation on the duration of the seismic signals like a energetic characteristic of the earthquakes. *BGJ, vol.IX, NI*.

- Christoskov L. et al., 1987. Real time and background data processing in the Bulgarian seismological network. *Proc. Xx gen. Assembly 1986, Kiel.* , Zurich.
- Deneva D. et al., 1988. On the discrimination between industrial explosions and weak earthquakes using records of local seismics networks. *Proc. of conference in Liblice, 1988, Praha.*
- Snoke J.A., 2009. FOCMEC: FOCal MECanism Determinations. VirginiaTech, Blacksburg, VA, USA, 2009, Manual.
- Solakov, D., 1993. An algorithm for hypocenter determination of near earthquakes. *Bulg. Geophys. J.* 19 (1), 56-69
- Solakov, D. et al., 2005. National Seismological Network – state and development. Proceedings of Scientific-practical conference on management in extraordinary situations and people protection, BAS, Sofia, 2005, 265-272.
- <ftp://www.orfeus-eu.org/pub/data/continuous/2006/>
- The maps in Fig1. and Fig2. are made with Quantum GIS and Natural Earth - Free vector and raster map data@naturalearthdata.com.

Данни и анализ на сеизмичните събития регистрирани от НОТССИ през 2012

Е.Ботев, В.Протопопова, И.Попова, Бл.Бабачкова, С.Величкова, И.Цончева,
Пл.Райкова , Вл.Бойчев, Д.Лазаров

Резюме. Предлаганото научно съобщение съдържа обобщена информация за резултатите от събирането, обработката и анализа на първичните данни за сеизмичните събития, регистрирани от Националната Оперативна Телеметрична Система за Сеизмологична Информация (НОТССИ) през 2012 г. Представена е карта на епицентрите на общо 1508 земетресения в частта от Балканския полуостров, ограничена от географска ширина 37° - 47° N и дължина 19° - 30° E. По-подробно се анализира сеизмичността за територията на България и прилежащите ѝ земи (повече от 930 сеизмични събития в район с координати $\lambda = 22^{\circ}$ - 29° E и $\varphi = 41^{\circ}$ - 44.5° N). Предлага се и каталог на земетресенията с магнитуд $M > 2,5$. Сеизмогенните прояви се обсъждат по зони, сравнени със съседни периоди време.